IGNITION AND COMBUSTION PHENOMENA ON A MOVING GRATE

with application to the thermal conversion of biomass and municipal solid waste

Maarten van Blijderveen

Ignition and combustion phenomena on a moving grate: with application to the thermal conversion of biomass and municipal solid waste
van Blijderveen, Maarten

PhD thesis, University of Twente, Enschede, The Netherlands, December 2011

ISBN 978-90-8891-368-6

Keywords: Municipal solid waste; combustion; solid fuels; ignition; moving grate; biomass

Cover: Picture of the burning waste in one of the combustion lines of the waste incinerator of GKS in Schweinfurt, 2009

This research has been carried out in the framework of the EU project NextGenBioWaste with funding from TNO, The Netherlands.

Printed by: Proefschriftmaken.nl || Printyourthesis.com
Published by: Uitgeverij BOXPress, Oisterwijk

IGNITION AND COMBUSTION PHENOMENA ON A MOVING GRATE

WITH APPLICATION TO THE THERMAL CONVERSION OF BIOMASS AND MUNICIPAL SOLID WASTE

PROEFSCHRIFT

ter verkrijging van
de graad van doctor aan de Universiteit Twente,
op gezag de rector magnificus,
prof.dr. H. Brinksma
volgens besluit van het College voor Promoties
in het openbaar te verdedigen
op vrijdag 13 januari 2012 om 12.45 uur

door

Maarten van Blijderveen
geboren op 25 juni 1982
te Warnsveld

Dit proefschrift is goedgekeurd door de promotor
Prof. dr. ir. G. Brem

De promotiecommissie:

Voorzitter:	
Prof. dr. F. Eising	Universiteit Twente
Promotor:	
Prof. dr. ir. G. Brem	Universiteit Twente
Leden:	
Prof. dr. ir. T. H. van der Meer	Universiteit Twente
Prof. dr. ir. S. R. A. Kersten	Universiteit Twente
Prof. dr. ir. L. Lefferts	Universiteit Twente
Prof. dr. ir. J. J. H. Brouwers	Technische Universiteit Eindhoven
Prof. dr. ir. B. J. Boersma	Technische Universiteit Delft
dr. ir. A. I. van Berkel	TNO

Summary

Combustion can be defined as a fast oxidation process of a solid, gaseous or liquid fuel at elevated temperatures. In any combustion process, ignition plays an essential role. Not only to initiate the combustion process, but also to maintain it. Especially in solid fuel combustion on a grate, where fuel is abundantly available, the ignition of the fresh fuel determines the stability of the combustion process. To be able to control the combustion process properly, the understanding of the ignition processes of solid fuels is of great importance.

For modeling purposes, the ignition of a solid fuel layer on a grate is often described by an ignition front traveling downwards through the fuel bed. The waste layer ignites from the top due to furnace and flame radiation, thus the combustion process takes place over the length of the grate. However, as there is almost no mixing of the solid fuel over the length of the grate, the process can be considered as a horizontal plug-flow process. For this reason the combustion process on the grate can be translated to a packed bed where the length coordinate of the moving grate corresponds with the time in the packed bed process. The packed bed can be modeled as a transient one dimensional model. Generally, to validate these one dimensional models, results from experiments in so called "pot furnaces" are used. In these experiments waste or an other solid fuel is piled on a fixed grate in a round tube and ignited from the top while air is fed via the grate and flowing upwards through the fuelbed. Thermocouples and gas sampling points at several heights in the fuelbed can be used to monitor the process. In case of a homogeneous fuel, at every height in the layer a subsequent sharp rise in temperature is measured going from the top to the bottom of the reactor. From these data, a fairly constant ignition front velocity can be derived. However, in the present work it is shown that one dimensional models based on a homogeneous fuel under-predict the velocity of the ignition front in waste by a factor of two. Apparently, not all phenomena which are important in waste combustion on a moving grate are captured in these simplified one dimensional models. This thesis deals with some of these ignition phenomena encountered in the combustion of municipal solid waste and biomass on a moving grate.

Solid fuels such as biomass and waste both contain fixed carbon and a large part of volatiles (more than 70 wt.%). The volatiles combustion should be considered as the combustion of a gaseous fuel, while the fixed carbon combustion can be considered as the combustion of solid (char) particles. Chapter 2 investigates the impact of gaseous combustion in a packed bed. To eliminate the reactions in the solid phase, natural gas combustion in an inert solid phase is considered. The chapter deals with the case where the combustion takes place inside the packed bed. This process is called filtration combustion and can be characterized by a thermal wave and a combustion wave. An analytical model from the literature is used to investigate the in-

fluence of different parameters such as gas composition, gas velocity, bed porosity and particle diameter on the propagation of the combustion front. The results are validated by experimental results. For these experiments a tube filled with alumina spheres is used. A premixed flammable gas mixture is fed through the packed bed and ignited in the lower region of the tube. Thermocouples at several heights monitor the combustion process. The trends found from the analytical model can be compared well with the experimental results. It is shown that the combustion wave travels downwards much slower than the combustion fronts generally measured in burning solid fuel beds. It is also shown that flashback is very unlikely to occur in waste combustion.

The one dimensional approach mentioned before can only be applied if the horizontal mass and energy gradients along the grate can be neglected. With the help of the Péclet number, it is shown in chapter 3 that the horizontal energy gradients can not always be neglected. As a result the ignition front propagation through a packed bed is divided in a horizontal direction and a vertical direction. The horizontal front propagation determines the flame stability in the furnace and the vertical front propagation determines the burnout of the fuel. Based on optical observations of ignition fronts and gas composition measurements below the ignition front it is concluded that the driving mechanism of the front propagation in both horizontal and vertical directions is char combustion (for low radiative heat fluxes from the furnace walls). This implies that the volatile combustion can be neglected, which simplifies the modeling of the ignition front propagation significantly. With this result, an analytical one dimensional model for the velocity of the ignition front is derived. The calculated ignition front velocity and combustion front temperature are a function of a dimensionless energy loss term and a dimensionless excess energy term. Based on these terms, upper and lower boundaries for the ignition front velocity are derived. The model is validated with experiments from the literature done by several researchers. The model can be applied to both horizontal and vertical directions when furnace radiation is low.

To investigate the possibility to ignite the fuel by preheated primary air, experiments are carried out in a pot furnace. In these experiments, a preheated primary air flow is fed into a shallow packed bed of either wood, RDF or char. The critical air temperature needed to ignite the bed and the corresponding bed temperature at the moment of ignition are recorded as a function of the primary air flow. In chapter 4, it is shown that a fuel bed of wood can be ignited solely by a primary air stream with a temperature as low as 230^oC. A fuel bed of char ignites even with a primary air temperature as low as 170^oC. For lower primary air velocities, both the critical air temperature and the bed temperature at ignition decrease. A remarkable observation is that with a deep fuelbed the ignition does not occur close to the grate, but $20-35cm$ above the grate. This can be explained by taking conduction inside the bed into account. The obtained

experimental results are translated into a spontaneous ignition model in chapter 5. The model is based on Semenov's analysis of thermal explosions and consists of the balance between the exothermic pyrolysis reactions and the convective heat transfer of the preheated primary air to the fuel. A single dimensionless parameter is derived which determines the critical air temperature and the fuel bed temperature at ignition as a function of the primary air velocity, the inert fraction and the fuel type. The results from the model agree well with the results from the experiments for wood and RDF. With the presented theory, the ignition phenomena occurring during char experiments can only be explained qualitatively. It seems plausible to assume that the temperature at which the heat of reaction of char oxidation becomes exothermic coincides with the spontaneous ignition temperature.

Chapter 6 deals with the startup of a waste incinerator. This is done by investigating the piloted ignition of several solid fuels such as wood, PVC and PMMA under a radiative heat flux. A model is developed to predict the ignition times for several materials and radiative heat fluxes. The model is based on the ignition temperature of the produced gas mixture at its lower explosion limit. From the energy balance at the moment of the pilot, it is calculated if the mixture can reach its ignition temperature at a certain time, called the ignition time. Experiments from the literature are used to validate the model and flashes observed during these experiments can be explained qualitatively by the model. Subsequently, the model is further developed to a full-scale furnace and it is shown that there is a critical primary air flow with respect to ignition. When the primary air flow is higher than this critical value, ignition can not be obtained. This is due to the fact that the produced gas mixture is not able to reach its lower flammability limit for high air flows.

In chapter 7 the results from the present study are summarized and used to describe the ignition and combustion phenomena in full-scale waste incinerators. A simplified expression for the ignition front velocity in both the horizontal and vertical direction is presented and applied to determine local front velocities based on local fuel properties. The local front velocities are integrated over the bed height to obtain the location where the front reaches the grate. It is shown that this two-dimensional ignition front model predicts the ignition front to be up to twice as steep as predicted by a one-dimensional model. In this chapter also guidelines for startup of moving bed furnaces are given. It is advised to start with a fuel which ignites easily under a pilot and is able to maintain an ignition front. Recommendations for further research are (1) to validate the translations done in the current work to full scale waste and biomass combustion and (2) to apply the results to a full scale combustion process.

Samenvatting

Verbranding kan worden gedefinieerd als een snelle oxidatiereactie van een vaste, gasvormige of vloeibare brandstof op een hoge temperatuur. In elk verbrandingsproces speelt ontsteking een essentiële rol. Dit is niet alleen om het proces te starten, maar ook om het in stand te houden. Vooral bij vaste stof verbranding op een rooster, waar de brandstof volop aanwezig is, bepaalt de ontsteking de stabiliteit van het verbrandingsproces. Om het proces goed te kunnen regelen, is kennis van ontsteking van groot belang.

Voor het modelleren wordt de ontsteking van een vaste brandstoflaag op een rooster vaak beschreven door een ontstekingsfront dat omlaag beweegt door de brandstoflaag. De brandstoflaag wordt aan de bovenkant ontstoken door oven- en vlamstraling, dus de verbranding vindt plaats over de lengte van het rooster. Echter, omdat de afvallaag bijna niet gemengd wordt over de lengte van het rooster kan het proces beschouwd worden als een horizontaal propstroom proces. Daarom kan het verbrandingsproces op het rooster vertaald worden naar een gepakt bed waar de lengtecoördinaat van het bewegende rooster overeenkomt met de tijd in het gepakt bed. Het gepakte bed kan gemodelleerd worden met een transiënt ééndimensionaal model. Meestal worden deze modellen gevalideerd met resultaten van experimenten in zogenaamde "pot ovens". Bij deze experimenten wordt afval of een andere vaste brandstof in een buis op een vast rooster gestort. Deze brandstoflaag wordt aan de bovenkant ontstoken en lucht wordt via het rooster van onder naar boven door de brandstoflaag gevoerd. Op verschillende hoogtes in de buis kunnen thermokoppels en gasmonsterpunten gebruikt worden om het proces te monitoren. Bij een homogene brandstof wordt op elke hoogte van de brandstoflaag, van boven naar beneden, een opeenvolgende scherpe toename van de temperatuur gemeten. Uit deze data kan een vrij constante snelheid van het ontstekingsfront afgeleid worden. Echter, het huidige werk laat zien dat de ééndimensionale modellen gebaseerd op een homogene brandstof de ontstekingsfrontsnelheid in een afvalverbrandingsoven met een factor twee onderschatten. Blijkbaar worden niet alle fenomenen die belangrijk zijn in afvalverbranding op een rooster beschreven met deze vereenvoudigde ééndimensionale modellen. Deze dissertatie beschrijft sommige van de ontstekingsverschijnselen die plaats vinden in afval- en biomassaverbranding op een rooster.

Vaste brandstoffen zoals biomassa en afval bevatten beiden gebonden koolstof en hebben een hoog vluchtig gehalte (meer dan 70 gewichts-%). De verbranding van de vluchtige componenten kan worden beschouwd als de verbranding van een gasvormige brandstof en de gebonden koolstofverbranding kan worden beschouwd als de verbranding van vaste (kool) deeltjes. Hoofdstuk 2 onderzoekt de invloed van de verbranding van gassen in een gepakt bed. Om de reacties in de vaste fase te elimineren, wordt de verbranding van aardgas in een inert gepakt bed beschouwd. Het

hoofdstuk beschouwt de situatie waar de verbranding in het gepakte bed plaatsvindt. Dit proces wordt filtratieverbranding genoemd en het wordt gekarakteriseerd door een thermische golf en een verbrandingsgolf. Een analytisch model uit de literatuur is gebruikt om de invloed van verschillende parameters zoals gassamenstelling, gassnelheid, porositeit van het bed en deeltjesgrootte van het bedmateriaal op de voortgang van het verbrandingsfront te onderzoeken. De resultaten zijn gevalideerd met experimentele resultaten. Voor deze experimenten is een met aluminakorrels gevulde buis gebruikt. Een voorgemengd brandbaar gasmengsel wordt door de buis met het gepakte alumina geleid en wordt in de onderste zone van de buis ontstoken. Op verschillende hoogtes monitoren thermokoppels het verbrandingsproces. De trends die gevonden zijn met het analytische model komen goed overeen met de trends die gevonden zijn met de experimenten. Het is aangetoond dat de verbrandingsgolf in deze situatie veel langzamer naar beneden beweegt dan de verbrandingsgolf in een brandend bed van vaste brandstof. Het is ook aangetoond dat het zeer onwaarschijnlijk is dat terugslag van vlammen plaatsvindt in afvalverbranding.

De ééndimensionale benadering die hiervoor genoemd is kan alleen toegepast worden als de horizontale massa- en energiegradiënten parallel aan het rooster verwaarloosd kunnen worden. In hoofdstuk 3 is het aan de hand van het Pécletnummer aangetoond dat de horizontale energiegradiënt niet altijd verwaarloosd kan worden. De voortgang van het ontstekingsfront is daarom opgedeeld in een horizontale en een verticale richting. De horizontale frontverplaatsing bepaalt de stabiliteit van de vlam en de verticale verplaatsing bepaalt de mate van uitbrand van de brandstof. Uit optische observaties van ontstekingsfronten en uit gemeten gassamenstelling onder het ontstekingsfront is geconcludeerd dat de vaste koolverbranding het drijvende mechanisme is voor de frontvoortgang in beide richtingen (voor lage warmtestralingsfluxen van de oven). Dit houdt in dat de verbranding van de vluchtige componenten in de gasfase verwaarloosd kan worden. Dit vereenvoudigt het modelleren van de voortgang van het ontstekingsfront aanzienlijk. Met dit resultaat is een ééndimensionaal analytisch model afgeleid voor de snelheid van het ontstekingsfront. De berekende frontsnelheid en temperatuur van het verbrandingsfront zijn een functie van een dimensieloze energieverliesterm en een energieoverschotterm. Een boven- en een ondergrens voor de frontsnelheid zijn afgeleid op basis van deze twee termen. Het model is gevalideerd met experimenten uit de literatuur die zijn gedaan door verschillende onderzoekers. Wanneer de warmtestraling van de oven laag is, kan het model toegepast worden op zowel de verticale als de horizontale voortgang van het ontstekingsfront.

Om de mogelijkheid om de brandstof te ontsteken met voorverwarmde primaire lucht te onderzoeken, zijn experimenten in een pot oven uitgevoerd. Bij deze experimenten is een voorverwarmde primaire luchtstroom door een ondiep gepakt bed van hout, RDF of vaste koolstof gevoerd. De kritische temperatuur van de lucht waar-

bij de ontsteking plaatsvindt en de temperatuur van het brandstofbed bij ontsteking zijn gemeten als functie van de primaire luchtstroom. Het is in hoofdstuk 4 aangetoond dat een gepakt bed van hout kan worden ontstoken door een luchtstroom met een temperatuur van slechts 230^oC. Een gepakt bed van vaste kool kan zelfs ontsteken bij een luchttemperatuur van 170^oC. De kritische temperatuur van de lucht en de temperatuur van het brandstofbed bij ontsteking nemen af bij lagere primaire luchtsnelheden. Een opvallende waarneming is dat bij een diep brandstofbed de ontsteking niet vlakbij het rooster, maar $20-35mm$ boven het rooster plaatsvindt. Dit kan worden verklaard door warmtegeleiding in het brandstofbed te beschouwen. In hoofdstuk 5 zijn de experimentele resultaten vertaald naar een model van spontane ontsteking. Het model is gebaseerd op Semenov's analyse van thermisch explosies en bestaat uit de balans tussen de exotherme pyrolysereacties en de convectieve warmteoverdracht van de voorverwarmde lucht naar de brandstof. Er is één dimensieloze parameter afgeleid die de kritische temperatuur van de lucht en de temperatuur van het brandstofbed bij ontsteking bepaalt als functie van de primaire luchtstroom, inertgehalte van de brandstof en het type brandstof. De resultaten van het model komen goed overeen met de experimentele resultaten voor hout en RDF. Met het gepresenteerde model kunnen de verschijnselen tijdens de experimenten met vaste koolstof alleen kwalitatief verklaard worden. Het lijkt aannemelijk dat de temperatuur waarbij de reactie van de vaste kool met lucht van endo- naar exotherm gaat, samenvalt met de spontane ontstekingstemperatuur.

Hoofdstuk 6 beschouwt het opstarten van een afvalverbrandingsinstallatie. Dit is gedaan door de ontsteking met hulp van een ontstekingsbron (bijvoorbeeld een vonk of een laserpuls) van verschillende materialen zoals hout, PVC en PMMA die aangestraald worden door een warmtestralingsbron te onderzoeken. Er is een model afgeleid dat de tijd die nodig is voor ontsteking voor verschillende materialen als functie van de stralingsflux berekent. Het model is gebaseerd op de ontstekingstemperatuur van het geproduceerde gasmengsel wanneer dat op zijn laagste explosiegrens is. Met de energiebalans op het moment van de vonk is te bepalen of het mengsel de ontstekingstemperatuur bereikt op een zeker tijdstip: de ontstekingstijd. Experimenten uit de literatuur zijn gebruikt om het model te valideren en de flitsen die zijn waargenomen in deze experimenten kunnen kwalitatief worden verklaard met het model. Vervolgens is het model doorontwikkeld voor ovens op ware grootte en is het aangetoond dat er een kritische primaire luchtstroom met betrekking tot de ontsteking bestaat. Als de luchtstroom groter is dan deze kritische waarde, zal het geproduceerde gasmengsel zijn laagste explosiegrens niet kunnen bereiken en zal er ook geen ontsteking plaatsvinden.

In hoofdstuk 7 zijn de resultaten van de huidige studie samengevat en gebruikt om de ontstekings- en verbrandingsverschijnselen in afvalverbrandingsovens van ware grootte te beschrijven. Er is een vereenvoudigde vergelijking afgeleid voor de snel-

heid van het ontstekingsfront in zowel de horizontale als de verticale richting. Deze vergelijking is gebruikt om met lokale eigenschappen van het brandstofbed lokale frontsnelheden te bepalen. Om de locatie te vinden waar het ontstekingsfront het rooster raakt, zijn deze lokale frontsnelheden geïntegreerd over de hoogte van het brandstofbed. Het is aangetoond dat dit tweedimensionale model van het ontstekingsfront een tot twee keer zo stijl front voorspelt als een ééndimensionaal model. In dit hoofdstuk zijn ook richtlijnen voor het opstarten van een afvalverbrandingsoven gegeven. Het advies is gegeven om te beginnen met een licht ontvlambare brandstof waarin ook een ontstekingsfront kan bestaan. Aanbevelingen voor verder onderzoek zijn onderverdeeld in (1) validatie van de vertalingen die gedaan zijn naar ovens van ware grootte en (2) toepassen van de resultaten op ovens van ware grootte.

Table of Contents

1

Introduction

What is this all about? That is the central question in this first chapter. It will give the reader an introduction on the context and goals of the research described in this thesis.

1.1 Introduction

Worldwide, more and more waste is produced. In Europe the amount of municipal waste produced, increases two percent every year with a total amount of 243 million tonnes in 2003 [53]. This means that on average each European inhabitant produces about 530 kilogram of municipal waste per year. The treatment of this waste differs largely from country to country as can be seen in figure 1.1. This has to do with the local composition of the waste, the available space for landfilling and national legislation on waste management.

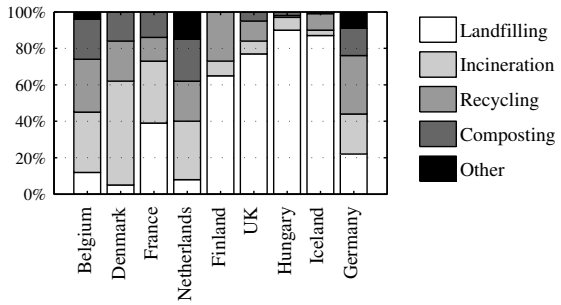

Figure 1.1: *The municipal waste treatment of several European countries for 2002. [53]*

Despite the long history in regulated waste treatment, which goes back to (and even before) the ancient Israelites, it lasted till the seventies of the previous century before waste treatment was regulated on a large scale. In 1979 the Dutch member of parliament Ad Lansink proposed a preferred order of treatment methods. This so called "Ladder van Lansink" (ladder of Lansink) consists of the following steps, in which prevention is the most favorable option:

1. prevention
2. re-use
3. recycling
4. incineration
5. landfill

Still, the Dutch waste policy is based on this ranking. Also in other European countries and on European scale similar rankings are used since the seventies and eighties. Unless this generally accepted ranking, a lot of waste is still landfilled as can be seen

in figure 1.1. However, the figure does not include the most preferable option of prevention which is hard to measure. In practice, not all waste can be prevented or is re-usable or recyclable. Moreover, for some waste components the environmental impact of incineration in modern incineration plants is less than the one for re-use or recycling. This shows the need for clean and effective incineration plants as a suitable and environmentally friendly alternative for re-use and recycling.

1.2 Waste incineration plants

The first waste incineration plant was erected in 1874 in Nottingham (UK) [10]. Before this time, waste was burned, but not systematically in a plant designed for this. From this moment, many of these waste incinerators are built in the UK and around the year 1900, 210 plants were built [72]. A drawing of such a waste incinerator can be seen in figure 1.2.

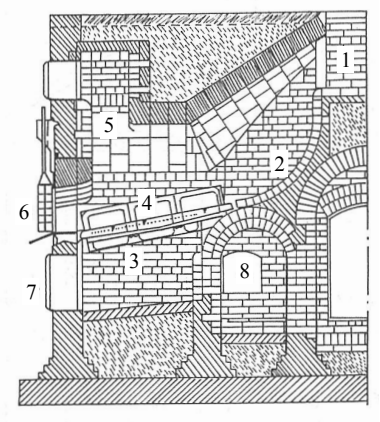

Figure 1.2: *An old waste incineration plant. 1-Waste feed channel; 2-Pre-drying zone; 3-Fixed grate; 4-Cooled cast iron walls; 5-Flue gas pass; 6-Ash and stoking opening; 7-Ash chute; 8-Combustion air opening. [72]*

The inclined grate technology used in these first waste incineration plants is still used nowadays in the most advanced plants. While the grates used before were fixed, almost all grates used nowadays are moving. Figure 1.3 shows a modern municpal solid waste incineration plant. The figure shows that the furnace is only a small part of the entire plant. The largest part is the flue gas cleaning system. The policy of the Afval Energie Bedrijf nicely shows the changing trends in waste management. They treat

the waste as a raw material to produce energy and useful materials. The materials resulting from the combustion and flue gas cleaning are used useful as much as possible. They state that from 1000 kg of waste only 5 kg can not be utilized and should be landfilled [3].

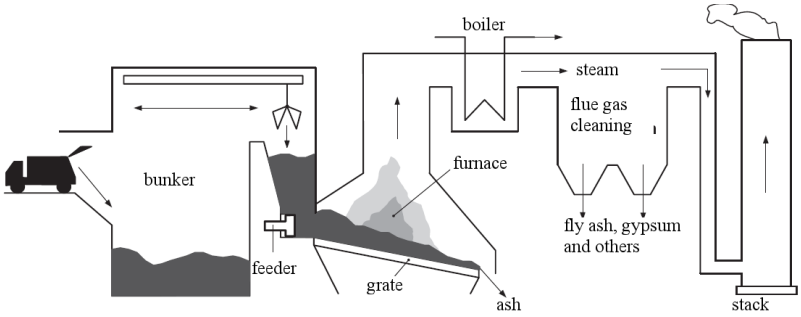

Figure 1.3: *A modern waste incineration plant in Amsterdam. Adopted from [90]*

When we focus on the furnace two main differences can be distinguished between several plants. First, several types of grates can be applied and second, different furnace geometries are in use. Most of the applied grates consist of rows of bars which move either against the waste flow (reverse acting grate) or along the waste flow (forward acting grate). Typically a forward acting grate is used when the grate is horizontal and a reverse acting grate is used with an inclined grate. The movement of the grate bars transports the waste through the furnace and results in good mixing of the burning waste. The air needed for the combustion is either fed through openings between the grate bars or through openings in the grate bars themselves. Also some plants are equipped with a roller grate. This type of grate consists of about six large slowly rotating rolls over which the waste is transported and mixed. In this case, the combustion air is fed through openings between the rolls. Figure 1.4 shows the three types of grates. A picture of a newly installed horizontal grate can be seen in figure

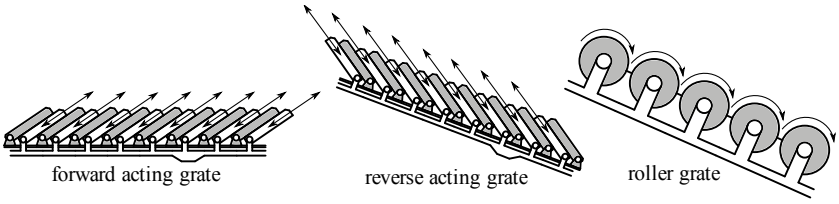

Figure 1.4: *The three mainly used grates in waste incineration plants.*

Figure 1.5: *A picture of a new horizontal forward acting grate. The waste enters at the back of the picture and travels towards the viewer. The boiler tubes at the furnace walls can be seen as well. Source: Martin GmbH für Umwelt- und Energietechnik*

1.5. This picture also shows the vertical boiler tubes at the furnace walls.

Also three main types of furnace geometries can be distinguished. They differ in the flue gas flow direction relative to the waste flow direction. The first type is called co-flow or parallel flow. In this furnace the flue gases flow in the same direction as the waste. In this furnace, the burnout of the flue gases is good because they pass the hot combustion zone. The second type is called counter-flow. In this case the flue gases flow upstream the waste and they help to dry and ignite the fresh fuel. Gas burnout can be a problem in this type of furnace. The final type is the cross- flow or center-flow furnace. In this furnace the flue gases flow normal to the waste direction. This type is in between the co- and the counter-flow type. The three types can be seen in figure 1.6.

The air needed for the combustion is fed through the grate, this air flow is called primary air. To enhance the burnout of the flue gases more air is fed into the furnace above the fuel bed. This air stream is called secondary air. Next to the waste feed rate and grate movement, these air flows are important values to control the combustion process.

1.3 Developments in waste combustion

Due to an increasing awareness of the health and environmental impact of the waste incineration more stringent regulations followed rapidly after each other both on European and on national level. An overview of Dutch, German and Swiss emission di-

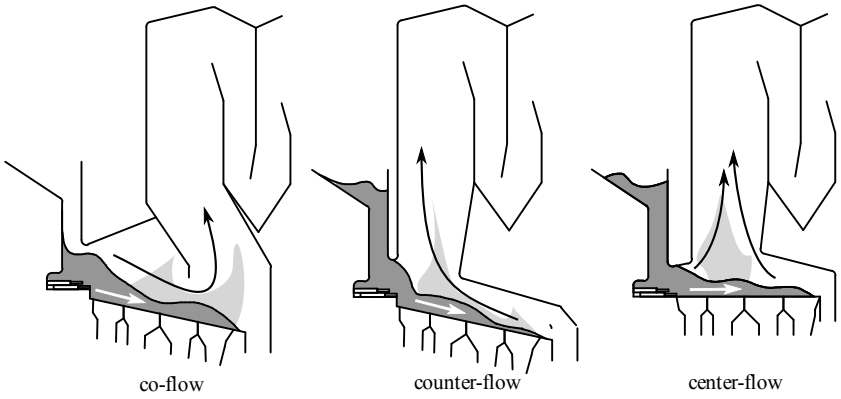

Figure 1.6: *The three mainly used furnace types in waste incineration plants.*

rectives together with the European directive are listed in table 1.1. The increasingly

Table 1.1: *Overview of emission legislation in Germany (TAL 74: Technische Anleitung Luft; 17 BImSchV: Bundes-Immissionsschutzgesetz), The Netherlands (RV 85: Richtlijn Verbranden; BLA: Besluit Luchtemissies Afvalverbranding) and European Union.*

Component	TAL 74 (1974, German) [42]	17 BImSchV (1990, German)	RV 85 (1985, Dutch) [42]	BLA (1993, Dutch)	Directive 2000/76/EC (2000, EU)
Total dust (mg/m^3)	100	10	50	5	10
HCl (mg/m^3)	100	10	50	10	10
SO_2 (mg/m^3)	-	50	-	40	50
HF (mg/m^3)	5	1	3	1	1
NO_x (mg/m^3)	-	200	-	70	200
C_xH_y (mg/m^3)	-	10	-	10	10
CO (mg/m^3)	1000	50	-	50	100
Cd (mg/m^3)	10	0.05	0.1	0.05	0.1
Hg (mg/m^3)	10	0.03	0.1	0.05	0.05
Sum other heavy metals (mg/m^3)	125	0.5	5	0.5	0.5
PCDD/F ($ng\ TE/m^3$)	-	0.1	-	0.1	0.1

stringent legislation transformed the waste combustion plants to chemical plants and half of the installation costs are needed for the flue gas cleaning equipment. The re-

sult is that modern waste incineration plants are generally cleaner than fossil fuel fired power plants.

To see the share of the hazardous emissions of waste incineration, table 1.2 compares the emissions from waste incineration to some other sources of emissions. In general, the emissions from waste incineration are only a fraction of the total emissions. Despite the low share of waste incineration on air pollution the public opinion is still that waste incinerators are dirty and especially dust (PM10), dioxins and heavy metals are thought to be the main pollutants resulting from waste incineration. Indeed, up to fifteen years ago waste incineration was strongly contributing to dust and heavy metal emissions and is was even the main emitter of dioxins. However, due to the legislation and technological development, the emissions of waste incinerators decreased drastically. It seems that the public resistance against waste incinerators can not keep up with the fast technological development. But even when the emissions can be reduced even further, prevention of waste should always be favorable.

Table 1.2: *Emissions from waste incineration and some other sources in 2005. [66, 1, 2]*

	PCDD/F (mg)	PM10 (kton)	Cu (ton)	Hg (kg)	NO_x (kton)	SO_2 (kton)
Waste Incineration	0.70	0.029	0.088	159	2.1	0.18
Energy sector	-	0.5	0.16	N/A	46	9.9
Traffic	1.34	20	69	34	332	70
Consumers	21.7	3.3	10	23	15	0.51
Fireworks	-	0.15	74	N/A	0.021 (N_2O)	N/A
Total	36.1	45	N/A	>600	481	129

Also methods are developed and already in use to utilize the fly ash, bottom ash and other residues from the incineration process. This results in a (almost) zero-waste process in which only a small amount of the residue has to be landfilled. In this approach the waste is not only a fuel, but also a raw material. A pitfall of treating waste like this is that it can hinder the prevention of waste.

Next to the trends in strongly reducing the emissions another trend that can be seen is that waste incineration plants are more and more regarded as power plants instead of waste treatment plants. Because about half of the combusted waste is biomass, also half of the produced energy is CO_2 neutral. Currently a lot of discussion on political level is going on about the question whether energy from waste combustion is renewable or not. Also with the treating waste as a fuel, renewable or not, it can hinder the prevention of waste. When this is kept in mind, the combustion of waste is a suitable treatment method for waste.

1.4 Ignition of the waste layer

The ignition of the waste layer is not only important at the startup of the plant, but also during continuous operation. The stability of the combustion process and the burnout of the waste are defined by the ignition behaviour of the waste layer. Rogers proposed a model for the several reaction zones in a burning fuel layer [74], this model can be seen in figure 1.7. Rogers states that straight reaction and ignition fronts are present in the burning fuel layer. His findings are based on one dimensional pot furnace experiments which he translates to two dimensional fuel beds.

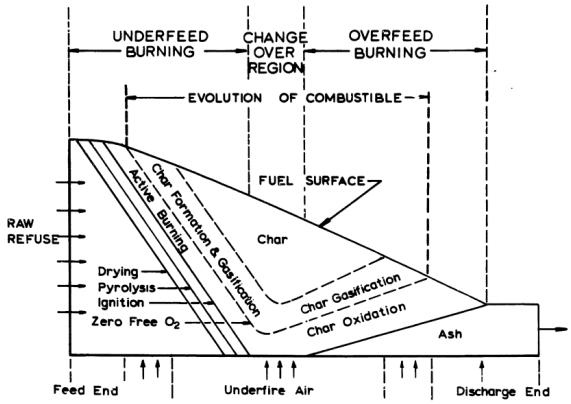

Figure 1.7: *The reaction zones in a burning fuel layer as proposed by Rogers [74].*

The pot furnace is a vertical tube with a porous grate at the bottom. This grate supports the fuel bed and air is fed through this grate. For an experiment, the tube is filled with a solid fuel and ignited at the top. During the experiment, the fuel bed burns slowly from the top to the bottom of the tube. Thermocouples at several heights in the fuel bed monitor the ignition and combustion processes. The generally accepted idea is that the results from the pot furnace can be translated to a two dimensional fuel bed by correlating the time in the pot furnace to the location in the two dimensional fuel bed by the vertical velocity of the fuel bed.

The one dimensional approach and the pot furnace are used more often by several researchers [39, 46, 76, 31, 88, 100, 75] to determine the ignition speed in a packed fuel bed as a function of process and fuel parameters. Also two dimensional experiments are carried out in full scale [84] and pilot plants [34] to obtain insight in the ignition and combustion processes. In the experiments a sharp ignition front which travels downwards is found. Generally, the velocity of the ignition front is found to be in the

order of 0.5 mm/s. This velocity depends mainly on moisture content and primary air velocity. For high values of the moisture content or air velocity the ignition front is extinguished. This ignition front can be measured in well defined fuel beds such as packed wood pellets or other fairly homogeneous (on bed scale) fuels. However, when inert is added or when different materials or fuel sizes are mixed, the ignition front propagation can not be observed that clear. As an illustration figure 1.8 displays the results from two pot furnace experiments presented by Ortmanns and Brem [64]. The temperature readings show that for wood a sharp and well defined ignition front travels downwards. For simulated waste however, a clear ignition front can not be distinguished.

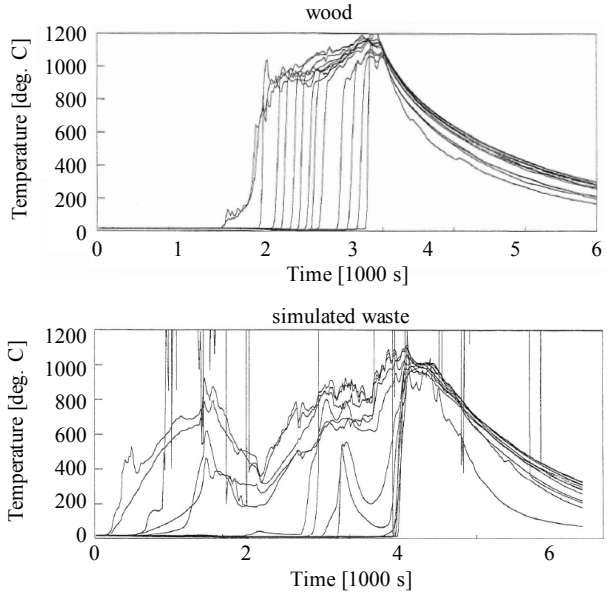

Figure 1.8: *Temperatures at several heights in the fuel bed as a function of time [64].*

As a result, when the derived models based on a sharp ignition front are applied on waste combustion, the ignition front is predicted to reach the grate about halfway the furnace. In practice, high temperature corrosion can be observed at the grate at already one quarter of the length of the furnace.

1.5 Scope of the thesis

The derived models for the ignition front propagation based on a sharp and constant moving ignition front are not able to describe the overall ignition processes in waste combustion. However, these models can be successfully applied on biomass combustion of a grate. Besides, the models give information on the physics encountered in the ignition inside a packed fuel bed. For waste combustion there is still the need for a model which can predict the ignition inside the highly inhomogeneous waste bed. To develop such a model, first the physics behind the ignition should be discovered.

The combustion and ignition of a solid fuel such as waste can be divided in a gaseous part and a solid part. Chapter 2 investigates the impact of gaseous combustion in a packed bed. To eliminate the reactions in the solid phase, natural gas combustion in an inert solid phase is considered. An analytical model from the literature is used to investigate the influence of different parameters such as gas composition, gas velocity, bed porosity and particle diameter on the propagation of the flame. The results are validated by experimental results. It is also shown that flashback is very unlikely to occur in waste combustion and other phenomena seem to be important to the ignition of waste on a grate.

Chapter 3 investigates the influence of two dimensional effects in the waste layer on the ignition of this layer. The one dimensional approach mentioned before can only be applied if the horizontal mass and energy gradients along the grate can be neglected. With the help of the Péclet number, it is shown in chapter 3 that the horizontal energy gradients can not always be neglected. As a result the ignition front propagation through a packed bed is divided in a horizontal direction and a vertical direction. An analytical one dimensional model for the velocity of the ignition front is derived. The model is validated with experiments from the literature done by several researchers. The model can be applied to both horizontal and vertical directions when furnace radiation is low.

In chapter 4 the possibility to ignite the fuel by preheated air is investigated. Therefore, experiments are carried out in a pot furnace. In these experiments, a preheated primary air flow is fed into a shallow packed bed of either wood, RDF or char. The critical air temperature needed to ignite the bed and the corresponding bed temperature at the moment of ignition are recorded as a function of the primary air flow. The obtained experimental results are translated into a spontaneous ignition model in chapter 5. The model is based on Semenov's analysis of thermal explosions and consists of the balance between the exothermic pyrolysis reactions and the convective heat transfer of the preheated primary air to the fuel. The results from the model agree well with the results from the experiments for wood and RDF. With the pre-

sented theory, the ignition phenomena occurring during char experiments can only be qualitatively explained.

Chapter 6 deals with the startup of a waste incinerator. This is done by investigating the piloted ignition of several solid fuels such as wood, PVC and PMMA under a radiative heat flux. A model is developed to predict the ignition times for several materials and radiative heat fluxes. The model is based on the ignition temperature of the produced gas mixture at its lower explosion limit. Experiments from the literature are used to validate the model and flashes observed during these experiments can qualitatively be explained by the model. Subsequently, the model is further developed to a full-scale furnace.

In chapter 7 the results from the present study are summarized and used to describe the ignition and combustion phenomena in full-scale waste incinerators. A simplified expression for the ignition front velocity in both the horizontal and vertical direction is presented and applied to determine local front velocities based on local fuel properties. The local front velocities are integrated over the bed height to obtain the location where the front reaches the grate. It is shown that this two-dimensional ignition front model predicts the ignition front to be up to twice as steep as predicted by a one-dimensional model. In this chapter also guidelines for startup of moving bed furnaces are given. It is advised to start with a fuel which ignites easily under a pilot and is able to maintain an ignition front.

2

Gas phase

In this chapter, measurements and a mathematical model on a burning gas inside a packed bed are presented. To focus on the reactions in the gas phase, an inert packed bed is used. It is shown that a combustion wave travels through the packed bed and in some cases, this wave travels against the direction of the gas stream. It is also shown that flashback is very unlikely to occur in municipal solid waste incineration on a grate.

2.1 Introduction

Experiments with a homogeneous fuel in a packed bed show a clearly the reaction front. Experiments done with a less homogeneous fuel such as MSW show no clear reaction front and the bed burns at different places [64]. There are some explanations why waste ignites faster than predicted by models based on a homogeneous material. Channeling inside the packed bed can be one of the reasons why the waste is igniting faster (see for example the work of Yang et al. [97]). Due to easy igniting pieces of waste a channel can be created when this piece is burned. In this channel the air resistance is lower so even more oxygen is available and combustion inside the channel is enhanced, increasing the channel even further (see figure 2.1). Another explanation for the faster ignition rate is that highly flammable materials are inside the packed bed which already release volatiles by the heat of the preheated primary air or heat from the combustion zone. Under certain conditions these gases will be able to flashback if they reach the reaction front.

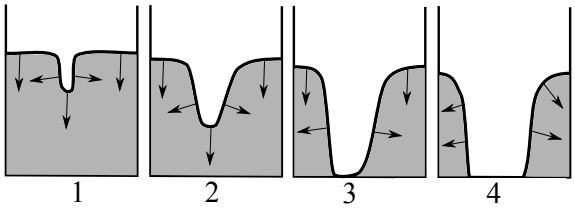

Figure 2.1: *Growth of a channel. [99]*

The behaviour of the volatile phase in waste combustion is the subject of this chapter. In practice, this phenomenon is a complex combination of (among others) pyrolysis, gas combustion and heat and mass transfer between the solid and the gas phase. To reduce this complexity the solid phase is regarded inert and the combustible gases are fed through this inert packed bed. In this case the solid pyrolysis (which is the source of the combustible gases) is not limiting the process. A model is presented to predict the combustion process of the gas inside the packed bed. The variation in flame temperature, solid temperature and flame velocity are investigated as a function gas mass flux, bed porosity and bed particle diameter. Experiments are carried out to validate the model. With the gained knowledge, the possibility of flashback in municipal waste combustion as described earlier in this section is investigated. But first, in the next section, a literature review will be given on gas phase combustion in an inert packed bed.

This chapter is an excerpt of the Msc. thesis written by Damink [28] which was carried out within the framework of the present study. For more details, experimental results

and an analytical model, the reader is referred to his work.

2.2 Literature review

2.2.1 Flashback of flames in porous media

In his dissertation Lammers [55] investigates the flashback of flames in porous burners. When the burning velocity of a free flame present above the burner is higher than the unburnt gas velocity the flame will move to the burner. When it reaches the burner the flame is cooled by the surface reducing its flame velocity resulting in a stabilized flame. Thus a flame on the ceramic foam burner is cooled by the ceramic material and so less NO_x is produced making ceramic burners very interesting for industrial applications.

Lammers showed that the stabilization of the flame is impossible for a range of unburnt gas velocities if the temperature of the environment (and the burner) becomes too large and so heat accumulates in the ceramic foam. Inside the foam the flame speed is increased significantly due to the increasing upstream effective heat conduction. It has to be mentioned that turbulence is not taken into account in his model for the upstream combustion wave. This may result in under-predicted flame velocities. An industrial burner with ceramic foam will loose its heat to the environment by radiation. When the flame can not get rid of its surplus of energy flashback will occur. This flashback is defined as an unstable transition from surface combustion to internal combustion. The most important factors for flashback are the temperature of the environment, emissivity, porosity, heat transfer coefficient and the conductivity of the material.

For his model some assumptions were made. First the temperature dependency of the solid conductivity is expected not to be relevant because the radiative transport of heat will be much larger than the conductivity. The dependency on the heat transfer coefficient to the gas velocity was found to be relevant but not taken into account due to the relative large uncertainty in the properties of the material used. So a fixed heat transfer coefficient is used in the model and no Nusselt relations are used. For the gas phase the skeletal mechanism of Smooke is used with constant Lewis numbers and simple expressions for the other transport and thermodynamic properties. Some conclusions from the dissertation:

- The risk at flashback is the highest at an equivalence ratio of unity;
- The criterion for flashback is highly sensitive to the heat transfer coefficient between the gas and the porous burner.

Besides focusing at the instant of flashback, one can also look at the processes occurring after the flame has entered the porous medium. This is done in the next section.

2.2.2 Filtration combustion

Filtration combustion is defined by Babkin et al. [7] as the propagation of a gaseous exothermic reaction in an inert porous medium.

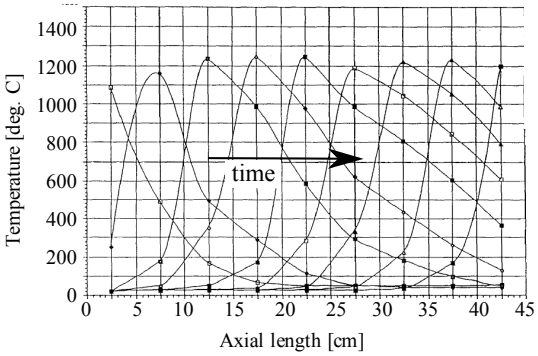

Figure 2.2: *Profiles of a moving combustion wave in a tube filled with an inert packed bed. The gas enters the tube at $x = 0$ and is ignited here. The figure shows that the combustion wave travels along the gas stream. [103]*

During filtration combustion experiments a combustible mixture is supplied to one end of a tube containing an inert granular material. The mixture is either ignited at the inlet or at the exit. With thermocouples at several locations along the tube the temperature inside the packed bed is measured. While the ignited end heats up a plane combustion wave appears. A typical result can be seen in figure 2.2. The figure shows the thermocouple readings at several positions along the tube at several instances. It can be seen that in this case, every $10cm$ a thermocouple is placed. From this figure a combustion wave velocity can be derived by dividing the distance between two thermocouples by the difference in time for them to reach their maximum temperatures. The measured velocities are constant over the entire length of the reaction tube, except for an initial section of a few millimeters long. It depends on the initial parameters if the combustion waves propagate either with or against the flow or become standing waves. The thermo-physical and structural characteristics of the porous medium, the reactivity of the combustible gas (rate and energy release of reaction) and the flow velocity are all important parameters determining the velocity of the filtration combustion wave. The pressure wave does not have a big effect on the combustion characteristics and can be neglected, but thermal and concentration

waves are of greatest interest. The process is characterized by a thermal wave velocity and a combustion wave velocity. The thermal wave can be made visible by initially preheating a narrow zone and filtering a gas without feeding fuel to the bed. Figure 2.3 shows a decaying thermal wave.

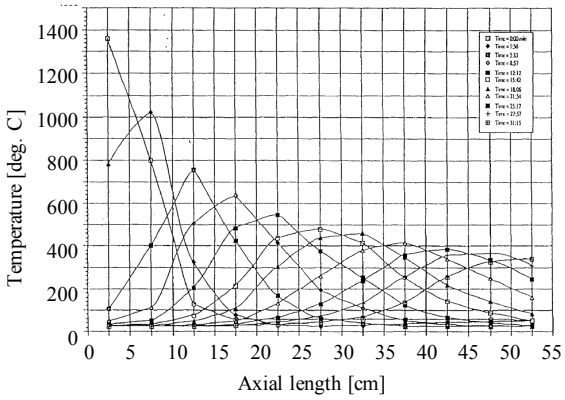

Figure 2.3: *Propagation of a thermal wave without fuel supply. A narrow zone of the packed bed at $x = 0$ is preheated and a gas without fuel is filtered through the bed [103]*

When the thermal wave and combustion wave overlap, the heat of reaction becomes localized in a moving thermal wave. Figure 2.4 shows that in the first $0.2m$ the gas is heated by the solid. This solid was already heated by the thermal wave initiated by the flame in a previous time step. When the gas ignites it releases heat to the solid. In this wave the temperature can be 2.8 times higher than the normal adiabatic flame temperature of the mixture.

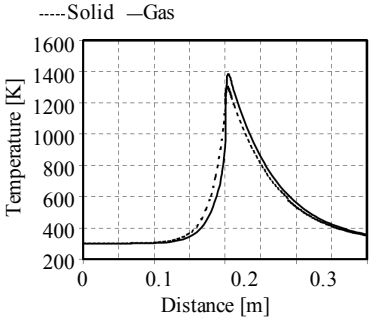

Figure 2.4: *The solid and gas temperature profile of a combustion wave. [23]*

Several regimes of combustion are distinguished in the literature, see for example the work of Babkin et al. [6]. The regimes are determined by the combustion front velocity. An overview of the regimes is given in table 2.1.

Table 2.1: *Overview of the several regimes in filtration combustion. [6]*

Regime	Wave velocity [m/s]	Mechanism
Low velocities (LVR)	$0 - 10^{-4}$	Solid heat conductivity, intensive interphase heat exchange
High velocities (HVR)	0.1 – 10	Convective gas movement under uniform pressure
Sound velocities (SVR)	100 – 300	Convective gas movement due to gradient pressure in the combustion wave
Low velocities detonation (LVD)	500 – 1000	Self-ignition under shock wave interaction with carcass elements
Normal detonation (ND)	1500 – 2000	Detonation under heat and pulse loss

The low velocity and the high velocity regimes are of interest in municipal waste combustion. The other three regimes can be described as flashback. This phenomenon will be dealt with later in this chapter.

Low velocity regime

Filtration combustion will occur in the low velocity regime if the particle diameters are sufficiently small or the filtration velocity of the gas is sufficiently high or if the mixture is outside the normal flammability limits (ultra lean or ultra rich). The low velocity regime can be characterized by the intensive heat exchange between the gas and the solid. In other words, the flame is attached to the solid phase as can be seen in figure 2.4. In this regime filtration combustion can be superadiabatic when heat is circulated from the hot-products to the cold incoming reactants by the solid phase. The reactive gases are preheated before they react so they can reach a flame temperature higher than the adiabatic flame temperature. Only when the combustion wave is co-current with the filtration flow the gas gains more energy from the solid than it looses to it. According to Zhdanok [103] this is the case for low (<0.5) and very high (>1.6) fuel equivalence ratios. For intermediate equivalence ratios the combustion wave can propagate counter-current to the gas flow. In this case subadiabatic combustion takes place because the reactants loose heat to the relative cold solid phase. The heat

circulation by the solid has a positive effect on the flame stability and flammability and even very low exothermic mixtures can be burnt efficiently.

High velocity regime

For sufficiently large particle diameters, low filtration velocities of the gas and mixtures within the normal flammability limits a transition between the low and high velocity regime occurs. During this abrupt transition the flame velocity increases by 3 to 4 orders of magnitude. In the reaction zone the thermal connection with the solid phase is broken and the flame is comparable with a homogeneous flame because the propagation is realized by the thermal conductivity of the gas instead of the solid. These gas conductivity and diffusion terms are usually ignored in models for the low velocity regime. In the high velocity regime also turbulence becomes important for the total process. The characteristics of the HVR are an incomplete burn-up of the fresh mixture and the turbulent non-uniform flame front. Experiments are not done in open tubes but in closed vessels. An investigation of the the transition from the low to the high velocity regime is given by Dobrego et al. [29].

In municipal waste combustion, combustible gases can be created under the solid ignition front either by preheated primary air or by heat from the reaction front. Gas composition measurements for both cases (see chapters 3 and 4) show that the concentration of the volatiles are well below the lower flammability limit for both cases. Because only in the low velocity regime the gases are able to ignite outside the normal flammability limits, this regime is the only relevant regime in municipal waste combustion. Therefore, in this study modeling and experimental work have been carried out in the low velocity regime.

2.3 Modeling

In modeling filtration combustion some assumptions and estimates have been made. The following assumptions are often used [23, 36, 102, 7, 103]:

- The packed bed is modeled as a continuum.
- The flow speed is sufficiently low so that the pressure is assumed to be constant. Achenbach [4] calculated a maximum pressure drop of $1600Pa$ showing that this assumption is reasonable.
- The porosity of a packed bed filled with spheres is estimated to be 0.4. The porosity depends on the packing of the bed and the shape of the particles.

- In all analytical models the combustion wave is assumed to move at a constant speed. In experiments it was seen that except for the starting region this is valid.
- Almost all researchers assume the bed to have an uniform porosity and they assume that there are no temperature gradients inside the particles ($Bi << 1$). Using bigger particles in experiments results in larger discrepancies with modeling results.
- The temperature is equals the ambient temperature on either side of the combustion wave. This is valid when the reactor is long enough.
- The solid thermal conductivity is considered to be large relative to that of the gas mixture.
- In models for the low velocity regime the diffusion and thermal conductivity of the gas are neglected. This assumption is not valid for the high velocity regime.
- The energy exchange between the gas and the solid is assumed to be proportional to the local temperature difference.
- The porous media is considered inert and does not participate in the reaction.
- In analytical models often a first order Arrhenius rate expression is used to describe the methane combustion. Most numerical models use the GRI database.
- No radial effects are considered. This is valid when Pe

Some discussions exist on the following assumption: the reaction front is assumed to be small relative to the width of the preheated zone. In most analytical models the gas temperature is considered to jump from T(0-) to T(0+) at the point where the temperature of the solid is equal to the ignition temperature. The reaction term is replaced by an energy release delta function dividing the system into a pre-reaction and post-reaction zone. Bubnovich et al. [23] question the assumption of the reaction front to be infinitely small. They derived an equation for this reaction front thickness which describes the front of several millimeters seen during experiments well.

2.3.1 Modeling equations

The system which describes the energy and mass conservation is [23] (see also figure 2.5):

$$
\begin{cases}
\dfrac{\partial(\rho_g Q)}{\partial x} = 0 \\[2ex]
\rho_g \dfrac{\partial Y_i}{\partial t} = -\frac{\rho_g Q}{\epsilon} \dfrac{\partial Y_i}{\partial x} + K_i \\[2ex]
\rho_g c_{p,g} \dfrac{\partial T_g}{\partial t} = \dfrac{\partial}{\partial x}\left(k_g \dfrac{\partial T_g}{\partial x}\right) - \frac{\rho_g Q c_{p,g}}{\epsilon} \dfrac{\partial T_g}{\partial x} \\
\qquad - \frac{1}{\epsilon} h A_s (T_g - T_s) - h_{wall}(T_g - T_0) - \Delta H_{CH_4} K_{CH_4} \\[2ex]
\rho_s c_{p,s} \dfrac{\partial T_s}{\partial t} = k_{eff} \dfrac{\partial^2 T_s}{\partial x^2} + \frac{1}{1-\epsilon} h A_s (T_g - T_s) - h_{wall}(T_s - T_0)
\end{cases}
\tag{2.1}
$$

In this system, ρ_g is the gas density, Q is the superficial filtration velocity, Y is the species mass fraction, ϵ is the porosity of the packed bed, c_p is the specific heat, T is the temperature, k is the thermal conductivity, h is the heat transfer coefficient, ΔH is the heat of reaction and K is the reaction rate. The subscript $_g$ denotes the gas phase and $_s$ denotes the solid phase. The first two equations are the mass conservation equations. The third equation is the energy conservation equation for the gas phase and the last equation is the energy equation of the solid phase (the packed bed).

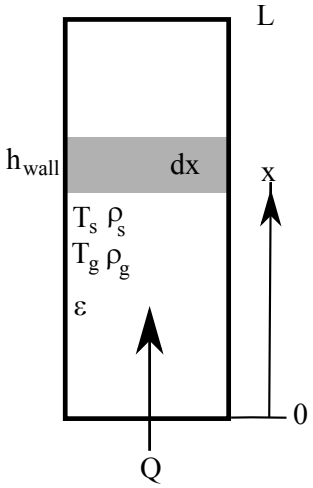

Figure 2.5: *Scheme of the system*

The diffusion of the gas species is small compared to the convection, so the diffusion is neglected. The boundary and initial conditions are:

$$\begin{aligned} &T_g = T_{g,0}; \quad \frac{\partial T_s}{\partial x} = 0; \quad Y_i = Y_{i,0} \quad \text{at} \quad x = 0 \\ &\frac{\partial T_g}{\partial x} = 0; \quad \frac{\partial T_s}{\partial x} = 0; \quad \frac{\partial Y_i}{\partial x} = 0 \quad \text{at} \quad x = L \\ &T_g = T_s = 293 + 1100 e^{-\left(\frac{x-0.5}{0.05}\right)^2}; \quad Y_i = Y_{i,0} \quad \text{at} \quad t = 0 \end{aligned} \tag{2.2}$$

The initial condition for the two temperatures is a sharp peak with a maximum at x=0.5m. These temperature peaks simulate ignition. When the simulated time is long, the influence of the height of the initial peaks can be neglected. This assumption holds in this case, because the times in the simulation are in the order of an hour.

Reaction kinetics

The overall reaction of ultra lean methane combustion will be approximated by a single step Arrhenius equation:

$$K_{CH_4} = k e^{-E/RT} \rho_g Y_{CH_4} \tag{2.3}$$

For the ultra lean ($0.1 \leq \phi \leq 0.47$) mixtures Futko [36] obtained the kinetic coefficients based on numerical calculations with the GRI mechanism:

$$\begin{aligned} E &\simeq 130 kJ/mol \\ k &\simeq 2.0 \cdot 10^8 s^{-1} \end{aligned} \tag{2.4}$$

Variable parameters

The average superficial gas velocity by:

$$Q = \frac{\dot{m}''_g}{\rho_g} \quad \text{with:} \quad \rho_g = \frac{p}{MRT_g} \tag{2.5}$$

The specific heat of air (of which the mixture mainly consists) is calculated by [23]:

$$c_{p,g} = 947 e^{183 \cdot 10^{-6} T_g} \tag{2.6}$$

The specific heat of the solid, in this case alumina is calculated by using [23]:

$$c_{p,s} = 29.6 + 2.61 T_s - 1.7110^{-3} T_s^2 + 3.3810^{-7} T_s^3 \tag{2.7}$$

The Nusselt relation introduced by Wakao et al. [92] is used for the heat transfer coefficient.

$$h = \frac{k_g}{d_p}\left(2 + 1.1 Re^{0.6} Pr^{1/3}\right) \quad \text{with:} \quad Re = \frac{Q d_p}{\nu_g} \tag{2.8}$$

The thermal conductivity of the gas is calculated with [24]:

$$k_g = 4.82 \cdot 10^{-7} c_{p,g} T_g^{0.7} \tag{2.9}$$

The volumetric wall heat losses depend on the reactor type used. In the combustion wave velocity experiments the tube is hot and energy is only lost by natural convection at the outside of the reactor. Based on an energy balance for a cylindrical control volume of diameter $d_{tube,i}$, the volumetric heat transfer coefficient for the heat transfer from the bed to the wall can be derived:

$$h_{wall,v} = h_{wall} \frac{4}{d_r} \tag{2.10}$$

in which h_{wall} is the heat transfer coefficient and $h_{wall,v}$ the volumetric heat transfer coefficient from the solid bed to the surrounding environment. For a detailed estimate of the heat transfer coefficient for the experiments the reader is referred to the work of Damink [28]. He estimates a volumetric heat transfer coefficient of $444 W/m^3 K$.

The total effective solid thermal conductivity is expressed as:

$$k_{eff} = k_s + k_r \tag{2.11}$$

The total effective solid thermal conductivity consists of a combination of the thermal conductivity (k_s) and a radiation term (k_r). It is difficult to calculate the effective thermal conductivity because the packing force and the packing arrangement needs to be known because the thermal conductivity is very sensitive to these parameters. Henneke [43] assumes the thermal conductivity of the packed bed to be 1% of the thermal conductivity of pure alumina. Pure alumina has a conductivity of about $18 W/mK$ so this results in a conductivty of $0.18 W/mK$ for the packed bed. Bubnovich [24] uses for the same sized alumina spheres a thermal conductivity of $1.32 W/mK$ and in another paper [23] the following polynomial is used:

$$k_{al} = -0.22 + 1.7 \cdot 10^{-3} T_s + 8.22 \cdot 10^{-8} T_s^2 \tag{2.12}$$

This results in a conductivity range from about 0.6 to $1.8 W/mK$ for the temperature range of the experiments. This polynomial is used in the model.

Experiments showed that the steel reactor tube became very hot. Because of the high conductivity of stainless steel of about $25 W/mK$ at high temperatures the hot zone is enlarged. Due to this high conductivity heat is moved upstream easier so the downstream velocity of the combustion wave decreases. To take the extra thermal conductivity of the tube into account this conductivity is averaged over the surface. The thermal conductivity of the stainless steel reactor is given by: $k_{tube} = 0.013T_s + 11$ [15]. The effective solid thermal conductivity including the conductivity of the reactor wall is given by:

$$\begin{aligned} k_s &= \frac{(1-\epsilon)k_{al}A_{bed} + k_{tube}A_{tube}}{A_{bed} + A_{tube}} \\ \text{with:} \quad A_{bed} &= \frac{\pi}{4}d_{tube,i}^2 \quad \text{and} \quad A_{tube} = \frac{\pi}{4}\left(d_{tube,o}^2 - d_{tube,i}^2\right) \end{aligned} \tag{2.13}$$

The outer diameter of the tube $d_{tube,o}$ is $0.051m$.

The radiation part is calculated by [25]:

$$k_r = 4Fd_p\sigma T_s^3 \tag{2.14}$$

In this relation, σ is the Stefan-Boltzmann constant and F is the radiation exchange factor to be about 0.5 for a packed bed with a porosity of 0.4 and an emissivity of 0.45 for the alumina spheres. For high temperatures the radiation is dominating the heat transfer inside the bed so $k_r >> k_s$ for high temperatures.

Fixed parameters

The used fixed parameters and reaction kinetics for the model are summarized in table 2.2.

Table 2.2: *The parameters used in the model.*

variable	value	ref.	variable	value	ref.
A_s	$\pi/d_p = 698m^{-1}$	[43]	p	$101\ kPa$	
D	$45mm$		Pr	0.7	[14]
d_p	$4.5mm$		ρ_s	$3690\ kg/m^3$	
E	$130kJ/mol$	[36]	σ	$5.669 \cdot 10^{-8}\ W/m^2K^4$	[14]
F	0.5	[25]	ϵ	0.4	[4]
k	$2.0 \cdot 10^8 s^{-1}$	[36]	$d_{tube,i}$	$45mm$	
$d_{tube,o}$	$51mm$				

2.3.2 Solution method

To solve the set of equations (2.1) the multi-physics partial differential equation solver *FlexPDE* is used which is based on finite elements. Each run at a specified equivalence ratio and mass flux results in a number of temperature profiles at different time steps. The peak solid temperature and the combustion wave velocity can be extracted from the data. Due to some instabilities in the solution for the peak gas temperature, the combustion wave velocity is derived from the locations where the gas temperature is $800K$. This can be done as figure 2.6 shows that the temperature profile before combustion zone (left part of the wave) does not change. In the zoomed plot it is clearly visible that first the gas is heated by the solid (the preheat region) followed by a region were the solid is heated by the gas to the point the peak temperature is reached (the reaction region). In figure 2.7 the mass fraction of CH_4 in the combustion wave is plotted. As can be seen the reaction front in this case is about $30mm$ wide.

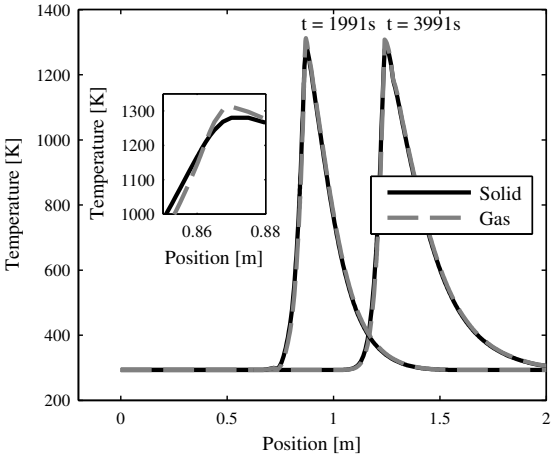

Figure 2.6: *The predicted gas and solid temperatures at t=1991s and t=3991s. The mass flux is* $0.55kg/m^2s$ *and* $\phi = 0.15$.

2.3.3 Results

Gas mass flux

Figure 2.8 shows the peak solid temperature (left) and combustion wave velocity (right) as a function of the equivalence ratio for different gas mass fluxes. The left

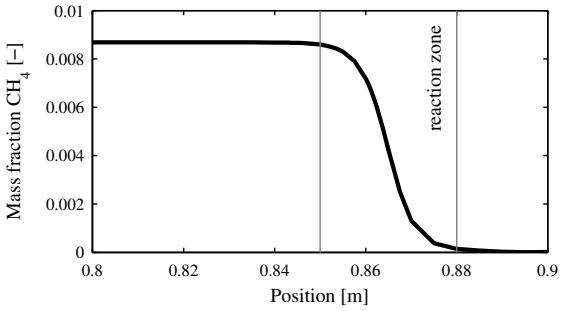

Figure 2.7: *The mass fraction of CH_4 at t=1991s for a mass flux of $0.55 kg/m^2 s$ and $\phi = 0.15$.*

figure shows that the peak solid temperature increases with increasing equivalence ratio. This is an expected result because more fuel is added to the system with an increasing equivalence ratio. Increasing the gas flow rate also leads to an increasing peak solid temperature. Also this can be attributed to the addition of more fuel by increasing the mass flow of the incoming gas stream. The increasing temperatures show that the increased cooling of the higher gas velocity is more than compensated by the increasing amount of available chemical energy.

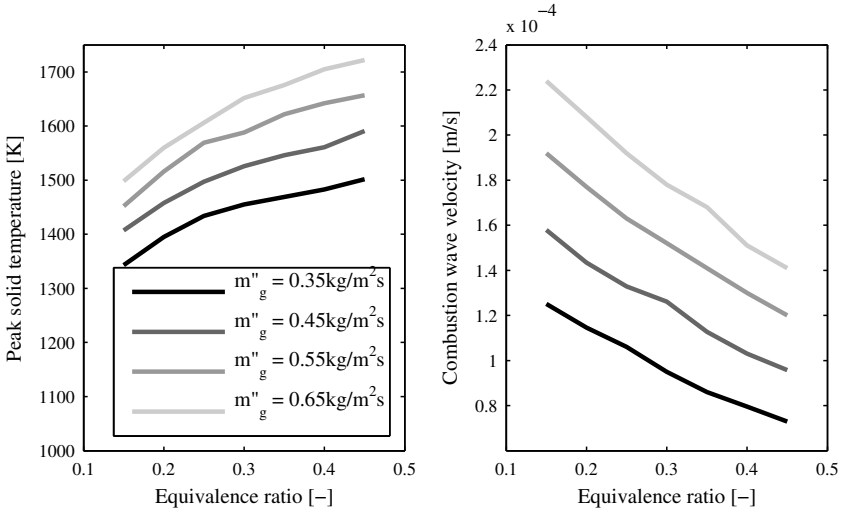

Figure 2.8: *The predicted peak solid temperature (left) and combustion wave velocity (right) as a function of equivalence ratio for different gas mass fluxes.*

At the same time, the combustion wave velocity decreases with increasing equivalence ratio. This is an expected result because the flame contains more energy to travel against the gas stream. Despite this, still not enough energy is put in the flame to make it travel upstream. For an increasing gas mass flux, the combustion wave velocity increases as well. Despite the higher energy content of the flame it is blown further downstream by the increasing gas flows.

Particle diameter

The influence of the particle diameter can be seen in the plots in figure 2.9. The left plot shows the peak solid temperature for two particle sizes and the right plot shows the combustion wave velocity for these particle sizes. The only model parameter that changes with particle size is the convective heat transport (through both the Reynolds and the Nusselt numbers). The temperature plots show that increasing convective cooling is more pronounced for the smaller particles due to an increased heat transfer coefficient for these particles.

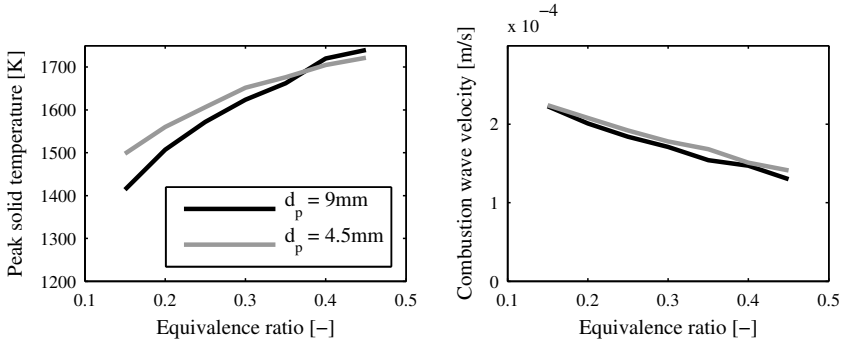

Figure 2.9: *The predicted peak solid temperature and combustion wave velocity for different particle diameters.* ($\dot{m}''_g = 0.65 kg/m^2 s$)

Despite the differences in convection for the different particle sizes, the combustion wave velocities hardly differ. This shows that the particle size (and thus the convective heat transfer) does not have a significant effect on the combustion wave velocity.

Zhang [102] validated his model with experiments done with different particle diameters and showed that the discrepancies with modeling results become bigger when the particle diameter is increased. This is caused by the fact that the model does not take into account temperature gradients inside the particles.

Adding nitrogen

When increasing the mass flux of the fuel/air mixture more energy is added to the system increasing the temperature. By adding nitrogen the mass flux can be increased without increasing the energy content of the mixture. Addition of nitrogen in an open flame will cool the flame since more gas needs to be heated with the same amount of energy. Adding nitrogen in the case of filtration combustion can be compared with a higher mass flux at a lower equivalence ratio since the methane mass fraction decreases. The left part of figure 2.10 shows that adding nitrogen does not have the same effect as adding nitrogen to open flames and even increases the peak flame temperature. Despite the higher temperature for an increasing nitrogen flow, the right plot shows that the velocity also increases.

The results for adding nitrogen can be compared to the results presented in figure 2.8. Also there, higher temperature are obtained when the equivalence ratio is decreased at an increasing mass flow.

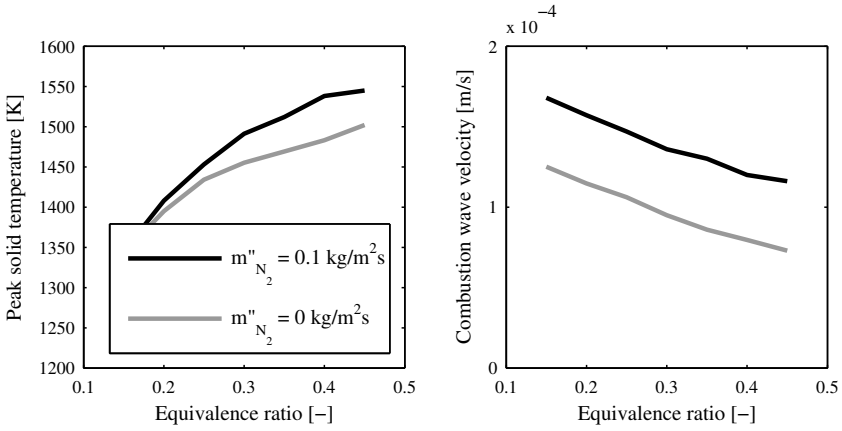

Figure 2.10: *The predicted peak solid temperature and combustion wave velocity for a case with and without extra nitrogen added.* ($\dot{m}''_g = 0.35 kg/m^2 s$)

Porosity of the bed

The effect of porosity of the packed bed can be seen in figure 2.11. The left plot shows that the peak solid temperature is only influenced slightly. However, the right plot shows that a small porosity results in a lower wave velocity. This is caused by the increased velocity of the thermal wave since less solid needs to be heated.

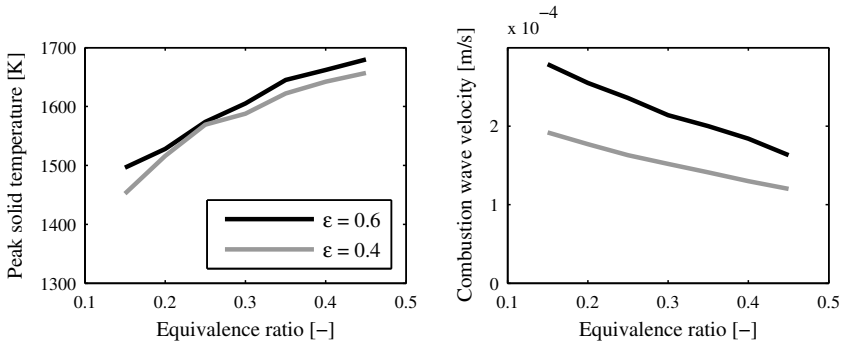

Figure 2.11: *The predicted peak solid temperature and combustion wave velocity for different packed bed porosities.* ($\dot{m}''_g = 0.55 kg/m^2 s$)

2.4 Experiments

2.4.1 Experimental setup

Figure 2.12 shows the experimental setup used for the experiments. Air, methane and nitrogen are fed from below into the premix section (2). The mass flux of the different gases are controlled by orifices which are calibrated with a wet gas flow meter. To prevent flashback in the supply tubes special safety valves are used. The premix section is filled with steel wool to improve mixing and prevent explosions. A highly porous plate (3) is used to carry the bed and prevent flame flashback from the ignition zone to the premix zone. In the ignition zone the gas is ignited by a heating coil wrapped around a small alumina tube (4). The packed bed (5) consists of alpha-alumina spheres of about $4.5mm$ in diameter. α-Alumina (Al_2O_3) is used, because of its high melting point of $2300K$, its relative low thermal conductivity,its low porosity and it is inert. The temperature in the bed is measured with K-type thermocouples. To reduce the wall heat losses the reactor is isolated with glass wool.

The reactor is made of stainless steel because of economical reasons and ease of manufacturing. Stainless steel is not the most convenient material for these experiments because of its relative low melting point of about 1700K and relative high thermal conductivity. More favorable materials to use are quartz glass or alumina but these materials are far more expensive and less convenient to manufacture. Since the material choice of the reactor limits the temperatures that can be reached also relative inexpensive K-type thermocouples can be used. Due to the temperature limit only runs with low mass fluxes and low equivalence ratios can be done without causing

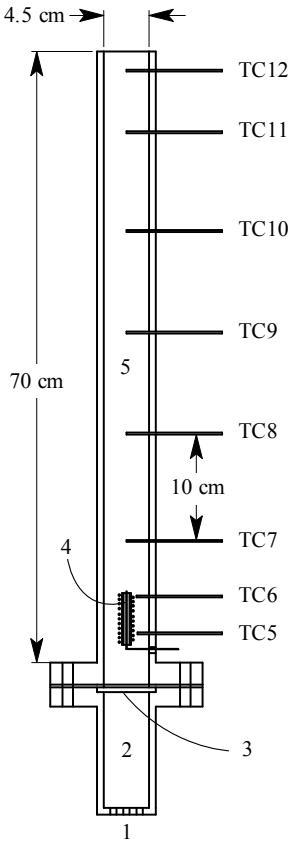

Figure 2.12: *A schematic overview of the experimental setup. 1-gas inlet; 2-premix section; 3-porous plate; 4-heating coil; 5-packed bed. The thermocouples are labeled TC5-TC12.*

damage to the experimental setup. The inner diameter of the tube is $4.5cm$ which is 10 times the particle diameter often used as a rule of thumb to neglect wall effects.

2.4.2 Procedure

The experiments are started by preheating the bed with the heating coil for about half an hour with a small mass flow of air. Then some methane is added to increase the heating rate of the bed. When sufficiently high temperatures are reached the mass flow of the air and the fuel are increased step by step. When the front starts to move

the power to the heating coil is turned off to prevent damage to the heating coil and partially burning of the mixture before they reach the combustion front.

2.4.3 Thermal wave

To get some insight in the thermal properties of the packed bed two runs are done to show the thermal wave. To start the experiment the bed is heated until thermocouple seven (TC7) reaches a temperature of $1073K$. Then the methane valve is closed to stop the reaction. Now only air is blown through the reactor at a chosen mass flux which causes the thermal wave to move downstream. Figure 2.13 shows the thermal wave at an air mass flux of $0.174kg/m^2s$. The left part of the figure shows the measured temperature versus time at different locations. When the shape of the wave does not change it is possible to extract the thermal wave velocity from such a plot by dividing the distance between the thermocouples by the time needed for the peak to reach the following thermocouple. However, due to the conductivity of the bed and the heat losses at the wall the thermal wave becomes less high and stretched out as can be seen in the right part of the figure where the temperatures are plotted against the position for different time steps. Because of this the maximum temperature measured at a thermocouple does not have to be the peak of the thermal wave. To extract the peak of thermal wave from the data the maximum temperature measured at the thermocouple has to be found while this temperature is larger than the temperature measured at the two thermocouples next to it. The thermal waves at the corresponding times are shown in the right part of the figure. From this figure the thermal wave velocity is derived by dividing the distance between the thermocouples by the time for the peak of the thermal wave to reach the next thermocouple.

2.4.4 Combustion wave

Figure 2.14 shows the measured data of a run with a mass flux of $0.45kg/m^2s$ and an equivalence ratio of 0.3. As can be seen in the figure the combustion wave becomes steady after thermocouple 10. Thermocouple 12 shows lower temperatures because this thermocouple is placed about $1cm$ under the top of the bed in a part of the reactor which is not isolated. The combustion wave velocity can be derived from the figure by dividing the distance between thermocouple 10 and 11 by the time needed to reach its maximum. Since the temperatures are plotted against the time the preheat regions are located at the right part of the waves.

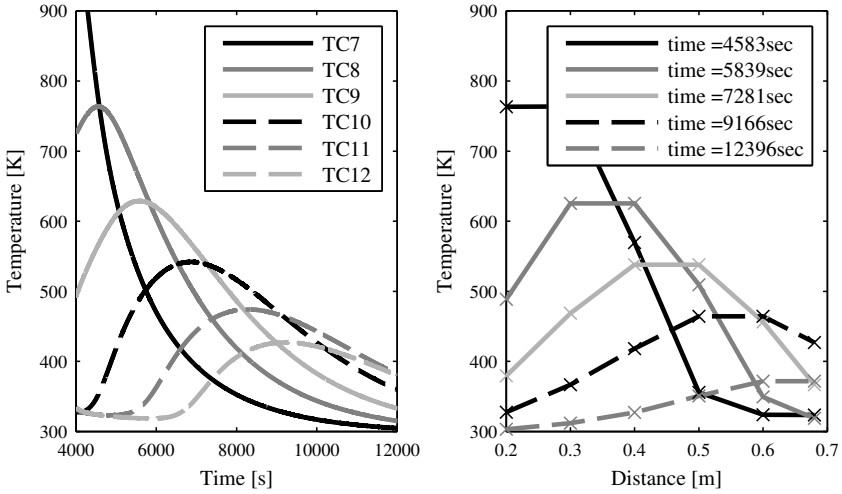

Figure 2.13: *The thermocouple readings as a function of time (left) and location (right) at an air mass flux of* $0.174 kg/m^2 s$

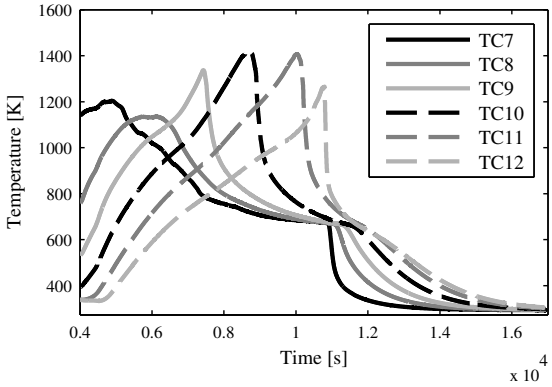

Figure 2.14: *The combustion wave* $\dot{m}''_g = 0.45 kg/m^2 s$ *and* $\phi = 0.3$

2.4.5 Remarks on the experiments

As discussed in the previous paragraph it takes a long time for the combustion wave to become stationary and so only a stationary combustion wave velocity can be derived between thermocouples 10 and 11. To improve the experimental setup a longer

reactor made from quartz glass or alumina has to be used.

Figure 2.14 shows that the temperatures in the lower part of the reactor remain rather high at a temperature of about $650K$ when the combustion wave already reaches thermocouples 10 and 11. It has to be mentioned that the heating coil is already turned off. When the methane supply is shut of, an instant drop in temperature is measured at thermocouple 7 just above the heating coil. The high temperatures can only be caused if energy is added to the lower part of the bed. An explanation may be the partly oxidation of the fresh mixture around the heating coil. Probably enough energy is released by the partial oxidation to keep the heating coil or a hot particle hot enough to maintain the oxidation. The effect can possibly be eliminated by shortly closing the methane valve to cool the lower part of the reactor. However it is rather hard to monitor the behaviour during the experiments. Measuring the CH_4, O_2 or CO_2 concentrations in the exhaust gases and/or by placing more thermocouples in the igniter zone would be useful to monitor the combustion process more accurately.

Despite these shortcomings in the experimental setup the trends found in the experiments are useful to validate the model.

2.4.6 Results and validation of the model

Figure 2.15 shows the predicted and measured peak temperatures and combustion wave velocities. The temperatures are measured at thermocouples 10 and 11 and the waves are derived between thermocouples 9 and 10 thermocouples 10 and 11. The model slightly over-predicts the peak solid temperature. Despite the small over-prediction, the influences of equivalence ratio, mass flux and addition of nitrogen are predicted reasonably well. The lower measured temperatures can be caused by the possible partial oxidation of the methane at the heating coil as described earlier.

The combustion wave velocities are also over-predicted, but also here the trends are predicted well. The slower wave velocities could be attributed to the wall effects. These are taken into account in the model as a volumetric heat loss, but the actual superficial heat loss might have a bigger impact than predicted by a volumetric heat loss. Also the heat generated around the heating coil can be a cause for the combustion wave to be able to slow down (i.e. it has the tendency to travel upstream).

2.4.7 Conclusions on the experiments and validation

Despite the low amount of experiments the trends predicted by the model can be validated. Also the peak temperatures are predicted well by the model. It is clear that

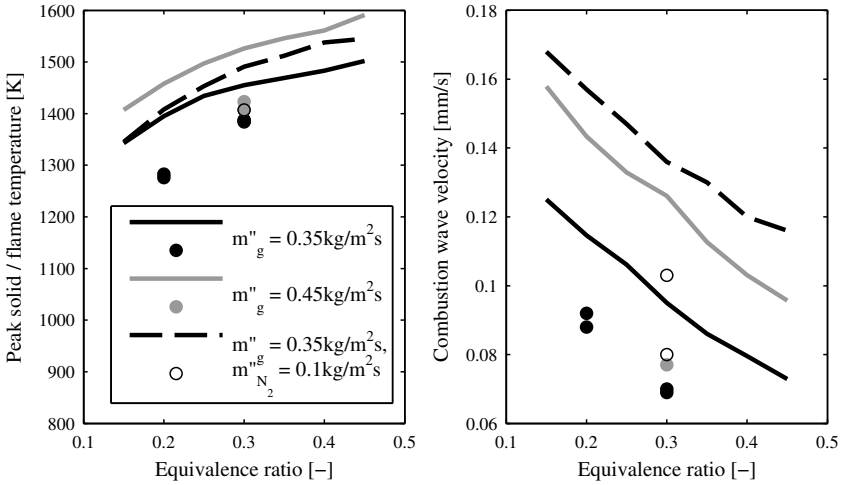

Figure 2.15: *The predicted and measured peak solid temperatures and combustion wave velocities. The temperatures are measured at thermocouples 10 and 11 and the waves are derived between thermocouples 9 and 10 thermocouples 10 and 11.*

the effect predicted by the models for increased equivalence ratios, mass fluxes and adding nitrogen are noticeable during the experiments.

2.5 Application to municipal waste incineration

As has been said in the introduction of this chapter, flammable gas concentrations under the ignition front are generally below the flammability limit. Therefore only the low velocity regime is interesting for waste combustion. It has been shown in the literature review that for these ultra low equivalence ratios in this low velocity regime the combustion wave travels along the gas stream. So despite the increased flammability of the mixture flashback does not occur.

However, because of the highly inhomogeneous composition of the waste, once in a while a situation could occur at which the conditions for the high velocity regime are fulfilled. In this regime, the gases should be at least at their lower flammability limit. In this regime the coupling between the gas and solid phase is broken, so the heat from the reaction front does not result in volatiles in this case. The heat from devolatilization can only come from the preheated primary air. In an extreme case, a batch of a highly flammable liquid such as methanol or octane is at the grate. It can

be estimated whether enough liquid can be evaporated by the preheated primary air to reach their LFL. The heat available in the air to evaporate is:

$$\dot{q}''_{air} = c_{p,air}\dot{m}''_{air}(T_{preheat} - T_{sat}) \tag{2.15}$$

The heat needed to evaporate enough liquid to reach its LFL is:

$$\dot{q}''_{evap} = \frac{M_{fuel}}{M_{air}} LFL\dot{m}''_{air} H_{evap} \tag{2.16}$$

The data for octane and methanol is listed in table 2.3. The table shows that there is not enough energy available in the preheated primary air to evaporate enough methanol or octane to create a flammable mixture. When it is not possible to create a flammable mixture with highly flammable liquids it is almost impossible to create such a mixture from a solid by pyrolysis. It can be concluded that flashback in MSW combustion is very unlikely to take place. This indicates that the upstream ignition front movement seen in for example wood combustion is mainly driven by the solid phase. This possibility will be treated more thoroughly in chapter 3.

Table 2.3: *Heat needed to evaporate a liquid to its LFL and the heat available for evaporation in the preheated primary air.*

fuel	LFL [-]	H_{evap} $[kJ/kg]$	M_{fuel} $[kg/mol]$	T_{sat} $[^oC]$	$\dot{q}''_{evap}$ $[kJ/m^2s]$	$\dot{q}''_a$ $[kJ/m^2s]$
octane	$0.95 \cdot 10^{-2}$	300	114	126	10	6
methanol	$6.7 \cdot 10^{-2}$	1100	32	65	72	32

2.6 Conclusions

- The model shows that the combustion front velocity is the same for $4.5mm$ and $9mm$ particles.
- The model shows that adding nitrogen to the gas mixture, the solid temperature increases. The combustion wave velocity increases as well.
- Experiments are carried out the validate the model. The model under-predicts both the solid temperature and the combustion wave velocity. The trends are well predicted.

- Due to the high primary air velocities common for the incineration of MSW the combustion wave will probably move downstream relative to the reaction front and does not have much effect on the reaction front going upstream.
- Flashback of a flame into cold unburned waste is unlikely to occur since the mixture must have an equivalence ratio around one. This is unlikely to achieve with preheated primary air and even impossible with the heat from the combustion zone.

3

Two dimensional front spread

This chapter investigates the mechanisms causing the ignition propagating in horizontal and vertical direction through a waste bed. The horizontal front propagation determines the flame stability in the furnace and the vertical front propagation determines the burnout of the fuel. Optical lab scale experiments are carried out to look inside a burning wood bed. Besides, a model is developed to predict the velocity and temperature of the ignition front in horizontal and vertical direction. The model is solved analytically and validated with experimental data from the literature. From the model an upper and a lower boundary for the ignition front temperature and velocity are derived. It is found that for both the vertical and the horizontal front propagation the char combustion is the driving mechanism for low radiative heat fluxes from the furnace. This implies that the volatile combustion can be neglected, which simplifies the modeling of the ignition front propagation significantly. In full scale plants, the radiation from the furnace walls can not be neglected.

3.1 Introduction

Combustion on a grate is common practice for the incineration of municipal solid waste. This grate technology is also used for energy production from biomass. To control such plants, physicochemical knowledge of the combustion process taking place on the grate is essential. Despite the robustness of the grate technology, the fire on the fuel bed may travel back and forth in the furnace. This may result in incomplete burnout or chute fire. In both these situations the ignition of the fuel is a key mechanism: poor burnout may occur with a fuel that is hard to ignite and chute fire may occur with a fast ignitable fuel. To control the combustion process and emissions, it is essential to stabilize the flame on the fuel layer and determine the ignition and combustion speeds through the fuel layer. The propagation of the ignition front is the subject of the current work.

In this work a two dimensional ignition front propagation through a packed bed of wood is investigated. Because waste is a highly inhomogeneous fuel, wood is used as a model fuel. Many models on the combustion of a solid fuel on a grate assume an ignition front which is initiated by the radiation of the furnace and the flames above the bed. After its initiation the front is assumed to travel downwards, see for example [39, 88, 91, 26, 31, 98]. This process is depicted in figure 3.1. In this model, only a thin one dimensional slice of the fuel layer is followed in time. The location of the front is correlated with time by the horizontal velocity of the fuel layer. This approach is only justified if the horizontal mass and energy gradients are small compared to the vertical gradients. Despite the wide use of this approach, the authors only found Van der Lans et al. [88] actually validating it for straw combustion.

It will be shown in this chapter that the one dimensional approach can not be applied to describe the combustion of a two dimensional fuel bed. In this work it is both experimentally and analytically investigated how a two dimensional ignition front evolves in time. As a first step the mechanisms in one dimensional front propagation are investigated. To investigate a two dimensional front propagation, optical experiments are carried out in a thin glass vessel. With the knowledge derived from the experiments, a model is developed to describe the front velocity in both the vertical and horizontal direction. The model is validated with experimental results from the literature. Finally, the experimental results obtained in lab scale setups are evaluated and translated to a full-scale incinerator.

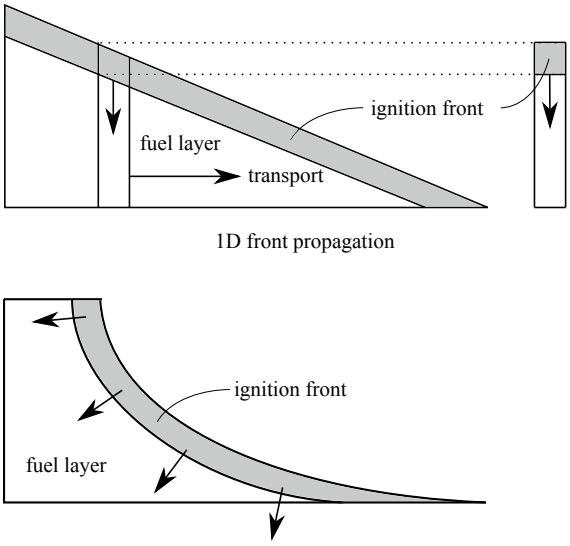

Figure 3.1: *Top: current model on ignition front movement through a packed bed. Instead of looking at the whole bed, only a one dimensional column is followed. Bottom: when the gradients in horizontal direction can not be neglected, a curved ignition front will result.*

3.2 Existence of two dimensional ignition fronts

The assumption whether the horizontal heat gradient can be neglected with respect to the vertical gradient can be verified with the Péclet number. This number gives the ratio of the convective heat transport due to the bed movement and the diffusive heat transport due to conduction and radiation inside the bed:

$$Pe = \frac{vL\rho c_p}{k_{eff}} = \frac{vL}{\alpha_{eff}} \tag{3.1}$$

In this equation v is the horizontal velocity of the fuel bed, L is a characteristic length and $\alpha_{eff} = k_{eff}/(\rho c_p)$ is the effective thermal diffusion coefficient of the bed. When $Pe >> 1$, the horizontal gradients can be neglected. The velocity of the fuel bed is determined by the grate movement and the feed rate. For waste combustion this velocity is around $8.4 cm/min$. This figure is generally higher for biomass combustion. For the characteristic length L the thickness of the thermal front seems an appropriate choice, because this is the length over which the thermal diffusion takes place. Experiments carried out by Ryu et al. [75] on $5-30 mm$ pine particles show that this

thermal front thickness is in the order of the particle size. The effective thermal conductivity k_{eff} is a combination of conduction and radiation. For high temperatures it can be shown that the conduction can be neglected compared to radiation:

$$\frac{k_{eff,rad}}{k_{eff,cond}} = \frac{4\sigma F d_f T_{f,avg}^3}{k_{cond}(1-\varepsilon)} \approx 160 \tag{3.2}$$

The radiation is described using an effective radiative conductivity $k_{eff,rad}$ [25]. In this equation σ is the Stefan-Boltzmann constant. The radiation exchange factor F is about unity [25]. The average combustion zone temperature $T_{f,avg} = \sqrt[3]{\frac{1500^4-300^4}{4(1500-300)}} = 1017K$ [79], the front thickness $d_f \approx 3 \cdot 10^{-2} m$ (an estimate for waste combustion), the thermal conductivity of the solid fuel $k \approx 0.15 W/mK$ (wood) and the porosity of the fuel bed $\varepsilon \approx 0.7$. For this process, the conduction is small compared to the radiation and can be neglected. This is also found by Shin and Choi [78].

With the numbers found, the Péclet number becomes (with $c_p = 1.9 kJ/kgK$ [68]):

$$Pe = \frac{v_b d_f}{\alpha_{eff,rad}} \approx 2 \tag{3.3}$$

The Péclet number is around 2, which shows that the horizontal heat gradient inside the bed can not be neglected. In fact, it seems to play an important role in the horizontal front propagation. This suggests that a two dimensional approach is needed.

Van der Lans et al. [88] found that the Péclet number is in the order of 10^4 for straw combustion. In contrary to our analysis, they use the length of the grate as the characteristic length. Besides, they assume conduction the main heat transport mechanism. These two differences result in a higher Péclet number than the one found in equation 3.3.

When the two dimensions of the front propagation are translated to relevant properties of the combustion process it can be said that the horizontal front propagation defines the location of the fire. The vertical front propagation determines the combustion rate and the burnout of the waste layer.

3.3 One dimensional ignition front propagation

As a first step, the one dimensional, vertical front propagation is considered. The heat needed to drive the ignition front downwards can be delivered by either the flames from volatile combustion or the combustion of the remaining char above the front.

To investigate the heat source responsible for the downward front propagation an analytical as well as an experimental approach has been applied. Firstly, optical experiments are carried out to observe the location of the volatile combustion. Secondly, gas composition measurements from Gort [39] inside the ignition front are evaluated to determine the location of the volatile combustion. Finally, the influence of the volatile content of the fuel on the ignition propagation is investigated with the help of measurements from Gort [39]. The findings from the experiments will be complemented by a flame speed analysis applied on a packed bed to see in which occasions the flame is able to burn inside the fuel bed.

3.3.1 Optical experiments

Optical experiments are carried out in a quartz glass tube to observe where the homogeneous combustion takes place. The tube is filled with wood pellets of about $5mm$ diameter and $10mm$ length. Two video cameras used to monitor the combustion process. One camera makes OH^* radicals visible with an UG11 filter. During the experiments different amplification levels are used for this camera, so the images from this camera can not be compared. The second camera is an ordinary camera which pictures will be used as a reference. Pictures are taken with the two cameras at the same time. The results for different air velocities can be seen in figures 3.2-3.5. Note that the picture and the OH^* image are not at the same scale.

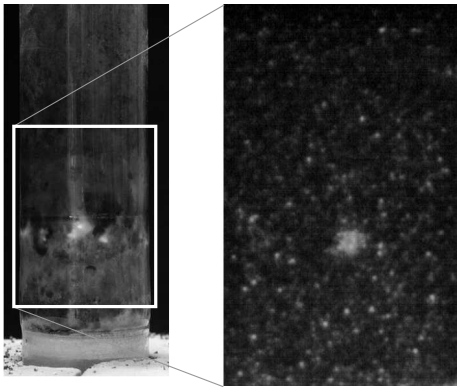

Figure 3.2: *Picture of the front (left) and OH^* spectroscopy (right) at an air velocity of* $0.052m/s$. *The OH^* spectroscopy shows a lot of noise because of the high amplification which was needed to show the very small amount of OH^* radicals.*

Figure 3.2 shows the front and the locations of OH^* radicals for an air velocity of $0.052m/s$. It can be seen that there are almost no OH^* radicals in the tube. The pic-

ture also shows hardly any flames. From this figure it can be concluded that glowing combustion does not produce OH^* radicals.

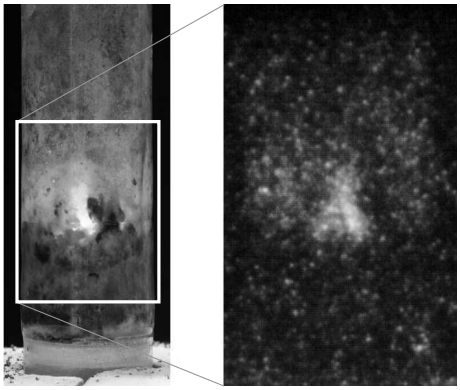

Figure 3.3: *Picture of the front (left) and OH^* spectroscopy (right) at an air velocity of* $0.10 m/s$. *The OH^* spectroscopy shows a lot of noise because of the high amplification which was needed to show the very small amount of OH^* radicals.*

When the air velocity is increased to $0.10 m/s$ some more flames (and OH^* radicals) are visible. This is shown in figure 3.3. Some flames are visible but not enough oxygen is available to burn all gases. Condensed tars have been found on the inside of the tube during and after the experiment.

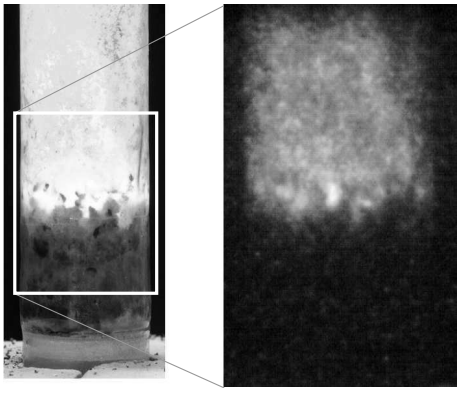

Figure 3.4: *Picture of the front (left) and OH^* spectroscopy (right) at an air velocity of* $0.28 m/s$. *A relatively broad glowing front can be seen in the picture.*

When the air velocity is increased to $0.28 m/s$ flames can clearly be distinguished (figure 3.4). When some more attention is paid to the images one can see that where the bed is glowing, no OH^* radicals are present. A conclusion can be that the flaming combustion takes place above the bed. Also the produced hydrogen, which has a high combustion velocity, seems to burn above the fuel bed. Due to the large heat losses to and through the wall the front is not straight but has a convex shape (the center of the tube burns faster). The pellets close to the wall can hide the flame. On the other hand, the glowing combustion inside the bed can be seen clearly in the pictures. An indication is given that the flaming combustion takes place above the bed (or at least not under the glowing front).

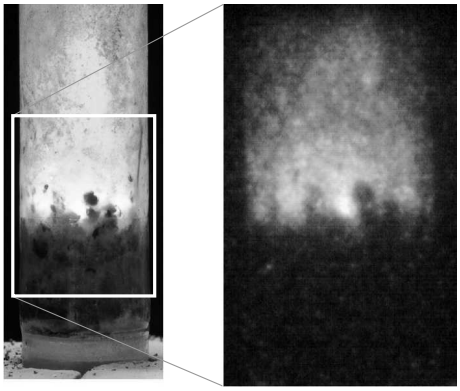

Figure 3.5: *Picture of the front (left) and OH^* spectroscopy (right) at an air velocity of 0.34 m/s*

Figure 3.5 shows the images of the experiment carried out with an air velocity of $0.34 m/s$. It can be seen from the picture that the flame is not as intense as is was in the previous experiment. When this picture is compared to the picture taken at an air speed of $0.28 m/s$ it can be noted that the latter shows a bigger glowing front. The higher air velocity causes the combustion to cool down. When the velocity is even further increased the front will be cooled too much and extinguishes.

These optical experiments indicate that there is hardly any volatile combustion for low air velocities. For higher air velocities the volatile combustion is clearly present, but it seems to occur mainly above the fuel bed.

3.3.2 Gas composition measurements

Gort [39] measured temperatures and gas compositions inside a burning packed bed. The used setup consists of a steel tube with a diameter of $300 mm$ and a length of

$800mm$. The fuel bed is ignited from the top with an electric radiant heater and primary air is fed through the fuel bed from below. Gort used wooden cubes of $30mm$ and air velocities of 0.05, 0.25 and $0.5m/s$. The gas extraction point is at a fixed location inside the fuel bed so the gas extraction point sees the front passing in time. Figure 3.6 shows the measured composition of the extracted gases as a function of time for three air flow velocities (0.05, 0.25 and $0.5m/s$). The figures also show the calculated oxygen balance of the flue gases. This oxygen balance is defined as the amount of oxygen depleted from the incoming air minus the oxygen found in the product gases CO and CO_2. Note that the oxygen present in the H_2O is not considered. Just below the ignition front at $0.05m/s$ the amount of oxygen in the product gases CO and CO_2 is higher than the oxygen which is depleted from the air supply. This indicates that oxygen from the wood is used to create CO and CO_2 under the front which can only happen when volatiles are burned under the front. When volatiles are burning under the front, the front will be speed up due to the effective transportation of heat.

The positive oxygen balance (more oxygen is depleted than is found in the CO and CO_2) is probably caused by the fact that the water and hydrocarbon concentrations are not considered. The hydrocarbons and water can contain a significant amount of oxygen.

Initially at 0.25 and $0.5m/s$ as much oxygen is depleted from the air as is found in the CO and CO_2. This may indicate that for these air velocities only char combustion takes place under the front, because this produces no H_2O. These observations lead to the conclusion that at low air velocities volatiles burn under the ignition front. This conclusion is in line with the first conclusion of Katalambula et al [52]. They measure the ignition mode (flaming or glowing) of a coal particle for several air velocities. They find that only under negligible and free convection the ignition is flaming.

3.3.3 Ignition with varying volatile content

To study the influence of volatile content on the ignition front in a packed bed, Gort carried out experiments [39]. He pyrolized wooden cubes of $30mm$ under nitrogen at a temperature of 300^oC for a certain time before burning them in a packed bed. The properties of the partly pyrolized cubes are listed in table 3.1.

ignition rate

Results from the experiments carried out by Gort are plotted in figure 3.7. He shows measured results for the ignition rate which is defined as the mass of the fuel that is

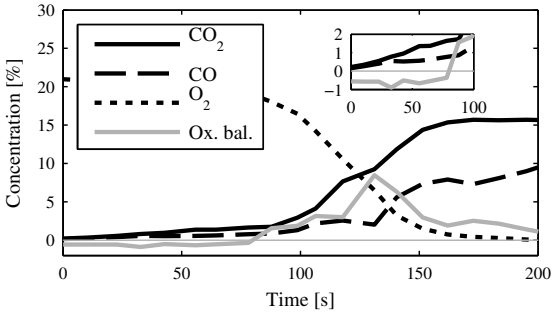

(a) Air flow velocity: $0.05 m/s$

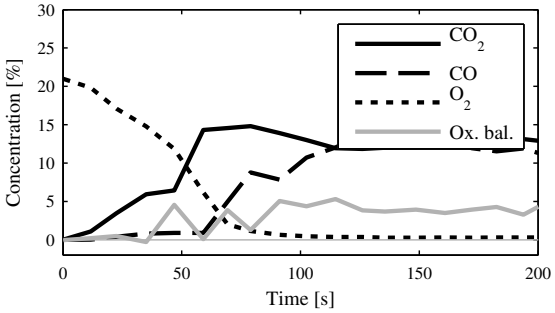

(b) Air flow velocity: $0.25 m/s$

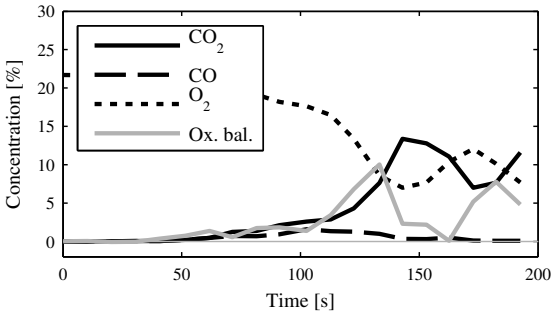

(c) Air flow velocity: $0.5 m/s$

Figure 3.6: *Measured gas compositions and an oxygen balance inside a packed bed of wood cubes as a function of time for three air velocities.*

Table 3.1: *Data from the dry and pyrolyzed wood [39].* [a] *The bed density can be calculated from the properties of the bed and the wood given in [39]. Assumed is that the volume of the wood particles in not changed during the pyrolysis.* [b] *The ignition speed is the ignition rate divided by the bed density. Note that the unit is millimeters per second*

	untreated	dry at 100^oC	15 min. at 300^oC	25 min. at 300^oC	35 min. at 300^oC
% volatiles (d.b.)	82.6	82.6	81.1	75.5	53.5
% moisture (as received)	10.4	2.5	5.0	0.9	0.0
ignition rate $[kg/m^2s]$	0.078	0.125	0.122	0.113	0.0790
particle density $[kg/m^3]$	615	565.2	569.5	508.2	356.9
bed density $[kg/m^3]$ [a]	200	183.7	185.1	165.2	116.0
ignition speed $[mm/s]$ [b]	0.390	0.681	0.659	0.684	0.681

ignited per second (in kg/m^2s). The figure show that the ignition rate decreases with decreasing volatile content.

ignition speed

The speed of the ignition front (in mm/s) is calculated with the data from table 3.1. This is done by dividing the ignition rate from the experiments by the initial density of the packed fuel bed. This ignition front speed is also plotted in figure 3.7. The values of the untreated wood are omitted from the figure because the relatively high water content influences the results too much. It can be seen in the figure that the ignition front speed is independent of the volatile content. This shows that the ignition front propagation is driven by heat transfer and not by chemical properties.

3.3.4 Flame speed in a packed bed

The flame speed in a packed bed can be calculated with a relation given by Williams [95]. Although this relation is valid for the flame speed of a one dimensional adiabatic open gas flame, it can be applied to a flame inside a packed bed.

$$\rho_g v_{fl} = \dot{m}_g''' d_{fl} \tag{3.4}$$

The flame speed is v_{fl}, the volumetric gas combustion rate is $\dot{m}_g'''$ (in kg/m^3s) and d_{fl} is the flame thickness (the zone at which the combustion reaction takes place). It can be shown that the volumetric gas combustion rate can be rewritten as follows:

$$\dot{m}_g''' = \frac{\dot{m}_g''}{\varepsilon d_{fl}} \tag{3.5}$$

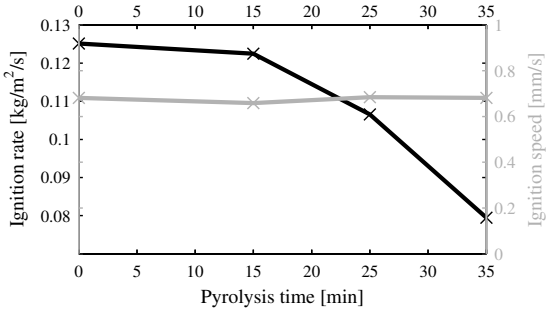

Figure 3.7: *The influence of pyrolysis time (at* 300^oC*) on the ignition rate (black line) and ignition speed (grey line). The ignition rate is taken from [39] (*$30mm$ *cubes of wood, air velocity equals* $0.1m/s$*)*

In which $\dot{m}''_g$ is the gas combustion rate per square meter, which is a more convenient parameter in our case and ε is the porosity. With equations (3.4) and (3.5) the flame speed can be expressed as:

$$v_{fl} = \frac{1}{\rho_g}\frac{\dot{m}''_g}{\varepsilon} = 0.064 m/s \tag{3.6}$$

In which $\rho_g = 1.2 kg/m^3$ (air at STP) and $\varepsilon = 0.7$ are used. The value for the gas combustion rate $\dot{m}''_g$ is approximated from the experimental results from Gort [39]. He measures a maximum combustion rate for packed $30mm$ wood cubed of $0.078 kg/m^2 s$. With a volatile content of 82.6%, the gas combustion rate will be maximum $0.064 kg/m^2 s$.

When the interstitial primary air velocity is higher than the calculated flame speed of $0.064 m/s$ (eq. (3.6)), the volatile-oxygen mixture is blown away and will not burn under the ignition front. It has to be noted that the analysis holds for an adiabatic situation. In the glowing char layer, energy is added to the volatile-oxygen mixture and the flame speed will increase. Hence it might be possible that the volatiles burn in the glowing char layer.

The calculated flame speed in equation (3.6) is valid for an adiabatic situation. But when the gas is flowing through a hot packed bed, energy is added to the gas. This results in a higher flame speed depending on the supplied energy. It has been shown in figure 3.11(b) that the gas phase burns inside the alumina layer, despite the high superficial velocity of $0.3 m/s$. This shows that the flame speed calculated in equation (3.6) is not applicable to a gas flowing through a hot packed bed. However, an important conclusion of this analysis is that for velocities higher than $0.064 m/s$ the gas can

not burn under the glowing char layer. This finding is in agreement with the findings from the gas measurements inside the combustion zone described in section 3.3.2.

3.3.5 Evaluation

For the vertical front propagation two sources of heat can be distinguished: (1) volatile combustion and (2) remaining char combustion. From different analyses it is found that only for low primary air velocities the volatiles can burn under the ignition front. For higher air velocities, the volatiles burn above the ignition front. When the volatiles burn above the ignition front, the heat transfer (either conduction of radiation) from volatile combustion to the fresh fuel will be minimal. The remaining source of heat is the char combustion. Equation (3.2) shows that the radiation is the prominent heat transfer mechanism inside a packed bed for high temperatures. It can be concluded that the vertical ignition front movement is dominated by the radiation from the char combustion. This implies that for ignition modeling the volatile combustion can be neglected completely, which simplifies modeling significantly.

3.4 Two dimensional ignition front propagation

The one dimensional approach will now be extended to a two dimensional approach. To investigate the ignition front propagation in two dimensions, optical experiments have been carried out in a two dimensional fuel bed.

3.4.1 Experimental procedure

A picture of the setup is shown in figure 3.8. The setup consists of a vessel of $17.5cm$ wide, $1.5cm$ deep and the height is about $40cm$. Air can be fed to the vessel from the bottom. To ensure a uniform flow over the width of the vessel, the air is fed through a porous plate. The backside and the upper part of the front-side of the vessel are insulated to minimize heat losses to the surroundings. Without the front-side insulation, the ignition front shrinks after the initial ignition and it even extinguishes after a while. The vessel is filled either with wood pellets or wood chips till a certain height. To ignite the wood, a layer of charcoal soaked in propanol is put on the right half of the fuel bed and lit. The experiments are recorded with a camera.

Several experiments are carried out to see the shape of the ignition front and its propagation mechanism in the two directions. The influences of both heat losses and volatile combustion are regarded. All experiments are carried out with an air velocity

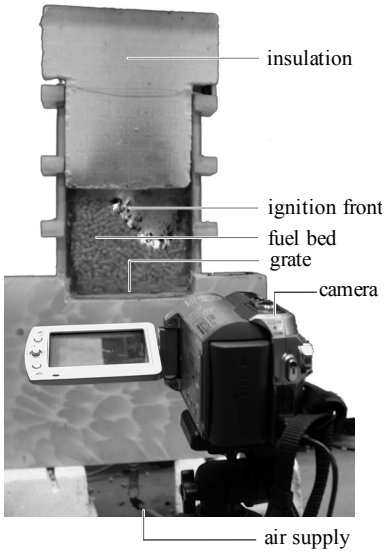

Figure 3.8: *Picture of the experimental setup to observe two dimensional ignition phenomena in a packed bed.*

of $0.3 m/s$. A typical result of an experiment can be seen in figure 3.9. Four images at equally spaced times are shown.

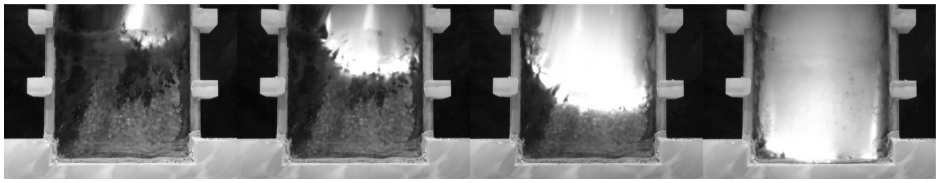

Figure 3.9: *Four pictures of the experiment with pellets. Together with the backside, the front-side is insulated as well. To take a picture, the front-side insulation is removed for a few seconds.*

3.4.2 Results and discussion

Base case

The base case is an experiment with wood pellets. The top of the fuel bed is at the same height as the lower side of the insulation on the front-side, so only the gas phase above the bed is insulated. In figure 3.10 four images of the experiment are combined in one picture. The location of the ignition front at four equally spaced times can be seen and are highlighted by the black lines. The experiment lasts for about 45 minutes. The front can be divided in two parts: the right side of the front which is fairly horizontal and the left side which is almost straight and at an angle of about 45^o. The horizontal part of the front expands towards the left. The vertical velocity of the front is $0.40 cm/min$ and the horizontal velocity is $0.38 cm/min$. Because these velocities are almost equal, this could indicate that the propagation mechanism for both (or all) directions is the same. However, with an equal front propagation mechanism in all directions a circle shaped front would be expected, which is not the case in the experiments. During the experiment wood particles from the top of the bed roll down along the inclined part of the front and are burned on the horizontal part of the front. This prevents the front from being too curved. It can be seen that where the inclined and the horizontal parts meet, the combustion is more intense than at other places. It is believed that this is caused by the combustion of the particles which rolled down.

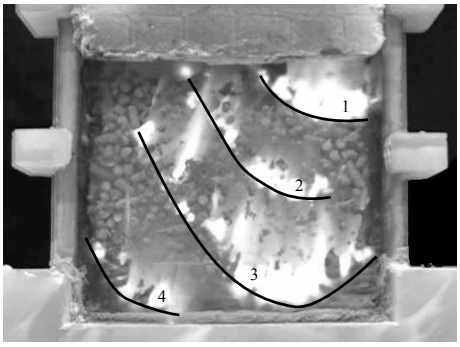

Figure 3.10: *Four pictures of the base case experiment combined in one image.*

Inert layer on top

To prevent interaction between the gas phase combustion and the fuel bed an inert layer of small alumina spheres is put on top of the bed after ignition. Again four pictures of the experiment are combined in one image (figure 3.11(a)). Besides the video camera recording the experiment, another camera monitors the location of the OH^* radicals with an UG11 filter, these radicals are an intermediate product of flaming combustion. This camera can only make a qualitative measurement. A result of this chemiluminescence measurement is shown in figure 3.11(b).

The normal pictures shown in figure 3.11(a) show that the front is straight and almost horizontal. Unlike in the base case, no inclined front at the left side is seen. Also hardly any flames are seen above the solid layer, but intense glowing is observed. The chemiluminescence image shows that almost all OH^* radicals exist in the alumina layer and hardly any OH^* radicals are visible above and below this layer. This shows that the volatiles are burned inside the alumina layer. The alumina layer prevents the gas phase to radiate to the fuel bed and because of its high temperature, the layer also insulates the fuel bed. In this case the vertical velocity of the front is $0.44 cm/min$, which is higher than in the base case. This is probably caused by the decreased heat loss from the ignition front to the gas phase due to the insulation by the alumina layer. The horizontal velocity is $0.34 cm/min$ which is slightly lower than in the base case. The lower horizontal velocity can be caused by the absence of flames above the solid bed and thus no heat can be transferred from the flames to the fresh fuel.

Full front-side insulation

To see the effect of heat losses from the front to the surroundings, the vessel is not only insulated at the backside, but also at the front-side. Every two minutes the front insulation is removed for a few seconds to take a picture. Four pictures of the experiment are shown in figure 3.9. The shape of the front is similar to the one from the base case. It can be seen that the horizontal part is larger and more straight than the one in the base case (figure 3.10). Also the inclined part is more steep in the current case. The vertical velocity of the front is $0.45 cm/min$, which is about equal to the one found with the inert layer on top. The horizontal velocity is $0.50 cm/min$ which is higher than the ones found in the base case and with the inert layer. This is an expected result, because less heat is lost to the surroundings and can thus be used to ignite the fresh fuel.

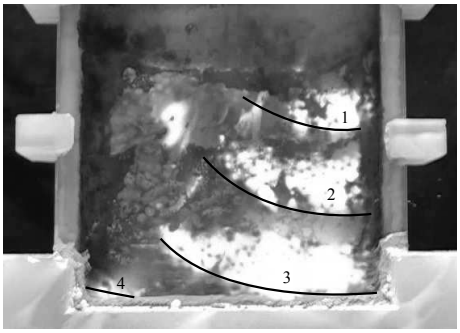

(a) Four pictures of the experiment combined in one image. A layer of alumina spheres is put on top of the fuel bed directly after ignition.

(b) OH^* chemiluminescence image of the ignition front.

Figure 3.11: *Results from the 2D ignition experiment with an inert layer on top of the fuel bed.*

3.4.3 Evaluation

A summary of the front velocities in both directions is given in table 3.2. The vertical velocities are significantly lower than the ones measured in the 1D ingition experiments (see table 3.1). This can be caused by the fact that the heat losses to the surroundings in the 1D ignition setup were much less than the losses in the 2D ignition setup.

The main observations of the 2D ignition experiments are:

- When an inert layer is put on top of the fuel bed, the volatiles almost completely burn inside that layer. The hot inert layer acts as an insulation layer for the fuel

Table 3.2: *Summary of the vertical and horizontal ignition front velocity for the three 2D ignition experiments*

	vertical velocity	horizontal velocity
base	0.40 cm/min	0.38 cm/min
inert layer	0.44 cm/min	0.34 cm/min
insulation	0.45 cm/min	0.50 cm/min

bed and the gas phase only interacts slightly with the fuel bed in this case. This causes the vertical front velocity to be higher than in the base case.

- When both sides of the vessel are insulated, the vertical front velocity equals the one obtained with the inert layer. The horizontal propagation velocity is slightly larger than the vertical one in this case.

3.5 Modeling

It has been shown that the main mechanism for the vertical propagation of the front is the radiation inside the fuel bed. Based on this knowledge, a model is derived to predict the vertical front velocity and the front temperature.

3.5.1 Modeling equations

The solid phase energy balance of the combustion zone (see figure 3.12) is as follows:

$$\sigma e F(T_f^4 - T_0^4) + hA_s d_f(T_f - T_0) + \dot{q}_0'' = \dot{m}_c'' \Delta H \tag{3.7}$$

The first term is the radiative heat loss from the front to the fresh fuel, where σ is the Stefan-Boltzmann constant, e is the emissivity of the fuel bed which is assumed to be unity, F is the view factor between the combustion zone and the fresh fuel. Because these two phases touch each other, the view factor can be assumed to be unity as well. T_f is the combustion zone temperature, which is assumed to be uniform over the height of this zone, T_0 is the initial temperature. The second term is the heat lost by convective cooling from the primary air flow, where h is the heat transfer coefficient, A_s is the specific surface area of the fuel bed. The third term is the nett energy flux from the front to the surroundings, which can be the reactor or furnace. For the vertical propagation $\dot{q}_0''$ only consists of losses and this term will be positive. The left

hand side gives the heat gain, where $\dot{m}_c''$ is the char combustion rate in the combustion zone per cross sectional area of the reactor and ΔH is the heat of combustion of char to carbon monoxide. The combustion of the carbon monoxide, which is formed at the surface of the char, takes mainly place above the combustion zone (i.e. in the flame) and does not contribute to a higher front temperature.

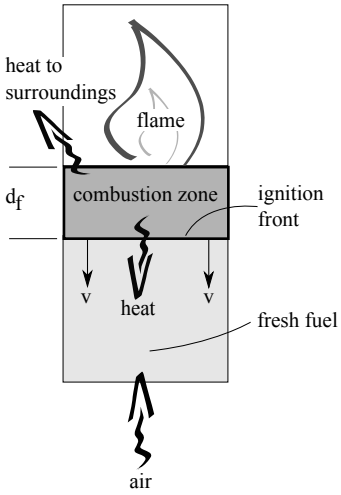

Figure 3.12: *Schematic overview of the combustion and ignition front.*

To solve this equation, the boundary condition at the lower boundary of the combustion zone can be used. At this boundary, the ignition takes place so it is called the ignition front. The boundary condition is as follows:

$$v_f \rho_s c_{p,s} (T_f - T_0) = \sigma e (T_f^4 - T_0^4) \tag{3.8}$$

The equation expresses that the heat needed to heat the fresh fuel to the combustion zone temperature equals the radiation from the combustion zone the this fresh fuel. In this equation, ρ_s is the packed fuel density, $c_{p,s}$ is the specific heat of the fuel and v_f is the ignition front velocity. Because this equation is an energy balance over an infinitely thin front, the convective cooling of the primary air flow can be neglected. To validate this relation,measurement data from Saastamoinen et al. [76], Fatehi and Kaviany [31] and Gort [39] are used. They measured the front velocity as well as the temperature in the combustion zone. Figure 3.13 shows the relation between the measured front velocities and the velocities predicted by equation (3.8). In about 80% of the cases the velocity predicted by equation (3.8) differs less than 20% from the measured velocity. It can be seen that the predicted velocities are generally higher than the measured ones. This is partly caused by the moisture contents

of the samples which is not included in equation (3.8). This comparison shows that equation (3.8) gives a reasonable relation between the front temperature and velocity.

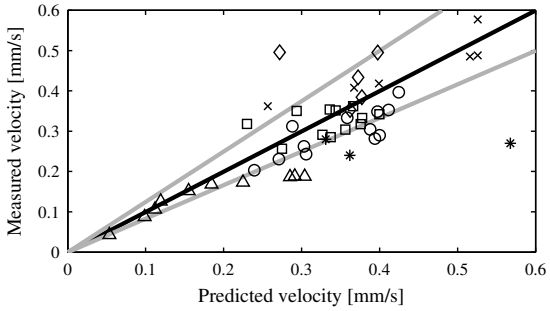

Figure 3.13: *The relation between the measured front velocities from [76, 31, 39] and the velocities predicted by equation 3.8. The black line denotes exact agreement and the two grey lines indicate* 20% *deviation.*

The two equations (3.7) and (3.8) have to be solved simultaneously to find v_f and T_f.

heat transfer coefficient

The heat transfer coefficient h can be found according to Bird et al. [17] as follows:

$$h = \frac{k(1-\varepsilon)}{d_p}\left(2.19Re^{1/3} + 0.78Re^{0.619}\right)$$
$$\text{with:} \quad Re = \frac{d_p Q}{\nu(1-\varepsilon)} \tag{3.9}$$

Here, ν is the kinematic viscosity of the air flowing through the bed, k is the thermal conductivity of the air and Q is the air flow rate. The term d_p is an equivalent particle diameter which is defined as:

$$d_p = \frac{6(1-\varepsilon)}{A_s} \tag{3.10}$$

It can be shown that for cubic particles the equivalent diameter d_p equals the particle diameter for a bed porosity of 0.67. This porosity is close to the porosities of packed fuel beds found in practice. For spheres, this relation is valid per definition.

front thickness

The optical experiments described in section 3.3.1 show that the glowing front thickness is in the order of the particle diameter. The models from Yang et al. [100] and

Shin and Choi [78] also show that the front thickness is in the order of the particle diameter. So as an approximation for the front thickness the equivalent particle diameter d_p from equation (3.10) is used.

$$d_f = d_p = \frac{6(1-\varepsilon)}{A_s} \tag{3.11}$$

The particle diameter now appears only in the heat transfer coefficient h and in the energy balance (3.7) and it can be seen that the particle diameter (or front thickness) is eliminated from the system of equations. The geometry of the particles appears in the system through the specific surface area of the fuel bed.

char combustion rate

The form of the char combustion rate $\dot{m}_c''$ is dependent on the overall equivalence ratio and can be expressed as:

$$\dot{m}_c'' = \begin{cases} f(K, h_{O_2}, Y_{O_2}) & \text{rich conditions (low air velocity);} \\ v_f \rho_c & \text{lean conditions (high air velocity).} \end{cases} \tag{3.12}$$

In the rich condition, the char combustion rate is a function of chemical kinetics, oxygen mass transfer and oxygen concentration. In rich conditions a char layer build up above the ignition and combustion front. This is described by Gort [39]. In lean conditions the combustion zone has a constant thickness. In this condition, the char combustion rate is determined by the front velocity.

heat losses to the surroundings

The heat losses to the surroundings are hard to determine exactly and depend mainly on the reactor design. The influence of the losses will be investigated with a sensitivity analysis.

radiation

The system of (3.7) and (3.8) can be solved analytically, but this will result in very complex expressions for v_f and T_f due to the fourth order temperature term in the radiation. To be able to solve this system analytically, the radiation term is approximated by second order accuracy. Note that the linearization used in equation (3.2) is not used in the model, because this would result in a temperature independent front

velocity. Experiments showed this is not the case and a linearization would be an over-simplification in this case.

$$\sigma e(T_f^4 - T_0^4) = \kappa(T_f - T_0)^2 \quad \text{with:} \quad \kappa = C\sigma e T_{f,avg}^2 \tag{3.13}$$

The result is a second order system, which can be solved easily. The term κ is the radiation approximation term. It can be shown that the constant C equals 1.65 for flame temperatures of 1350 K. To validate the approximation for the radiation, the results from the simplified model are compared to the exact results from equations (3.7) and (3.8) in figure 3.14. Both systems are solved numerical and only one situation is modeled and no losses are modeled. The figures are just to compare the second order simplification with the exact solution. It can be seen that the temperature is not influenced that much by the approximation. The velocity however, is changing more. This is due to the sensitivity of the front velocity on the temperature which is cubic. So a small change in temperature can lead to a significant change in velocity, especially for high temperatures. The error in the velocity is about 20% in this case. There are two reasons why this linearization is legitimate for predicting ignition front velocities:

- in the experiments on ignition front velocity, errors of around 20% are common;
- the losses to the surroundings are difficult to predict and measure. It will be shown later that the velocity can be predicted with about only 60% accuracy due to these unknown heat losses.

The drawback of this method is that the constant κ is a function of the variable $T_{f,avg}$ which is not known yet. An initial guess has to be made for κ to solve the system.

3.5.2 Dimensional analysis

Equations (3.7) and (3.8) can be solved simultaneously to find the combustion zone temperature T_f and the ignition front velocity v_f. The rearranged system is:

$$\begin{cases} T_f - T_0 = \dfrac{\dot{m}_c'' \Delta H - \dot{q}_0'' - \kappa(T_f - T_0)^2}{h A_s d_f} \\ \\ v_f = \dfrac{\kappa(T_f - T_0)^2}{\rho_s c_{p,s}(T_f - T_0)} \end{cases} \tag{3.14}$$

In the system, the primary air velocity is not included directly. However, the often measured relation between the primary air flow velocity and the front velocity (see

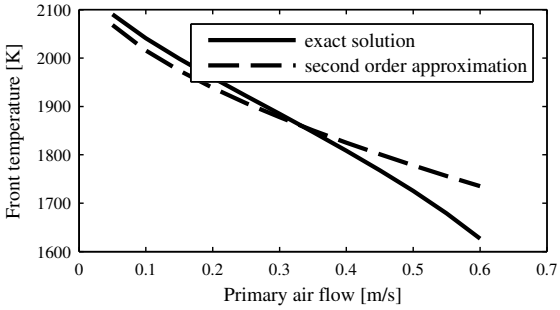

(a) Front temperature results of the exact solution and the second order approximation.

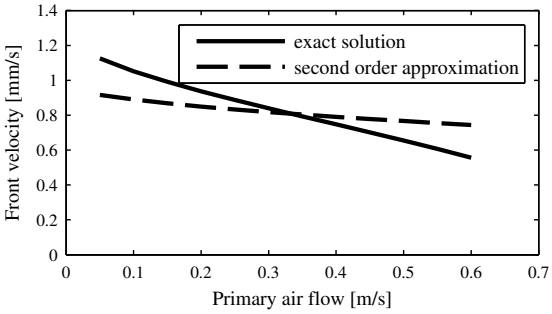

(b) Ignition front velocity results of the exact solution and the second order approximation.

Figure 3.14: *Front temperature results (a) and ignition front results (b) of the exact solution from equations (3.7) and (3.8) and the second order approximation from equation (3.13).*

for example [39, 76]) appears in the system through the heat transfer coefficient h, which is a function of the primary air velocity.

The variables T_f and v_f are made dimensionless as follows:

$$\begin{aligned} T_f &= T_0 \theta_f \\ v_f &= \frac{\kappa T_0}{\rho_s c_{p,s}} \psi \end{aligned} \tag{3.15}$$

In this equations, θ_f is the dimensionless temperature and ψ is the dimensionless ignition front velocity. When the initial system is expressed in the non-dimensional variables, the following non-dimensional system is the result:

$$\begin{cases} \theta_f - 1 = \dfrac{\dot{m}_c''(\psi)\Delta H - \dot{q}_0'' - T_0^2(\theta_f - 1)^2}{T_0 h A_s d_f} \\ \\ \psi = \theta_f - 1 \end{cases} \tag{3.16}$$

From the dimensionless system (3.16) it follows that only a solution for $\theta_f - 1$ has to be found to solve the system. So the system of two equations with two variables can be reduced to one equation with only one variable (ψ or $\theta_f - 1$) when the equation for ψ is substituted. The solution to this equation is:

$$\theta_f - 1 = \psi = -\frac{1}{2}Ex + \frac{1}{2}\sqrt{Ex^2 - 4Lo} \tag{3.17}$$

with:

$$\begin{aligned} Ex &= \frac{h A_s d_f}{\kappa T_0} - A\frac{\rho_c \Delta H}{T_0 \rho_s c_{p,s}} \\ Lo &= \frac{\dot{q}_0''}{T_0^2 \kappa} - (1 - A)\frac{Q \rho_a \Delta H_{CO} \varepsilon}{T_0^2 \kappa} \end{aligned} \tag{3.18}$$

For $A = 1$ the excess energy term Ex gives the energy that can be used for the front propagation and the loss term Lo gives the energy losses from the front. As stated before, the expression of the char burning rate is dependent on the stoichiometry of the combustion. For rich combustion (low air flow rates) A will be zero and for lean combustion A will be unity. It will be shown below that only the lean combustion ($A = 1$) is relevant in this case.

Experiments from Gort [39] show an ignition rate of around $0.07 kg/m^2 s$ for both 10 and 30mm cubes. At this ignition rate, the char ignition rate is $0.011 kg/m^2 s$ (with a fixed char content of 15%). For stoichiometric combustion, the air flow rate should be $0.12 kg/m^2 s$, which corresponds to an air velocity of $0.10 m/s$. Already for air velocities above $0.10 m/s$ the char combustion can be assumed to be lean. For this reason, only the lean combustion regime will be considered. In this regime, the heat loss term Lo is only dependent on the heat losses from the front to the surroundings. These losses will be influenced by the experimental conditions. However, the experimental setup primarily determines these losses. For this reason Lo is regarded constant for each experiment and ψ only varies with the excess energy term Ex for each experiment.

For the lean regime, the excess energy term Ex has to fulfill the following conditions:

$$-2\sqrt{Lo} < Ex < 0 \tag{3.19}$$

This can be explain as follows:

- If $Ex > 0$, the convective heat loss is larger than the heat produced by the reaction. No ignition will take place in this case.
- For $Ex < -2\sqrt{Lo}$, there exists no real solution for (3.17) can be found and extinction is the result. The physical background for this extinction will be shown later (eq. (3.20)). This requirement can also be stated as: $\psi > -1/2Ex$. Which is a useful boundary of operation.

There is only one requirement for Lo: $Lo > 0$. The heat lost from the system is represented by Lo, this heat loss can not be negative.

In the second criterion, $\psi > -1/2Ex$ is mentioned as a lower boundary for ψ. When the heat losses are zero ($Lo = 0$) the upper boundary for is found: $\psi < -Ex$.

From the viewpoint of process control, only a few parameters can be used to control the ignition front velocity: the heat transfer coefficient h, the initial temperature T_0 by using preheated primary air and the energy flux from the fuel to the surroundings $\dot{q}''_0$. The model seems not to depend on oxygen concentration in the primary air (if still in the lean regime). However, the heating of the inert nitrogen can be regarded as losses to the surroundings. So when the oxygen concentration is increased, it is to be expected that both the ignition front velocity and the combustion zone temperature increase. The other parameters are fuel properties which can not be changed online. However, the model shows that an increased char content results in an higher excess energy term. This will result in an higher ignition velocity. On the other hand, an increased product $A_s d_p$ results in a lower excess energy term and thus a lower ignition velocity and a higher chance on extinction.

3.5.3 Results

The model is validated with experimental data from Gort [39], Saastamoinen et al. [76] and Horttainen et al. [46]. These researchers measured the vertical ignition front velocities in a packed bed of wood for various wood types, particle sizes and primary air velocities. They all used lab-scale setups.

To validate the model with the measured front velocities, the measurement data have to be made dimensionless according to (3.15). For this, an approximation for the radiation approximation term κ (eq. (3.13)) has to be made depending on the average front temperature $T_{f,avg}$ which is not known in advance. The system has been solved iteratively to converge to matching values of κ and $T_{f,avg}$. This is due to the simplification made in (3.13) on the radiation term. The values of κ are listed in table 3.3 together with the relevant properties of the fuels from which the experimental data is used.

Table 3.3: *Relevant properties of the fuels used for validation. $\Delta H = 33\ MJ/kg$ and $\rho_c = 0.155\rho_f$ are used for the lower heating value of char combustion and char density respectively.*

Fuel type	A_s $[m^2/m^3]$	ρ_f $[kg/m^3]$	$c_{p,f}$ $[kJ/kgK]$	ε [-]	d_p $[mm]$	ref.	κ $[W/m^2K^2]$
cubes 10mm	200	200	2.7	0.7	9.0	[39, 14]	0.1600
cubes 30mm	70	200	2.7	0.7	25.7	[39, 14]	0.1680
spruce chips 5-20mm	251	157	2.7	0.62	9.1	[76, 14]	0.1790
chips 1x35mm	193	58	2.7	0.87	4.0	[76, 14]	0.1935
pellets 5mm	533	640	2.7	0.32	7.7	[46, 14]	0.1570
pine chips 5-20mm	171	145	2.7	0.71	10.2	[46, 14]	0.1550
shavings	945	120	2.7	0.74	1.7	[46, 14]	0.1765
pine chips 2 5-20mm	171	145	2.7	0.71	10.2	[46, 14]	0.1595
pellets 10mm	259	550	2.7	0.41	13.7	[46, 14]	0.1480

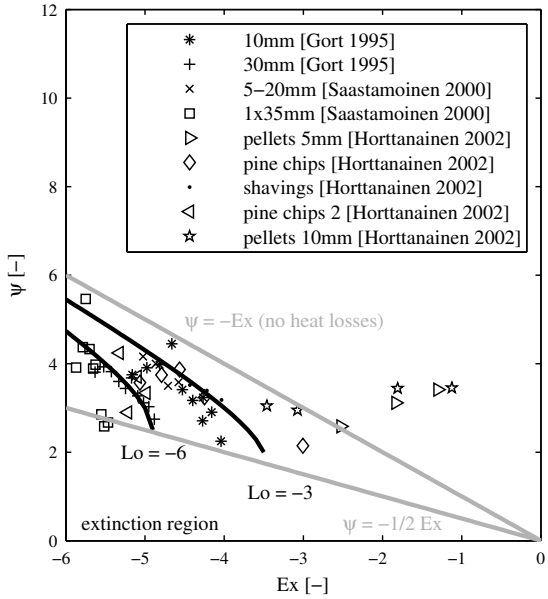

Figure 3.15: *The results from the model (eq. (3.17)) for the lean regime. Plotted is the dimensionless ignition front velocity ψ against the excess energy term Ex for several values of the heat loss term Lo. Experimental data from literature is included for validation. The region between the grey lines is the region in which a mathematical solution for ψ can be found and thus ignition may take place. (see text for explanation)*

The result from the model is shown in figure 3.15 together with the experimental results. The upper grey line gives the values for ψ (or $\theta_f - 1$) for $Lo = 0$. As described before, when $Lo = 0$, no heat losses are present. For vertical front propagation, this is the asymptotic situation and the dimensionless ignition front velocity ψ can not be in the region above this line. The lower grey line gives the lower boundary for ψ for which a real solution can be found from equation (3.17). This line results from the criterion $psi > -1/2Ex$ mentioned before. When the criterion for this line ($Ex = -2\sqrt{Lo}$) is rewritten with physical parameters (with the use of (3.15)) and the second equation of (3.16)) the following equation can be found:

$$v\rho_c \Delta H = hA_s d_f (T_f - T_0) + 2(T_f - T_0)\sqrt{\dot{q}_0'' \kappa} \tag{3.20}$$

The left hand side of this equation is the heat produced by the combustion of char. The first term of the right hand side is the convective loss and the second term is a kind of root mean square of the radiative (κ) and other heat losses ($\dot{q}_0''$). The equation shows that when the heat losses are equal to the heat produced by the combustion, the threshold for extinction is reached. This is physically correct. Also Shin and Chio [78] mention criteria for extinction. However, they only give qualitative relations.

Figure 3.15 shows that the experimental results should be between the two grey lines representing the upper and lower limit for the ignition front velocity.

The two black lines give ψ for a constant value of Lo. Because in the lean regime the heat losses are assumed constant for each experiment, the experimental results should follow the trends for constant values of the loss term Lo. The two data-sets from Gort [39] follow the trends reasonably good (at least for lower Ex). With exception from the 1x35mm particles from Saastamoinen [76] and the pellets of Horttainen [46] the data-sets from the other researchers follow the trends reasonably well. The difference between the model and the results from Horttainen can be explained by the fact that the pellets have a density of about twice the density of untreated wood. It is known that the thermal conductivity is linear dependent on the density. Besides, the packed pellets have a porosity which is twice as low as the other analyzed beds. This results in a lower radiation-conduction ratio (see (3.2)) and radiation is not the most important heat transfer mechanism anymore. The model under-predicts the values for ψ, which is expected.

In figure 3.16 a dimensional result is given. The front velocity v_f is plotted against the primary air velocity Q (appearing only through h). Results for four values of the term $\frac{\Delta H \rho_c}{\rho_f c_{p,f} T_0}$ are plotted. This term gives the ratio between the heat produced by the glowing char and the heat needed to heat up the fuel bed. For a fuel or a fuel mixture with a high volatile content (for example plastics) or a high inert content (for example glossy paper), this term decreases and the figure shows that the front velocity decreases. It is important to note that the total heating value of the fuel does not

determine the front velocity, only the heating value of the remaining char is relevant for the vertical front propagation.

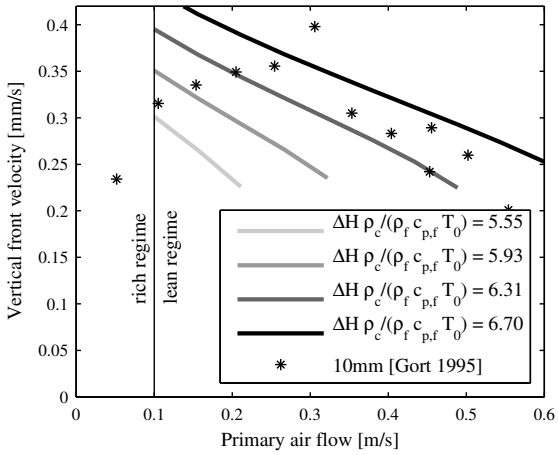

Figure 3.16: *The dimensional results from the model (eq. (3.17)) for the lean regime. Plotted is the dimensional vertical ignition front velocity v_f against the primary air velocity Q for several values of $\frac{\Delta H \rho_c}{\rho_f c_{p,f} T_0}$. Furthermore, $\kappa = 0.16$ and $\dot{q}''_0 = 60 kW/m^2$ are assumed.*

As in figure 3.15, the extinction region can be seen in figure 3.16 as well. For low values of $\frac{\Delta H \rho_c}{\rho_f c_{p,f} T_0}$ and high values of Q, no real solution for the front velocity could be found. The figure shows that in this case, the minimal front velocity is $0.2 m/s$. This value is also found by Gort [39] for 10mm particles with 10% and 30% moisture content.

heat losses

The value of Lo is dependent on the losses to the surroundings. These losses are mainly determined by the experimental setup, but also the fuel type has some influence. It is beyond the scope of this work to exactly determine the losses, so exact values of Lo are not presented for the experiments.

However, an estimate can be made for the inaccuracy of the model due to the unknown heat losses. If the system is close to extinction (relative high heat losses), the relation $Ex \approx -2\sqrt{Lo}$ holds. With (3.15) and (3.17) the following is valid close to extinction:

$$v_f = \frac{\kappa T_0}{c_{p,f} \rho_f} \sqrt{Lo} \tag{3.21}$$

From this, and the definition for κ (eq. (3.13)) and Lo (eq. (3.18)), the following relation holds:

$$v_f \sim T_{f,avg}^2 \sqrt{\dot{q}_0''} \tag{3.22}$$

From this relation, it can be seen that the dimensional velocity is quadratically dependent on the average dimensional front temperature. An estimate for the accuracy of the measured temperature would be 10%. This implies in an uncertainty for the velocity of about 20%. The linearization of the radiation which has been done before is shown to be within this uncertainty. If it is assumed that the major part of the heat losses are due to radiation, the velocity is even dependent on the fourth power of the temperature. In this case the uncertainty is even 40%. So an accurate front temperature is needed to quantify the front velocity with reasonable accuracy.

3.5.4 Application on two dimensional ignition front propagation

For the horizontal front propagation, two driving heat sources can be distinguished: (1) radiation from the char combustion to the virgin fuel and (2) radiation from above via the flame and furnace walls (see figure 3.17).

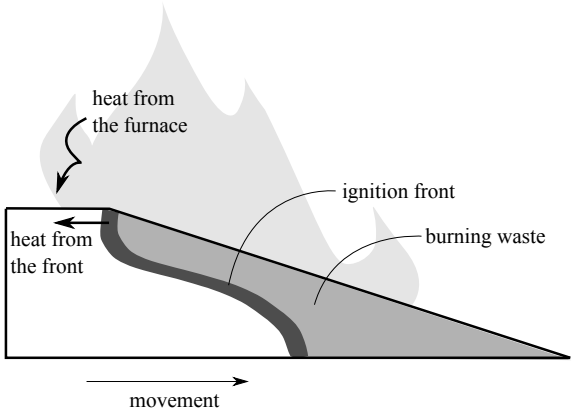

Figure 3.17: *The two heat sources for the horizontal front movement: (1) radiation from the char combustion to the virgin fuel and (2) radiation from above via the flame and furnace walls.*

If the radiation from the furnace is small, the char combustion is the driving mechanism for the horizontal front movement. In that case, the model presented in the sections before is also valid for the horizontal front movement.

On the other hand, when the radiation from the furnace walls is large, the fresh fuel will be ignited by this heat flow. Chapter 6 of this thesis deals with the piloted ignition

of solid fuels under a radiative heat flux. The results in this chapter show that with an radiative flux of $140 kW/m^2$ (calculated flux in the first zone [87]), the time needed to ignite 30% moist red oak is less than 30 seconds. This means that the waste almost directly ignites when it enters the furnace. In practice, this is not experienced. It is explained in chapter 6, that a critical primary air flow exists above which the fuel will not ignite. For a radiative heat flux of $140 kW/m^2$, this critical primary air flow is $0.02 kg/m^2 s$, which is smaller than the usually applied $0.3 kg/m^2 s$. This means that ignition can not be achieved by radiation of the furnace alone and the heat from the ignition front is important again.

3.5.5 Sensitivity analysis on the heat transfer coefficients

Because the radiative heat transfer plays an important role in this work, a sensitivity analysis on the parameter κ that is used to linearize the radiation term (eq. (3.13)) has been carried out. Besides, a sensitivity analysis on the heat transfer coefficient h has been carried out. The results of these sensitivity analyses are presented dimensional in figures 3.18.

The figures show that the solution is much more sensitive to a variation of the radiative heat transfer than it is for the convection. This is an expected result, since also Shin and Choi [78] predict the radiative heat flux to be about 4 times higher than the convective heat flux.

3.6 Application on full size waste and biomass incineration

The derived model can be used to control the combustion process in waste and biomass incineration plants. The lower limit of operation as can be seen in figure 3.15 can be used to prevent the flame to travel too close to the chute. It has been explained before that the horizontal front movement accounts for the flame stability.

For low radiative fluxes from the furnace to the fuel bed, the mechanisms for the front propagation in the two (or all) directions are the same and the horizontal and vertical ignition front velocity are more or less coupled. So when the flame travels to the entrance of the furnace, it is likely that the fire will reach the grate earlier. On the other hand, when the flame travels to the exit of the grate, probably the fire will reach the grate later. This can result in bad burnout. Besides, when the flame is at the backside of the grate, the time for the waste to achieve burnout is less. These two effects of a low ignition front velocity are important for the control of the combustion process.

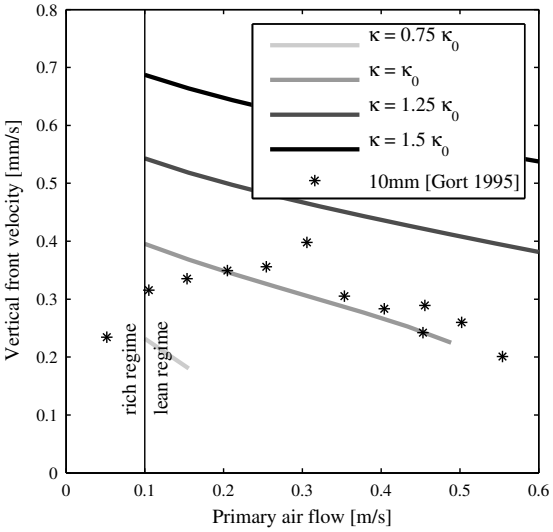

(a) The predicted influence of the radiative heat transfer κ.

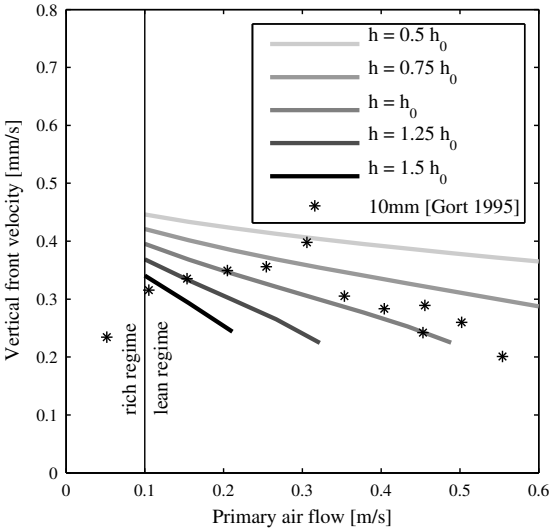

(b) The predicted influence of the heat transfer coefficient h.

Figure 3.18: *The dimensional front velocity as a function of the primary air flow velocity for varying values of* κ_{eff} *(a) and* h *(b).*

However, the application of the experimental and modeling results on a full size waste incineration process should be done with care. On these four main points a full size process differs from the experiments described in this chapter:

- inhomogeneous fuel (only for waste combustion);
- radiation from the hot furnace walls;
- moisture content;
- mixing.

These differences are elaborated in the next sections.

3.6.1 Inhomogeneous fuel

The inhomogeneity of the fuel can cause fluctuating front velocities in any direction. Ramström and Larfeldt [69] measured an unexpected high temperature on top of a 90% biomass and 10% plastics fuel bed close to the entrance of the furnace. This high temperature was found to be independent of the moisture content and may be caused by the easy ignition of plastics. Beside this, they found that the moisture is mainly present in the wood and that the plastics are almost dry. Also close to the entrance they measured relatively high grate temperatures. Their explanation is that spontaneous ignition occurs early on the grate. However, another explanation could be the easy ignition of the plastics as well, causing the ignition front to travel fast though the fuel layer to the grate.

Not only variations in chemical properties can influence the front propagation, but also variations in thermal properties can have an effect. The metals in the waste are highly conducting and this can result in a faster heat transfer to the fresh fuel and thus a faster ignition front propagation.

On the other hand, a moist area in the fuel bed can cause the front to slow down or even stop in either direction.

3.6.2 Radiation from the hot furnace walls

For low radiative heat fluxes from the furnace (for example in the two dimensional optical experiments) the leading mechanism for the front movement in the two directions is the radiation from the char combustion. As has been explained earlier in this chapter (derived from chapter 6), for high radiative fluxes from the furnace, the location of the ignition at the surface to the fuel layer is determined by the primary air velocity.

The furnace radiation is largely dependent on the furnace geometry. In case of a parallel flow furnace, the radiation to the fresh fuel will be considerably less than in a counter flow furnace. A realistic maximum wall temperature is 850^oC [50]. The temperature in the first zone in a counter flow furnace will be close to this value, but in a parallel flow furnace the wall in the first zone is most likely colder.

For the vertical ignition front movement, the furnace radiation is not important. Because the fresh fuel is covered with ash and glowing char, the furnace radiation can not reach the fresh fuel under the ignition front.

3.6.3 Moisture content

The presence of moisture is not included in the current model, but for relatively small moisture contents, the influence could be roughly approximated by decreasing Ex (in fact, decreasing $\Delta H/\rho_s$). Because the latent heat of evaporation is neglected by this method, this simplification is not suitable for larger moisture contents. However, figure 3.15 shows that for increasing moisture contents (decreasing Ex), the ignition fronts will be slowed down (following the constant Lo lines) and they will extinguished when Ex is too low. Extinction can also happen in the horizontal direction.

3.6.4 Mixing

In modern incinerators the mixing of the fuel bed on the grate takes place due to the movement of the grate. In lab-scale experiments in pot furnaces, no grate movement or mixing occurs and also the model does not include this. When mixing is considered, the convective transport of heat (by mixing the hot burning fuel with cold fuel) will be an important heat transfer mechanism and it can be even more important than radiation inside the fuel bed. The result is that in equations (3.7) and (3.8) the radiation term should be replaced by an effective convective heat transport term due to mixing. This term is dependent of the path and velocity of the fuel particles and. Warnecke [94] calculated that the waste makes a circular motion on a forward acting grate. This makes it difficult to estimate an effective convective heat transport term, because the locations of the "loops" should be known. The increased heat transport by mixing will increase the excess energy term (i.e. Ex will become more negative) and decrease the loss term Lo (see equation 3.18) and a larger front velocity will be the result.

3.7 Conclusions

When the furnace radiation is small, for both the vertical and horizontal propagation of the ignition front, the glowing char appears to be the main source of heat. As a consequence, the volatile combustion can be neglected completely which simplifies modeling significantly. A model is developed to predict the vertical front propagation velocity. The results from the model are compared to experimental results and the trends are predicted good. It is difficult to predict the actual experimental front velocities because of the unknown heat losses in the experiments. However, an upper and a lower boundary for the front velocity are derived. Because the ignition propagation mechanisms are the same for both directions, the model can be applied for simulating front propagation velocities in all directions. For high furnace radiation, the front location at the surface of the fuel bed is determined by the primary air velocity.

4

Spontaneous ignition experiments

A fuel bed can be ignited by blowing preheated air through it. This chapter presents experiments on this process. The minimum air temperature needed to ignite packed beds of wood, char and RDF are measured. This temperature is called the critical air temperature. Also the bed temperature at ignition and the time to ignition are measured. This temperature is called the spontaneous ignition temperature. The influence of moisture content, particle size and the air velocity are investigated. Wood chips are shown to ignite under an preheated primary air flow of $230 - 245^{o}C$ *and char at an air flow of* $170 - 200^{o}C$*. Increasing the primary air velocity results in both an increased critical air temperature and spontaneous ignition temperatures.*

4.1 Introduction

Combustion of municipal solid wastes on a grate is one of the dominant processes in municipal solid waste combustion (MSWC). However, grate firing is not only used for MSWC but also for combustion of other solid fuels, such as wood and other biofuels, e.g. straw or chicken-manure, to produce heat and power. For optimal process control, it is vital to understand the burning process inside the bed [90].

Many MSWC suppliers are using preheated primary air to be able to burn wet fuels or accelerate the ignition of the waste [89]. For primary air with temperatures up to 150^oC only drying of the fresh waste occurs. For higher temperatures, drying and pyrolysis can occur simultaneously and this can lead to spontaneous ignition [20]. By preheating the primary air to temperatures above 150^oC, the waste can deliberately be ignited in the zones where this is needed. On the other hand, by using preheated air, the waste can be ignited undesirably in zones where ignition is unwanted (for example close to the entrance of the grate). To be able to control the ignition of a fuel bed by preheated air, the effect of some key parameters such as primary air flow rate and temperature are investigated in this work. Besides, mechanisms which are responsible for the spontaneous ignition of the fuel bed by preheated air are investigated.

In the present work spontaneous ignition is defined as the transition from a negligible or slow fuel reaction rate to a rapid oxidation of either the volatiles or the solid fuel without the presence of an external source such as a spark or a flame. The sudden rise in temperature of the bed is used as an indicator to describe this phenomenon. The lowest bed temperature from which this rise starts, is called the spontaneous ignition temperature. The minimum air temperature needed for spontaneous ignition to occur is called the critical air temperature and the elapsed time required to suddenly rise the temperature is called ignition time.

Not much research is done on this topic. Van Kessel et al. [89, 90] investigated the combustion of waste with preheated primary air in a lab scale batch reactor. They mention the possibility of spontaneous ignition of waste at air temperature of 180^oC and they disprove the theory that this is caused by recondensation of moisture on relative dry parts of the waste. However, no further attention is paid to this phenomenon. Also research is done on the ignition of single particles in a heated air stream by Kuo and Hsi [54], but this work focuses on the mode of ignition (flaming or glowing) and the ignition time at temperatures between 400^oC and 600^oC. They do not deal with the lowest air temperature at which ignition occurs. The research which shows the most resemblance with the present work is the research on self-heating, self-ignition and thermal runaway done by Semenov [77] and Frank-Kamenetskii [33]. Often their analyses are applied to the ignition of coal and char [61] and cellulosic

materials [83]. These works show that coal can spontaneously ignite with ambient temperatures well below 100^oC. Cellulosic materials need a higher temperature to ignite. Times to ignition are in the order of days or even longer. In our work, the used temperatures are higher and different processes will occur.

Since the combustion characteristics are difficult to measure in full-scale plants, the moving bed is simulated by a batch type fixed bed reactor. Although the heat and mass transfer in transverse direction and additional particle mixing by the grate bars affect the local combustion performance, the heat and mass transfer in vertical direction is the dominant factor (see chapter 3). Therefore, a lab scale packed bed reactor in the form of a pot furnace can be used as a simplified system to simulate the moving bed. The time elapsed in the fixed bed corresponds to the residence time of fuel in the moving bed as has been described by Gort [39].

This chapter presents the effect of primary air flow velocity, particle size, moisture content and addition of inert to the fuel bed on the spontaneous ignition behaviour of several solid fuels. Because MSW is very inhomogeneous in both composition and particle size it is difficult to investigate the influence of fuel parameters on the ignition behaviour, wood is used as a model fuel. To see the effect of the volatile content, char is used as a model fuel as well. The inhomogeneous character of MSW is investigated in the experiments by using RDF.

In this chapter, firstly an analytical evaluation of spontaneous ignition is given. This evaluation is based on Semenov's analysis of thermal explosions [77]. Secondly, the experiments which are carried out are described and the results from these experiments are presented and discussed. Then the results of the experiments are evaluated in the light of the theoretical background and Semenov's analysis is applied to predict the spontaneous ignition and critical air temperatures for wood. Finally some conclusions on the experimental observations and the model results are drawn.

4.2 Spontaneous ignition theory

Semenov's analysis of thermal explosions [77] is used as a theoretical background on spontaneous ignition of packed beds. In Semenov's analysis, the radial (or horizontal) temperature gradients are assumed to be flat, but this will not be the case in a waste incinerator. However, when a small part of the waste layer is considered (for example the drying zone where preheated primary air is usually applied) the horizontal temperature gradient can be assumed to be flat in that area. Note that in the classic Semenov's analysis, the system transfers heat to the surroundings through the reactor wall of which the thermal resistance is much lower than the one of the fuel bed. In our case, the system interacts with a uniformly preheated airflow over the total sur-

face area of interest, so this system can be treated as zero dimensional. To be able to properly use Semenov's analysis, the outer temperature of the particles should not differ too much from the interior temperature. In the experiments used to measure the ignition temperatures of wood a slowly increasing air temperature is used. Due to this slowly increasing air temperature the times to ignition (at least 40 minutes) are much longer than the time for the core of the $1cm$ thick particles to heat up to 225^oC with an air temperature of 230^oC (about 3 minutes). This shows that at the moment of ignition the temperature inside the particles can be regarded uniform.

The base of this analysis is formed by an energy balance of the fuel bed. In our case, this balance consists of two parts:

- The heat generated by exothermic pyrolysis or oxidation of the fuel;
- the convective heat transfer between the primary air flow and the fuel bed.

In figure 4.1 these two energy streams are plotted as a function of the fuel bed temperature. The thick curved line denotes the heat generated by the reactions (q''_{react}). It is assumed that the reaction rate is controlled by the kinetics. For low temperatures this is a valid assumption. The three parallel straight lines denote the convective heat transport from the fuel bed to the air stream for three primary air stream temperatures (q''_{conv}). These lines cross the x-axis at the air temperature (T_0). When q''_{conv} is negative, the fuel bed is heated by the primary air flow.

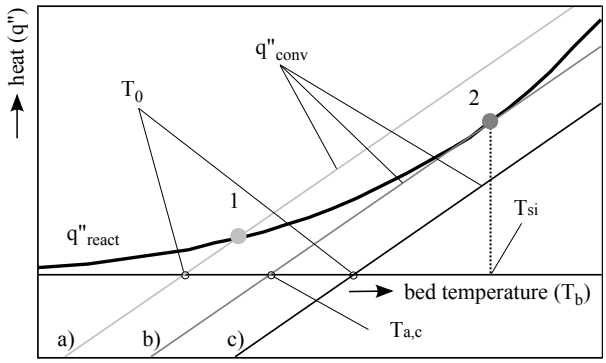

Figure 4.1: *Heat produced by the reaction (thick curved line) and the heat lost (positive values) or gained (negative values) due to convective heat transfer by the air stream for three values of T_0. Adopted from [77].*

Depending on the air temperature, ignition might take place or not. In situation a) in which the air temperature is too low to ignite the fuel bed is denoted by the light grey line. At the start of this situation, the temperature of the fuel bed is low and the

hot air stream heats the fuel bed. The reaction is still very slow and not much heat is produced by the reaction. When the temperature of the fuel is higher than T_0, the air stream cools the fuel. However, the heat produced by the reaction is larger than the heat lost to the air stream and the fuel will continue to heat up. When the fuel passes point 1, the heat lost to the air stream gets larger than the heat produced by the reaction and the fuel will be cooled by the air stream. Point 1 is a stable point and it has to be noted that the temperature in this point is higher than the temperature of the air stream even if there is no ignition.

When the air stream temperature (T_0) is chosen high, the heat lost to the air stream is always smaller than the heat produced by the reaction and ignition will occur. This is situation c) in figure 4.1. However, the moment of ignition can hardly be determined and thermal runaway is encountered from the moment the experiment starts. Thermal runaway is the situation where the heat gains are larger than the heat losses. An increase in temperature is the result. So in that sense, ignition occurred from the very moment the experiment started.

The threshold for ignition is given by situation b) (the dark grey line). The heat lost by the air stream is never larger than the heat produced by the reaction, so eventually ignition will occur. This situation gives the lowest air stream temperature at which ignition will occur. The temperature at point 2 is a critical temperature and the air temperature T_0 corresponding to this situation is the critical air temperature (T_{crit}). It has to be noted that at point 2, the slopes of the two lines are equal and a small deviation in either the reaction heat or the convective heat transport can result in a relative large difference in the spontaneous ignition and critical air temperature.

It is possible to change the convective cooling by altering the heat transfer coefficient. This can be done by changing the flow velocity of the air stream. When this velocity is increased, the heat transfer coefficient will increase as well and the heat lost by convective cooling will be more (the straight lines in the figure will become steeper). A higher T_0 is needed to ignite the fuel. When the air velocity is very low, the reaction rate for oxidation reactions (such as char combustion) will be determined by mass transport and this analysis will not be valid anymore. Besides changing the air velocity, also the particle size can be changed to influence the heat transfer coefficient. For smaller particles, the heat transfer coefficient will be higher and again a higher T_0 is needed to ignite the fuel bed.

4.3 Experimental

4.3.1 Experimental setup

The experiments were carried out at the laboratories of the Dutch research institute TNO in Apeldoorn. The schematic diagram of the experimental apparatus is shown in figure 4.2, the reactor is a lab scale packed bed reactor. The height of the reactor is $1350mm$ with an inner diameter of $150mm$. The reactor is insulated with glass fiber on the outside. The grate is located at the bottom of the reactor and consists of a distributor plate made of ceramic. Four thermocouples (Pt/Rh, type S) are used to monitor the temperature of primary airflow and temperature inside the bed at different heights. The primary air can be heated up to 275^oC and the air flow rate can be given up to $50m^3/h$. Every 20 seconds temperature and flow rate signals are send to a computer. The primary air is fed from the bottom of the fixed bed reactor through the grate. The air is preheated by an electric heater, installed in the supply line. The reactor is placed on a balance to monitor the mass of the fuel bed. Samples of the flue gases are extracted and analyzed.

The lower two thermocouples are positioned in the bed close to the grate. The thermocouples are protected from convection as well as radiation (after ignition) by small tubes covering the end of the thermocouples.

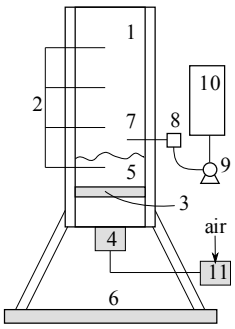

Figure 4.2: *Schematic overview of the experimental setup. 1-reactor; 2-thermocouples; 3-grate; 4-air flow heater; 5-fuel bed; 6-balance; 7-gas suction probe; 8-heated sample line; 9-suction pump; 10-gas analyzers; 11-air flow controller.*

4.3.2 Materials

Wood chips

The wood chips consist of a mixture of wood species resulting from forest cutting. Wood mainly consists of cellulose, hemicellulose and lignin and in general they cover respectively $40-60$, $20-40$ and $10-25 wt\%$ [96]. The pyrolysis and combustion processes of wood are complex because of the simultaneous degradation of the three components. The decomposition temperature range of the components is $315-400^oC$, $220-315^oC$ and $150-900^oC$, respectively [96]. Because lignin has such a wide temperature range for decomposition, it decomposes less easily than hemicellulose and cellulose. For temperatures below 300^oC the wood decomposition is mainly attributed to hemicellulose.

For some experiments, the wood chips moisture content has been changed to the desired value to study the effect of moisture content on the critical air temperature and spontaneous ignition temperature. This is done by adding some water assumed that by means of diffusion it will spread through the wood homogeneously [20].

The proximate and ultimate analysis of the wood chips is given in table 4.1 and in figure 4.3 a picture of the wood chips is shown. Because the wood chips are shredded forest residue, the composition can vary. The largest dimension of the chips is about $40mm$.

Table 4.1: *Proximate and ultimate analysis of the wood chip, wood charcoal (from literature) and RDF.*

	wood chips	char [37]	RDF
%C	50.0	92	50
%H	6.56	2.45	6.5
%O	41.5	3	30
%N	0.34	0.53	0.8
%S	0.29	1	0.3
%vol.	82.34	9.4	75
%ash	1.38	1	
%moist (a.r.)	9	6.0	3
H_b $[MJ/kg]$ (d.b.)	19.9	34.4	21
H_l $[MJ/kg]$ (d.b.)		33.9	20

Figure 4.3: *Some of the used fuels. Upper left to right: small char (*$10-15mm$*), medium char (*$15-30mm$*), large char (*$30-40mm$*). Lower left to right: wood chips (*$10-40mm$*), stones (*$10mm$*).*

Char

Two types of wood char have been used in the experiments. The first type of char is called commercial char. This char is generally used in barbeque's. The exact production process and the initial material are unknown but it is known that the fixed carbon content of this char is at least 82%. To study the particle size effect it has been manually cut into the desired size (small: $10-15mm$, medium: $15-30mm$ and large: $30-40mm$).

The second type of char is called lab char. This type of char is made in our laboratory by keeping the wood chips in nitrogen at 350^oC for three hours. The resulting char has a volatile content of around 40%, which is notably higher than the volatile content of the commercial char.

The commercial char as well as the inert material used in the experiments are illustrated in figure 4.3. In table 4.1, the proximate and ultimate analysis of char is given.

Refuse derived fuel (RDF)

Refuse derived fuel is made of the paper, plastics, wood and other organic components from municipal solid waste. The components are dried and pelletized to pellets

of 16 – 18mm. The proximate and ultimate analysis of the used RDF is listed in table 4.1.

4.3.3 Experimental procedures and programme

All the experiments with wood and commercial char have been performed with 300 gram and 250 gram of fuel, respectively. To find the critical primary air temperature and the spontaneous ignition temperature the following three methods can be used:

Constant temperature method; in this method the air is heated quickly to a constant value. When no ignition takes place, the fuel is removed and a fresh batch is put into the reactor. A new experiment is started with a slightly higher air temperature. When ignition is found, the current air temperature is the critical one. This method is suited to find the critical air temperature and the ignition time. However, for wood and char, the spontaneous ignition temperature can not be found with this method. This will be further explained in section 4.5.1. The RDF, lab char and some wood experiments are carried out with this method.

Slowly increasing temperature method; this method is basically the same as the previous one. However, the air is heated slowly to the desired value. Consequently, with this method it is not possible to determine the ignition time. In contrary to the previous method, this method is suitable to find the spontaneous ignition temperature. Besides, the critical air temperature can be found as well. The char experiments are done following this method.

Stepwise increasing temperature method; in contrary to the other two methods, in this method the fuel is not removed from the reactor when no ignition takes place. Instead the air temperature is increased by steps of 10^oC when no ignition takes place. With this method the spontaneous ignition temperature and the critical air temperature can be found. It has to be made sure that the temperature history does not influence the results. For wood this is the case and this method gives the same results as the previous method. This method is used in the wood experiments.

More comments on the effect on the ignition parameters of the three methods will be given in section 4.5.1.

To study the effect of primary air flow velocity on the critical air temperature and spontaneous ignition temperature a number of experiments have been carried out at five air flow velocities (0.1, 0.2, 0.3, 0.4 and $0.5 m/s$). Besides, the effect of inert in the fuel has been investigated by substituting a portion of the sample with inert (stone).

Finally, to see the effect of the size of the commercial char particles on the critical air temperature and on the spontaneous ignition temperature and time, three sample sizes are prepared (small, medium and large) by manually cutting the char into the desired size. Overall, more than 100 experiments have been carried out.

4.4 Results and discussion

4.4.1 Wood experiment results

The effect of primary air flow velocity

Figures 4.4(a) shows the spontaneous ignition temperature for wood as a function of primary air flow velocity at a constant moisture content. Figure 4.4(b) shows the critical air temperature. It can be seen that both the critical temperature needed for spontaneous ignition to occur and the spontaneous ignition temperature increase with increasing primary air flow velocities. This is an expected result, since for higher air velocities more heat is lost to the air flow due to a better convective heat transfer and a higher air temperature is needed to ignite the wood. This is also described in section 4.2. With the constant temperature method, the ignition time is found to be around 5 minutes (see figure 4.15).When no ignition took place, the bed temperature was about 5^oC higher than the air flow temperature for all air velocities. This indicates there is an exothermic process going on indeed. Despite this exothermic process, no thermal runaway is encountered. This situation is denoted by point 1 in figure 4.1.

Especially for the lowest air flow velocity, the scattering of the data considerable. This can be caused by the sensitivity of the location of point 2 in figure 4.1 as is explained in section 4.2. When the air flow is low, the heat transfer coefficient is low as well and the lines denoted by q''_{conv} in figure 4.1 are close to horizontal. The more horizontal the lines are, the bigger the effect of a minor deviation of the reaction heat or convective heat transfer are. In general for wood the reproducibility of the results is fairly good and the measurements are all within 10% deviation.

The effect of inert in the sample

Experiments have been performed to investigate the effect of inert on the spontaneous ignition temperature of the wood. For this purpose, stones are used as inert mixed with wood chips in 20 and $40 wt\%$ (inert) proportion for air flow velocities of $0.2 m/s$ and $0.3 m/s$. The results are compared to the normal situation without inert.

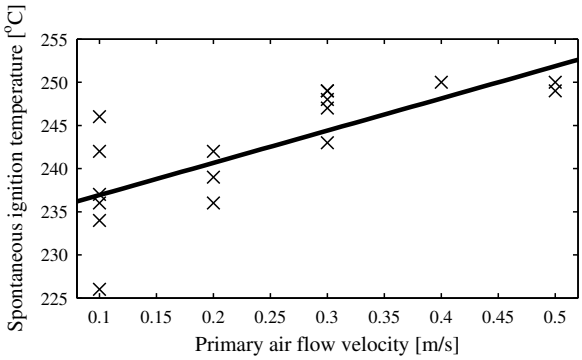

(a) Spontaneous ignition temperature

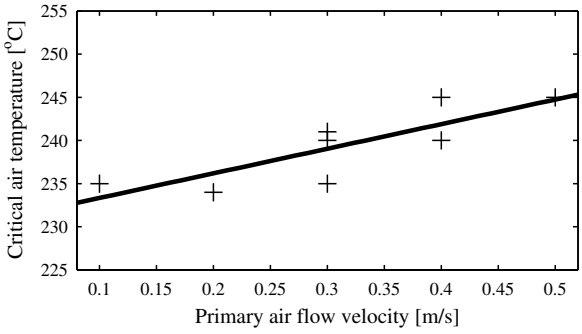

(b) Critical air temperature

Figure 4.4: *The measured spontaneous ignition (a) and critical air temperature (b) for wood chips as a function of the air flow velocity.*

As it is depicted in figures 4.5(a) and 4.5(b), increasing the percentage of inert in the mixture will increase the spontaneous ignition temperature and critical air temperature. This is due to the fact that the inert absorbs more energy given by the primary air without producing heat. To compensate that and to start the ignition more energy is needed, so the ignition temperature increases. This can also be explained with the help of figure 4.1: by adding inert to the fuel bed, the heat produced by the reaction decreases. This means that the line q''_{react} in figure 4.1 will be less steep and a higher air temperature is needed to ignite the fuel. Also the spontaneous ignition temperature (point 2) will be higher. For the last mixture of inert with wood chips ($40wt\%$), ignition occurs late for an air flow velocity of $0.2m/s$ and no ignition occurs for the air flow velocity of $0.3m/s$ within three hours. This is probably caused by the fact that, at higher flow velocities the loss due to the convection are higher than at lower air flow

velocities.

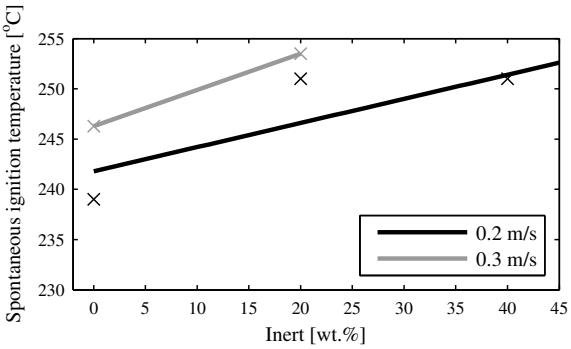

(a) Spontaneous ignition temperature

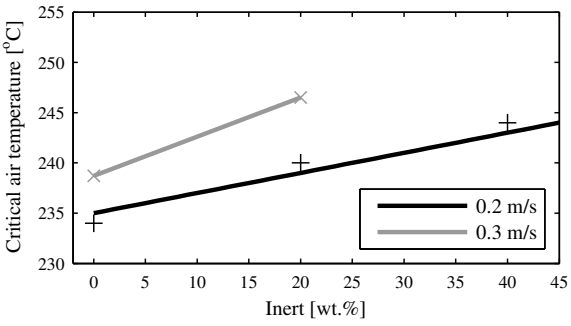

(b) Critical air temperature

Figure 4.5: *The measured spontaneous ignition (a) and critical air temperature (b) for wood chips as a function of the mass percentage inert for two air velocities.*

The effect of moisture

To investigate the effect of the moisture on the spontaneous ignition temperature of wood chips samples, the wood chips samples were moistened by spraying the needed amount of water on it and storing them for two days to make the water diffuse through the sample. Experiments with a fuel moisture contents of $9-12.7$, $18-20$, 30 and $50 wt\%$ have been carried out. In all experiments with a moisture content of the wood lower than $50 wt\%$ comparable critical air and spontaneous ignition temperatures have been found.

However, no ignition could be obtained for wood chips with a moisture content of 50% on a 150 minutes experiment. The grate temperature was only 1^oC higher than the primary air temperature compared to the results for dryer samples which were $5-7^oC$ higher. As the evaporation of the moisture needs energy, the exothermic devolatilization is inhibited. Yet, if the fuel bed had been kept for a longer time at this condition, (temperature and air flow velocity) it would probably have been ignited.

On the whole, with these moisture contents only a few experiments have been performed, therefore, it is not possible to get a reliable relationship between the fuel moisture content and spontaneous ignition temperature. However, after the moisture is evaporated, the particles can be assumed to behave as dry particles so it is reasonable to expect no change in spontaneous ignition and critical air temperatures with varying moisture content. Only the ignition time is likely to change due to the longer evaporation stage.

4.4.2 Char experiment results

An understanding of the oxidation rate of chars at low temperature is important for predicting self-heating and spontaneous ignition temperatures. Factors affecting the spontaneous ignition of char that have been investigated are: the primary air flow velocity, primary air temperature, particle size, the production method of the char and the addition of inert to the sample.

In figures 4.6 and 4.7 a typical constant temperature measurement result for the experiments for char can be seen. Figure 4.6 shows the mass of the char and the bed temperature during the experiment and figure 4.7 shows the concentrations of several components in the flue gas. It takes some time before the gas samples reach the analyzers, so there is a delay in the measured gas concentrations. In this case, the measurement for the bed temperature shows an ignition time of 1.5 minutes, which is significantly shorter than the ignition time for wood, which was 5 minutes (see figure 4.15). Ignition can be identified by the increase in temperature from figure 4.6, but also the sudden decrease of O_2 and the increase in CO_2 show that combustion is taking place (figure 4.7). Because the gas analyzer was located in a different room, there is a significant time delay for the gas analysis results. Note that these results are obtained by a constant air temperature. The spontaneous ignition and the critical air temperature are obtained by using a slowly increasing air temperature.

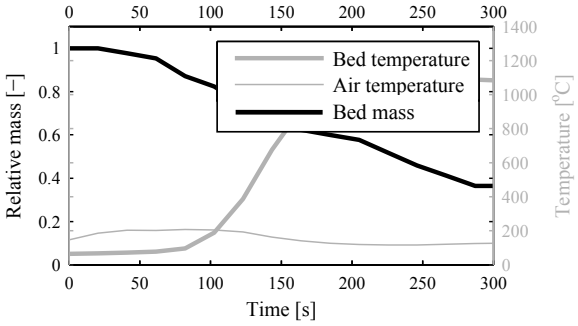

Figure 4.6: *Measured bed mass (black line) and air and bed temperatures (grey lines) as a function of time for lab char. The superficial air velocity is* $0.1\,m/s$ *and the air temperature is* 200^oC.

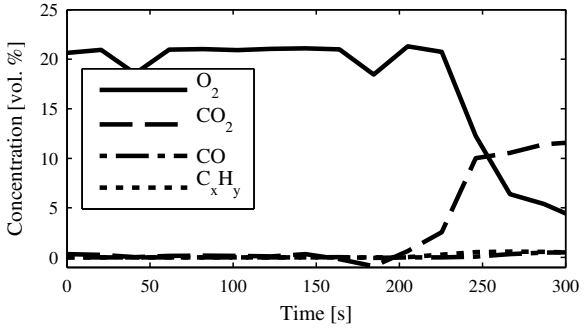

Figure 4.7: *Measured concentration of* O_2, CO_2, *CO and* C_xH_y *as a function of time for lab char. The superficial air velocity is* $0.1\,m/s$ *and the air temperature is* 200^oC.

The effect of primary air flow velocity

The effect of the air flow velocity on the spontaneous ignition characteristics of commercial char samples has been examined. Figure 4.8(a) shows the measured spontaneous ignition temperature of medium size char particles. Because for char, most of the experiments are slowly increasing temperature experiments, the critical air flow temperature is determined in an other way compared to the wood experiments. Figure 4.8(b) shows the minimum measured (out of minimal four experiments for each air velocity) air temperature at which ignition occurs. It also shows the maximum air temperature at which no ignition occurs. The reproducibility of the results for char are not as good as the ones for wood.

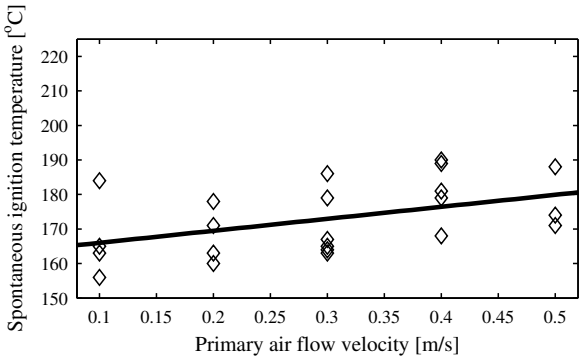

(a) Spontaneous ignition temperature

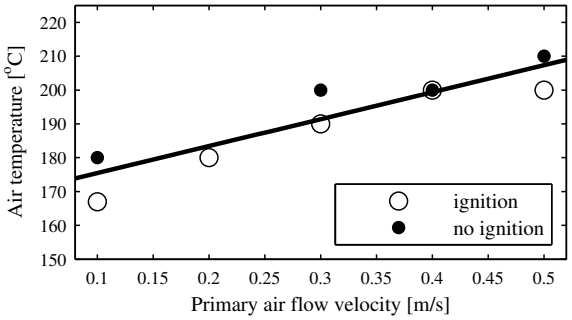

(b) Minimum measured air temperature at which ignition did occur (open symbols) and maximum measured air temperature at which ignition did not occur (closed symbols).

Figure 4.8: *The measured spontaneous ignition (a) and critical air temperature (b) for commercial char as a function of the air velocity.*

The figures show that both the spontaneous ignition and the critical air temperature for char are significantly lower than the ones for wood. This is probably caused by faster exothermic reaction mechanisms for char at lower temperatures. As can be seen in figure 4.8(a), the spontaneous ignition temperature of the commercial char increases with the flow velocity. For high air flow velocity experiments, the air temperature reaches the set air temperature in the heat controller quickly though, the heat transfer to the char and even more important: inside the char, may not be that quick due to a high Nusselt number. This means that the inside of the particles is still cold and no reaction takes place there yet, while the temperature of the outside of the particles (which is the measured temperature) can be high already. For low

air velocities, the Nusselt number is smaller and the temperature distribution inside the particles will be more constant. This means that for relative low measured outer temperatures the particles will be able to start the runaway reactions.

Despite the clear trend, not all batches of char have behaved the same. From figure 4.8(a) it can be seen that when ignition takes place, this is in all cases at a temperature below 190^oC. However, some batches of char did not ignite, even when the bed was at a temperature of 250^oC. This means that not all batches of char are the same and may be a small variation in geometry or mineral content results in a significant different ignition behaviour. It is also remarkable that the lowest temperatures at which ignition occurred in figure 4.8(b) are always lower (or equal for $0.4m/s$) than the maximum temperature at which ignition did not take place. This shows that the reproducibility of the char experiments is low, probably due to variations in the composition and geometry of the char. With MSW the reproducibility can be expected to be even lower. With this knowledge, the trend line in figure 4.8(b) has to be interpreted as the minimal air temperature at which spontaneous ignition could occur.

When no ignition took place, the bed temperature of the char was lower than the air temperature. This indicated that there is an endothermic process going on at temperatures lower than the spontaneous ignition temperature.

The effect of addition of inert to the sample

To see the effect of inert on the spontaneous ignition, again the two flow velocities (0.2 and $0.3m/s$) with small particle size have been considered. As it is depicted in figure 4.9, an increase of the spontaneous ignition temperature with increasing inert content has been measured. This is caused by the absorption of heat by the inert fraction thus decreasing the available amount of energy to start the spontaneous ignition. Ignition did not occur for an air velocity of $0.3m/s$ and 40% inert.

The effect of particle size

The particle size of commercial char may be an important factor in determining whether or not spontaneous ignition occurs. In general, the rate of oxidation is depending on the external surface area per unit volume of the coal particles which increases with decreasing particle size.

It is measured that the spontaneous ignition temperatures for small size particles are about 5^oC lower than those for medium size particles. The lower spontaneous ignition temperatures may be caused by a larger specific external surface area of the

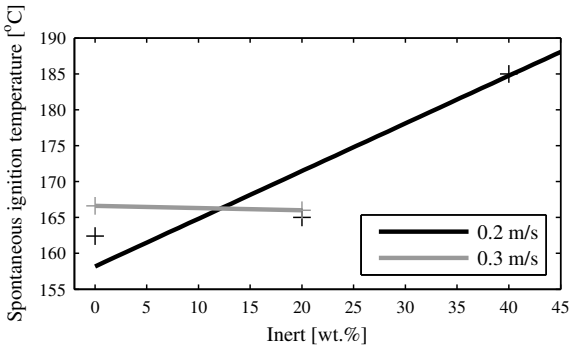

Figure 4.9: *Measured spontaneous ignition temperatures for small size commercial char as a function of the mass percentage inert for two air velocities.*

smaller particles, resulting in faster oxidation of the char. However, the difference is too small for detailed conclusions.

4.4.3 RDF experiment results

In figure 4.10 typical experimental results for RDF can be seen. The ignition time in this experiment is about 40 minutes, which is an order longer than in the case of wood and char. This can be caused by the fact that the RDF has a higher density ($500 kg/m^3$ versus about $200 kg/m^3$ for wood and even less for char), so the RDF does not heat up as fast as wood or char. The air temperature does not have a clear influence on the ignition times, however, when the air velocity is reduced to $0.1 m/s$, the the ignition times are around 80 minutes. This supports the idea that the heating of the fuel determines the ignition time, not the kinetics.

For RDF there is a typical pre-ignition stage which lasts from 2000 seconds until ignition at 2250 seconds in this case. This behaviour is probably caused by the different decomposition mechanisms for the several components found in RDF.

Figure 4.11(a) shows the spontaneous ignition for RDF as a function of primary air velocity. Figure 4.11(b) shows the critical air temperature as a function of the air velocity. Like with wood and char, the increasing trend with air velocity is observed here. It is noted that the spontaneous ignition temperature cannot be determined precisely due to the pre-ignition stage. However, figure 4.10 shows that the bed temperature is higher than the air temperature at ignition.

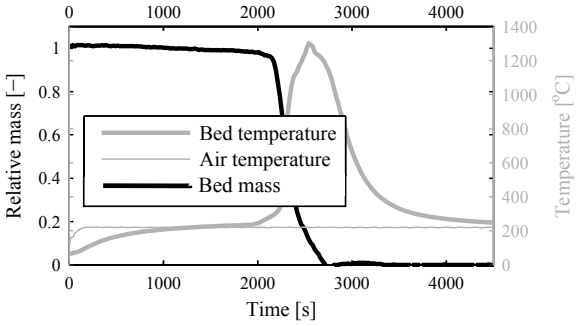

Figure 4.10: *Measured bed mass (black line) and air and bed temperatures (grey lines) as a function of time for RDF. The superficial air velocity is* $0.3 m/s$ *and the air temperature is* $220^{o}C$.

4.4.4 General experimental observations

In this section, some qualitative observations that are made during the experiments are described.

When two equal experiments with wood chips were carried out successively, an increase in critical primary air temperature and spontaneous ignition temperature has been noticed in the second experiment. The effect is even stronger if the first experiment is done with low air flow velocities. During inspection of the reactor, it is noticed that a significant amount of unburned volatiles condensed on the reactor wall. Subsequently, in the second experiment, the condensed tars will consume energy to evaporate and a higher temperature is needed to provide enough energy to ignite the fuel. For further investigation, two consecutive experiments with two air flow velocities (0.2 and $0.3 m/s$) have been carried out. It is found that both the critical air temperature and the spontaneous ignition temperature are in general $5^{o}C$ higher when a wood experiment is preceded by another wood experiment. To avoid this memory effect, the first wood experiment is followed by a char experiment to burn the condensed tars from the reactor wall. The char is only used to clean the reactor and no data is used from these runs. It has been shown that the measured temperatures for wood are more reproducible when an experiment with char is performed between the two wood experiments.

In some of the commercial char experiments, a significant delay of the spontaneous ignition has been observed. In general, for all experiments the initial ignition does not occur at the exact location of one of the thermocouples inside the fuel bed. In this case the ignition front has to travel a certain distance through the bed to be sensed by one of the thermocouples and the measured ignition time will be an over-estimation.

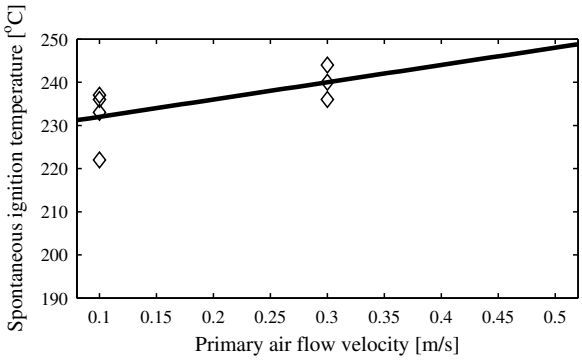

(a) Spontaneous ignition temperature

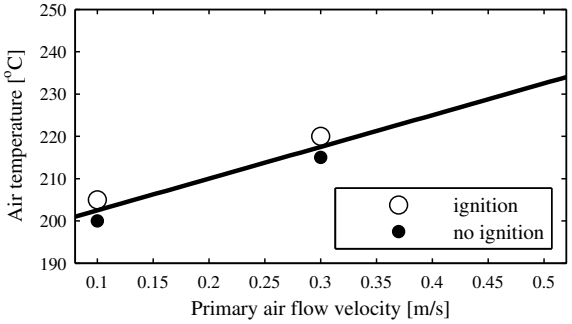

(b) Minimum measured air temperature at which ignition did occur (open symbols) and maximum measured air temperature at which ignition did not occur (closed symbols).

Figure 4.11: *The measured spontaneous ignition (a) and critical air temperature (b) for RDF as a function of the air velocity.*

Because the wood ignition is accompanied with a flame which can be sensed by the higher thermocouples easily, this delay is expected to be minimal for wood. However, the char ignition is only heterogeneous and the delay in ignition time can be significant. This is especially the case with large char particles.

To study the process behaviour after spontaneous ignition has occurred, two experiments at different air flow velocities with more than 1 kg wood chips have been carried out in the laboratory setup as a comparison. These experiments have been conducted, since in every other experiment only 300 gram of wood has been used covering only the first two thermocouples.

The first experiment is carried out at an air flow velocity of $0.2 m/s$ and an air temperature of $230^o C$. Figure 4.12 shows the temperatures measured by the thermocouples at the specified bed heights for this air flow velocity. It can be seen that the ignition first occurs at $20 cm$ above the grate, and the temperature at $5 cm$ above the grate increases subsequently. After that the high-temperature front travels upwards. The duration of the conversion process after the breakthrough is small ($5-15 min$), compared to the time before the breakthrough $40 min$.

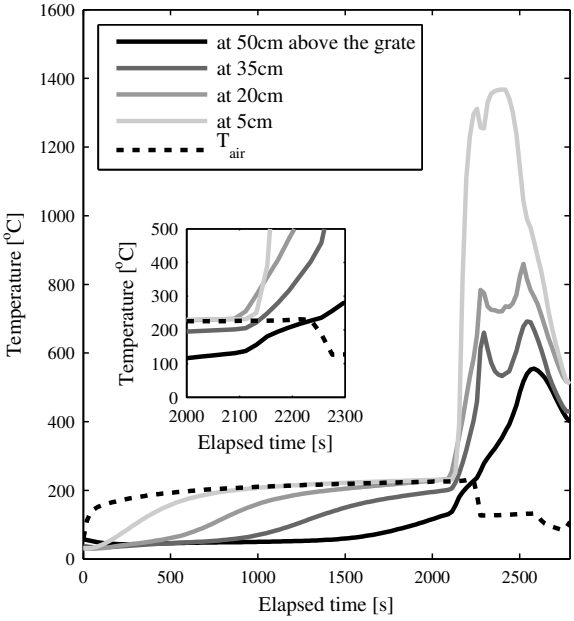

Figure 4.12: *Measured temperatures in a deep fuel bed of wood chips. Air flow velocity is* $0.2 m/s$. *Air flow temperature is* $230^o C$. *The inset shows the moment of ignition in more detail.*

The second experiment was carried out at an air flow velocity of $0.3 m/s$ and primary air temperature of $230^o C$ (see figure 4.13). At this flow velocity the spontaneous ignition starts in the bed at $35 cm$ above the grate. Next, the thermocouple below (at $20 cm$ above the grate) and above (at $50 cm$ above the grate) show an increase in temperature. Finally, the thermocouple located $5 cm$ above the grate shows an increase in temperature. The time taken for the ignition at $0.3 m/s$ is slightly higher than $0.2 m/s$. This may be due to the cooling effect by the higher air flow velocity.

From the above experiments, we may conclude that:

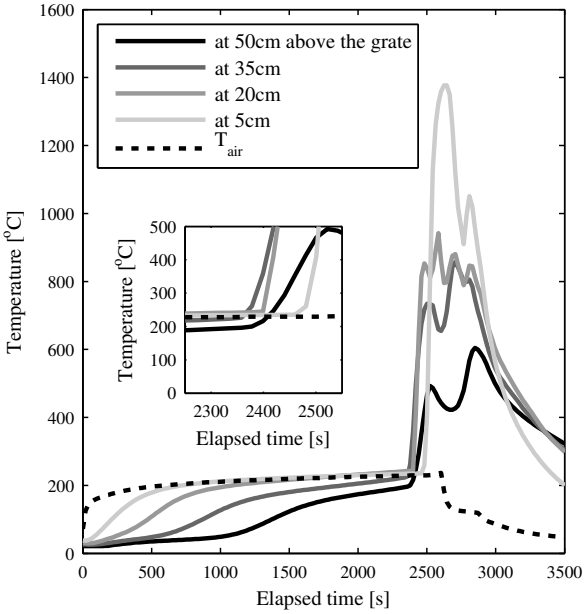

Figure 4.13: *Measured temperatures in a deep fuel bed of wood chips. Air flow velocity is* $0.3 m/s$. *Air flow temperature is* $230^o C$. *The inset shows the moment of ignition in more detail.*

- The initial ignition does not occur at the grate, but $20-35 cm$ above the grate. After the initial ignition, a reaction fronts travels upwards and another reaction front travels downwards;
- For a flow velocity of $0.2 m/s$, the reaction front travels quickly downwards, due to the presence of dry fuel and already formed char in the bottom of the fuel bed. Besides, close to the grate, the air is still oxygen-rich. However, for the flow velocity of $0.3 m/s$ this front does not travel downwards fast.

It is not clear why the ignition does not take place at the grate. It can be caused by the inhomogeneous composition and geometry of the fuel bed. Another explanation could be that, as it is described in section 4.2, a small deviation in reaction or convective heat transfer parameters can cause a relative large deviation in spontaneous ignition and critical air temperatures. The deep bed experiments show that it is difficult to predict at which height in the fuel bed the ignition will take place.

An experiment with wood chips was carried out with an air flow of $0.3 m/s$ and a temperature of $230^o C$. No ignition took place and the bed temperature stabilized and

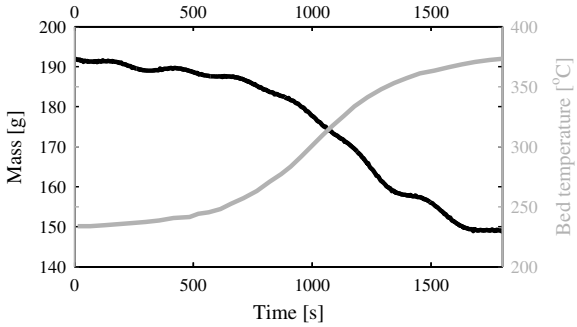

Figure 4.14: *Measured temperature and fuel bed mass as a function of time. A band-stop filter is applied on the mass signal to eliminate oscillations between* 4 *and* $40mHz$*. The experiment was started with an air flow velocity of* $0.3m/s$ *and a temperature of* 230^oC*. At* $t = 0$ *the air flow was turned off.*

after a while, the air flow was shut off. Figure 4.14 shows the change in bed temperature and mass after the air flow was stopped. A band-stop filter is applied on the mass signal to eliminate frequencies between 4 and $40mHz$ that are most likely a measurement error. From the rising bed temperature and the decreasing mass it can be concluded that an exothermic reaction is remaining after the air flow is turned off. This behaviour can be explained with the help of figure 4.1. With the air flow still on, the stable point 1 is reached and the bed is cooled by the air flow. When the air flow is now stopped, the convective cooling ceases and the exothermic reaction is able to proceed. The measured behaviour shows that the exothermic reaction proceeds without oxygen so it is a pyrolysis reaction. If this pyrolysis reaction was the only reaction, the temperature should have increased exponentially. However, a new stable temperature of around 380^oC is reached. This shows that besides the exothermic pyrolysis reaction also one or more endothermic pyrolysis reactions are going on at higher temperatures (above 300^oC). In section 4.5.2 the pyrolysis reactions are described into more detail.

4.5 Evaluation

4.5.1 Differences in experimental methods

The different results from the different methods to determine the ignition temperature described in section 4.3.3 will be explained with the help of the results of the

wood experiments.

A typical measurement result with the constant air temperature method for wood can be seen in figures 4.15 and 4.16. Figure 4.15 shows the mass of the fuel and the bed temperature during the experiment and figure 4.16 shows the concentrations of several components. It takes some time before the gas samples reach the analyzers, so there is a delay in the measured gas concentrations. The measurement for the bed temperature shows an ignition time of 5 minutes. Note that this is with an air velocity of $0.1 m/s$. Again, ignition is indicated by both the temperature increase from figure 4.15 and the decrease and increase of oxygen and carbon dioxide respectively (figure 4.16).

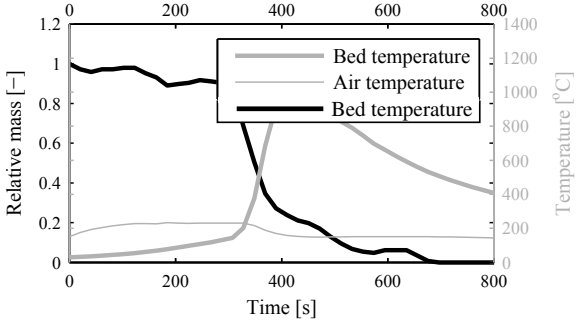

Figure 4.15: *Measured bed mass (black line) and bed and air temperatures (grey lines) as a function of time for wood chips. The superficial air velocity is* $0.1 m/s$ *and the air temperature is* $230^o C$.

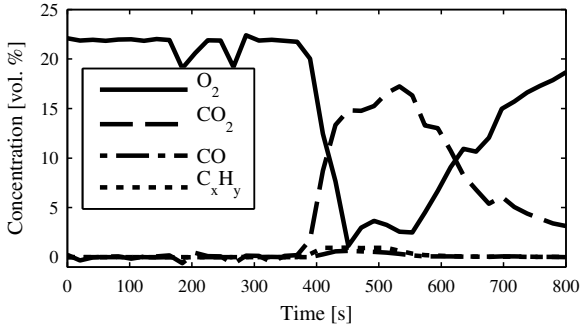

Figure 4.16: *Measured concentration of* O_2, CO_2, *CO and* C_xH_y *as a function of time for wood chips. The superficial air velocity is* $0.1 m/s$ *and the air temperature is* $230^o C$.

It can be seen that the bed temperature is only 150^oC when it ignites. However, this is not the spontaneous ignition temperature of the wood. The temperature measurement does not show a clear ignition point. Because the heat lost to the air stream is always smaller than the heat produced by the reaction, no clear moment of ignition can be defined. The thermal runaway (which is ignition in our case) starts as soon as the experiment starts (black line in figure 4.1). If the air temperature is chosen closer to the critical air temperature, this effect will be less pronounced and if the air temperature is close enough, the spontaneous ignition temperature can be measured, but this is a time consuming procedure. This illustrates that the constant temperature method is not suitable for determining the spontaneous ignition temperature.

An example of an experiment carried out with the slowly increasing air temperature method is shown in figure 4.17 for $0.3m/s$. By slowly increasing the air temperature (T_0 in figure 4.1) point 2 in figure 4.1 is reached slowly and can be determined accurately. The first notable difference with the constant air temperature experiment is that the time to ignition is at least an order of magnitude longer. This is inherent to the measurement method, because the bed is slowly brought to its runaway point. This shows that this method is not suitable for measuring ignition times. The second important difference is that the bed temperature is higher than the air temperature at ignition. Besides, the start of the runaway (ignition) can be seen clearly at 4285 seconds and a temperature of 247^oC. However, more experiments are needed to determine the critical air temperature.

The critical air temperature can be determined together with the spontaneous ignition temperature in a single experiment when the stepwise increasing air temperature is used. The result from such an experiment is shown in figure 4.18. The critical air temperature is 240^oC and the spontaneous ignition temperature is 249^oC (which is almost the same as in the slowly increasing temperature method).

4.5.2 Heats of reaction

In reality, the shape of the heat of reaction line is not as simple as depicted in figure 4.1. The reaction mechanism of wood is complex, but the kinetics of several types of wood are well documented. As has been posed in section 4.3.2, wood pyrolysis is often modeled by the sum of the pyrolysis of its main components (i.e. hemicellulose, cellulose and lignin) [40, 96, 63]. The kinetics of these pyrolysis reactions are not differing too much in literature. Hemicellulose is the most reactive and decomposes between around 220^oC and 315^oC. Cellulose decomposes between 315^oC and 400^oC and lignin decomposes slowly over a wide temperature range ($160^oC - 900^oC$) [96]. So for temperatures below 300^oC, wood degradation can be attributed to hemicellulose degradation for a great extent. Although the kinetics of these three reactions are fairly

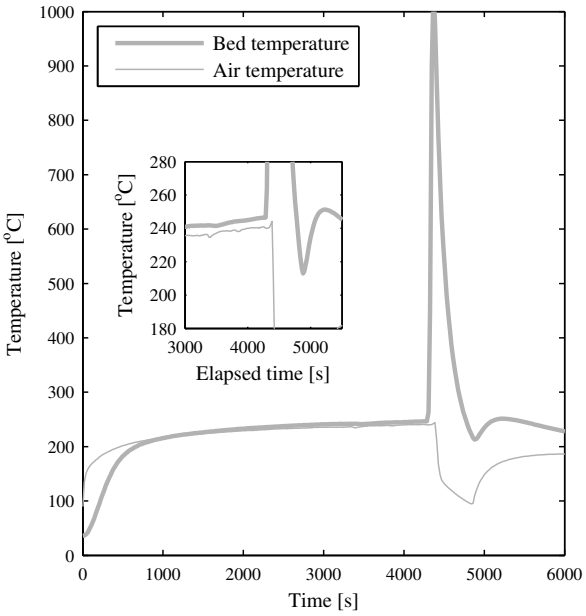

Figure 4.17: *Measured bed and air temperatures as a function of time for wood chips and a low heating rate. The superficial air velocity is* $0.3 m/s$ *and the air temperature is slowly increasing to* $240^o C$.

well known, values for the heats of reaction are scarce in literature. However, Yang et al. [96] found that hemicellulose and lignin pyrolysis are exothermic and cellulose pyrolysis is endothermic. The overall heat of pyrolysis has been measured by Rath et al. [71]. The most important conclusions that can be drawn from the papers from Yang et al. and Rath et al. [96, 71] are:

- wood pyrolysis is slightly exothermic at temperatures between $200^o C$ and $325^o C$ mainly due to the hemicellulose pyrolysis;
- between $320^o C$ and $380^o C$ the endothermic cellulose pyrolysis determines the heat of reaction;
- the degradation of wood for temperatures up to $300^o C$ can be attributed to the hemicellulose degradation.

From this it can be concluded that the spontaneous ignition temperature of wood will be above $200^o C$, which is in agreement with the experiments. Note that the reaction heat comes from an exothermic pyrolysis reaction. This means that also elevated

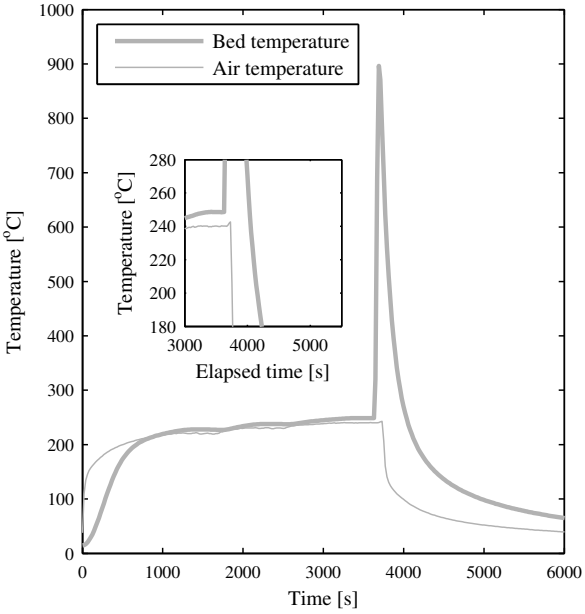

Figure 4.18: *Measured bed and air temperatures as a function of time for wood chips and a low heating rate. The superficial air velocity is* $0.3 m/s$ *and the air temperature is increased stepwise:* $220 - 230 - 240^o C$.

temperatures can be reached without oxygen at all. At around $320^o C$ the endothermic cellulose pyrolysis starts and the temperature of the fuel bed will stabilize without oxygen (with oxygen the fuel would have been ignited already). This behaviour is seen in the experiment where the air flow was stopped after no ignition took place (see figure 4.14).

For wood charcoal, no ignition data is found in the literature for the temperature ranges considered in the measurements. The heat of reaction is measured at the University of Twente using differential scanning calorimetry (DSC) for three types of wood charcoal in air. The charcoal samples are produced by keeping wood pellets for three hours at either $350^o C$, $500^o C$ or $650^o C$ in a nitrogen environment. The results can be seen in figure 4.19. It can be seen that the charcoal interaction with oxygen switches from endothermic to exothermic between $150^o C$ and $200^o C$. From this data it can be concluded that the spontaneous ignition of charcoal cannot be lower than $150^o C$. This statement is supported by the experiments. These heat of reaction profiles could also explain why the bed temperature is lower than the air temperature

at temperatures below the spontaneous ignition temperature, since the reaction is shown to be endothermic at these temperatures. This might lead to the idea that the temperature where the reaction gets exothermic is close to the spontaneous ignition temperature. The DSC results show that the temperature at which this happens is strongly dependent on the temperature at which the char was produced. This can be an explanation for the wide spread of the results for the char experiments.

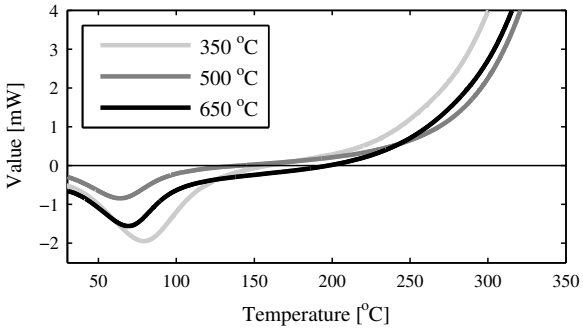

Figure 4.19: *Heats of reaction of three types of char as a function of temperature.*

4.5.3 Application of Semenov's analysis

It appears that Semenov's analysis is able to describe the ignition phenomena in a packed bed qualitatively. But when the heat produced by the reaction and the convective heat losses depicted in figure 4.1 are known, Semenov's analysis can be used to determine the spontaneous ignition and critical air temperature also quantitatively. In this section Semenov's analysis is applied on the ignition of a packed bed of wood.

Semenov's analysis starts with a reacting system at a uniform temperature. This assumption has to be validated for the experiments. Thermocouple readings on top of the grate and at 5cm above the grate in the bed differ only 2^oC after 11 minutes of heating a wood bed with 200^oC air flowing at $0.3m/s$. Figures 4.17 and 4.18 show that the ignition times in case of wood are in the order of one hour. This shows that there are no vertical temperature gradients just before ignition. The fuel bed is wide enough to assume that the horizontal gradients can be neglected as well. So the assumption that the fuel bed is at a uniform temperature before ignition is justified.

The convective heat transfer flux is expressed as:

$$\dot{q}''_{conv} = h(T_a - T_b)A_s d_b \tag{4.1}$$

In which h is the heat transfer coefficient and A_s is the specific surface area of the packed fuel. The heat transfer coefficient h can be found by the Nusselt-Reynolds relation according to Bird et al. [17].

As has been said before, for temperatures below 300^oC the decomposition of wood is determined by the pyrolysis of the hemicellulose. The heat gained by the reaction can be expressed as:

$$\dot{q}''_{react} = k_{hc} \exp\left(-\frac{E_{hc}}{RT}\right) \rho_{hc} \Delta H h_b \tag{4.2}$$

ΔH is the heat of reaction and h_b is the total height of the fuel layer in the reactor, ρ_{hc} is the density of the hemicellulose in the wood, k_{hc} is the pre-exponential factor, E_{hc} is the activation energy, R is the ideal gas constant and T is the temperature of the wood. Because before ignition, a uniform temperature can be assumed throughout the fuel bed, the height of the fuel bed is not important.

Most of the kinetic data found in the literature does not focus on the low temperatures encountered in the spontaneous ignition experiments. However, Órfão et al. [63] have carried out TG analyses on wood, cellulose, hemicellulose and lignin at low temperatures. They give the kinetics for the pyrolysis of the three wood components in nitrogen but they also found that in air the pyrolysis reactions occur at lower temperatures. They do not mention the kinetic data for hemicellulose in air, but it can be found by fitting an Arrhenius equation on their TGA curve. The result is: $E_{hc} = 107 kJ/mol$ and $k_{hc} = 8.9 \cdot 10^8\ 1/s$.

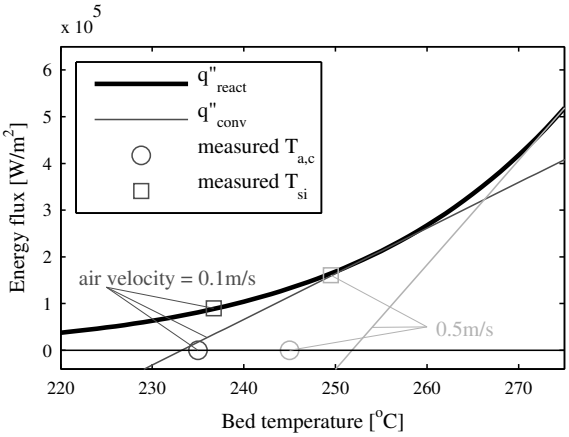

Figure 4.20: *Semenov's analysis applied to the spontaneous ignition of wood for three air velocities.*

The heat gained by the reaction (equation (4.2)) is plotted in figure 4.20 with the thick black line as a function of the bed temperature. The convective heat losses are (equation (4.1)) plotted for two air velocities ($0.1 m/s$ and $0.5 m/s$) with the two thin lines. In both situations the critical air temperature and the ignition temperature of the fuel bed can be seen. Also the measured ignition temperatures and the critical air temperatures are shown for these two air velocities. Both situations can be compared to situation b) in figure 4.1. The figure shows that the model is able to predict the critical air temperatures well. However, it over-predicts the measured spontaneous ignition temperatures by 5-10%. A straightforward reason for this over-prediction is that the solid temperature is calculated with the model, while the gas temperature between the solids has been measured. With solid phase runaway, the gas temperature is always lower than the solid temperature so the spontaneous ignition temperature is measured too low. The over-prediction of the measured spontaneous ignition temperature can also be caused by the inaccuracy in the kinetic data. Not many kinetic data are available at these relatively low temperatures and that is why no kinetic data could be found for the wood used in our experiments. Besides, the composition of the forest residue used in the experiments is unknown. Because the predicted values are very sensitive to the kinetics, an over-prediction of more than 10% is can be expected. Because the trends and the phenomena seen in the experiments compare well with the theory, it can be stated that the model is physically sound. To increase the accuracy of the predictions, more research on the details of the reactions is needed.

4.6 Conclusions

According to the objectives of the work, the conclusions can be categorized in three main parts: (1) general results, (2) influence of key parameters and (3) spontaneous ignition mechanisms. The general conclusions which can be drawn from the experiments are summarized in table 4.2.

Table 4.2: *Measured critical air and spontaneous ignition temperatures and ignition times for wood, char and RDF.*

	wood chips	char	RDF
T_{crit} [^oC]	230 – 245	170 – 200	205 – 200
T_{ign} [^oC]	230 – 255	155 – 190	220 – 245
ign. time [min]	5	2	60

The effect of several key parameters on the ignition behaviour is experimentally investigated. The results can be summarized as follows:

- The primary air velocity has a significant effect on both the critical air temperature and the spontaneous ignition temperature. Increasing the primary air flow velocity increases both temperatures. For high flow velocities the critical air temperature and spontaneous ignition temperature tends to become constant;
- Addition of inert to the wood and char fuel bed increases the spontaneous ignition temperature as well as the critical air temperature needed for the ignition;
- No significant influence of moisture content (up to $30 wt\%$) on spontaneous ignition behaviour for wood chips has been found;
- No significant difference in spontaneous ignition behaviour between small ($10-15mm$) and medium ($15-30mm$) sized char particles has been measured. No reliable results could be obtained with large ($30-40mm$) sized char particles.

With the help of Semenov's analysis of thermal explosions the mechanisms determining the spontaneous ignition behaviour are derived. The main conclusions are:

- The spontaneous ignition behaviour is determined by the combination of convective heat transfer between the primary air flow and the fuel bed and the heat gained by the reactions in the fuel bed;
- For wood, the heat gained by the reactions is determined by the exothermic hemicellulose pyrolysis. This causes the spontaneous ignition temperature to be higher than the critical air temperature;
- For all experiments with char, the spontaneous ignition occurs at a temperature below the air temperature irrespective of the air flow velocity. If ignition did not occur, the bed temperature will be below the air temperature. This indicates that until ignition the reactions in the char are endothermic. This idea is supported by DSC measurements on char;
- RDF shows a typical pre-ignition stage. This is probably caused by the inhomogeneous composition of this fuel.

5

Spontaneous ignition modeling

This chapter describes a newly developed model which predicts the spontaneous ignition temperature of the fuel bed and the critical temperature of the primary air at which the fuel bed ignites. The influence of primary air flow rate and addition of inert are modeled for a packed bed of wood. From the model a dimensionless parameter is derived in which all investigated parameters (fuel type, air flow rate and inert fraction) are combined. This parameter appears to be sufficient to describe both the spontaneous ignition and the critical air temperature. The results from the model are validated with experiments presented in chapter 4. The model over-predicts both the temperatures by $6-7^{o}C$*. However, the trends are predicted well. For char, a minimum spontaneous ignition temperature is derived from DSC measurements. The temperature at which the interaction of char and oxygen from the air switches from endo- to exothermic seems to coincide with the spontaneous ignition temperature.*

5.1 Introduction

In this chapter a model to predict the spontaneous ignition and the critical air temperature of a packed bed of wood or char is described. The model is used to investigate the influence of the air flow velocity and the amount of inert on the spontaneous ignition temperature and the critical air temperature. Finally, the model results are compared with experimental results from chapter 4.

5.2 Theory

The observed ignition phenomena presented in chapter 4 can be explained by Semenov's analysis of thermal explosions and the two main parameters are: 1) the heat gained by the reaction and 2) the heat lost by (convective) cooling. Details of this theory are described in section 4.2.

Another explanation of the observed ignition phenomena might be that the pyrolysis gases form a flammable mixture with the incoming air (i.e. the pyrolysis gas is at its lower flammability limit). In this case the ignition temperature is the temperature at which the composition of the pyrolysis gases is a flammable mixture with the air flow and the temperature in the bed should be above the ignition temperature. For a higher air flow, more pyrolysis gases are needed to reach the lower flammability limit and thus a higher bed temperature is needed. However, two TGA experiments on wood carried out at Sintef [18] showed thermal runaway without ignition. One experiment was carried out with an argon flow of $20 ml/min$ and an oxygen flow of $5 ml/min$, the second experiment was carried out with an argon flow of $39.5 ml/min$ and an oxygen flow of $10.5 ml/min$. As a result, the experiments are carried out at an oxygen concentration of 20% and 21% respectively. The sample temperatures and the program temperature are displayed in figure 5.1. The TGA furnace is actively cooled. The measured temperature profiles indicate solid phase thermal runaway. If gas phase ignition would have been occurred, a sharp increase in temperature to a high value would have been seen. Besides, no sharp increase in H_2O concentration is measured, indicating that no gas phase ignition has occurred. The thermal runaway is controlled by the active cooling of the TGA furnace. The experiment with the low flow rate shows a larger temperature overshoot than the experiment with the high flow rate. From the low flow rate experiment, it can be concluded that no gas phase ignition occurs at a temperature of even 280^oC. The experimental results presented in chapter 4 show that wood ignites with air temperatures as low as 230^oC. It can be concluded that this ignition is not primarily caused by gas phase ignition.

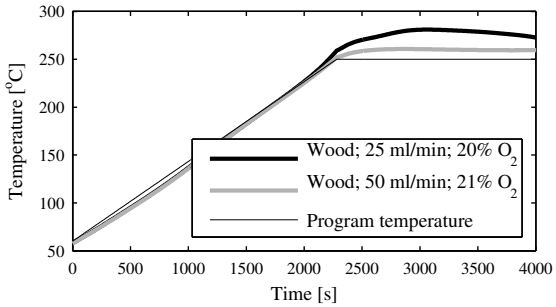

Figure 5.1: *Sample temperatures (black lines) and program temperature (grey line) versus time for TGA experiments carried out at Sintef [18].*

5.3 Modeling

As explained above, ignition is determined by the balance between two terms:

1. heat gained by the reaction
2. heat lost by (convective) cooling

These two terms are analyzed in this section.

5.3.1 Heat gained by reaction

The heat produced by the reaction equals:

$$\dot{q}''_{react} = K\Delta H d_b \tag{5.1}$$

In which K is the overall reaction rate per unit volume, ΔH is the heat of reaction and d_b is the height of the fuel layer in the reactor. In the next sections the reaction rates for char and wood will be investigated into detail.

Char

Ismail and coworkers found that at low temperatures ($< 125^oC$) the interaction between pure oxygen and Saran (a type of polymer) char consists mainly of chemisorption of oxygen at the char surface [49]. At higher temperatures (between 125^oC and 240^oC) also oxidation becomes important. Above 240^oC oxidation is determining the

conversion. Although the used char as well as the oxygen concentration are different in the spontaneous ignition experiments (which are carried out in air), the results form Ismail et al. serve as a good indication of the occurring processes.

TGA experiments on three types of charcoal have been carried out at Sintef [18]. The charcoal samples are produced by heating wood pellets for three hours at either 350^oC, 500^oC or 650^oC in a nitrogen environment. For the 500^oC-sample, the TGA results show a mass increase at 180^oC, showing that chemisorption is faster than oxidation, see figure 5.2. For the 350^oC- and 650^oC-sample, a negligible mass change is found at temperatures above 160^oC. This indicates that the chemisorption rate and the oxidation rate are equal. However, the absolute rate of the two separate processes can not be determined for the three samples.

The TGA results correspond with the findings of Bergström [16]. He determined the ignition temperature, chemisorption rate and the CO_2 release at ignition as a function of the spruce wood char preparation temperature. The results are plotted in figure 5.3. He found that the ignition temperature is minimal for a production temperature of 450^oC. Besides, he observes a maximum reactivity for a production temperature of 430^oC. It can be seen that for production temperatures of 350^oC and 550^oC the O_2 uptake and the CO_2 release are about the same. This is in line with the results from the TGA experiments. The wide spread in the measured spontaneous ignition temperatures for char [86] can be attributed to this high dependency of the ignition phenomena on char production temperature. Since it is unlikely that all used char is produced at the same temperature, fluctuations in ignition temperature from batch to batch can arise.

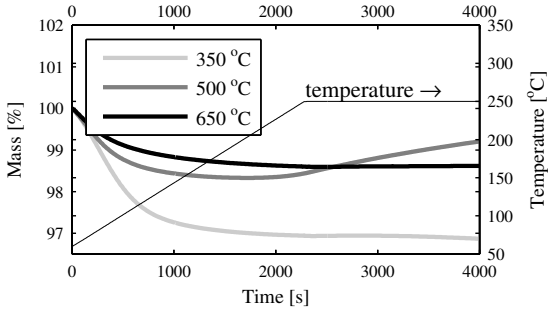

Figure 5.2: *Mass profiles of char in a TGA in an oxidizing and inert environment. The temperature in the oven is also shown. Adopted from [18].*

Despite the unknown kinetics, a lower boundary for the spontaneous ignition temperature can be estimated with the help of the reaction heat of char oxidation. The

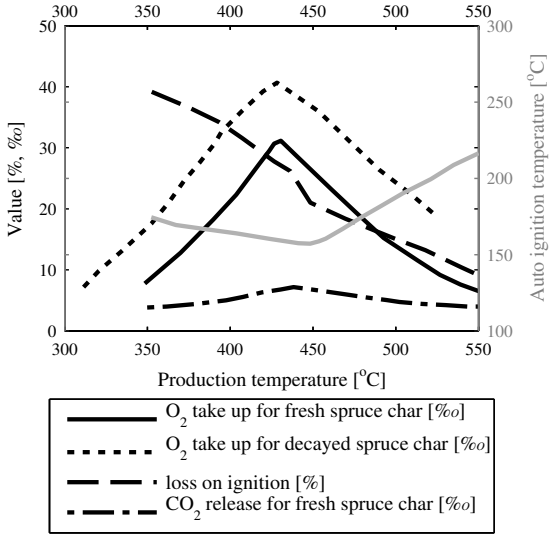

Figure 5.3: *Some char reactivity and ignition parameters as a function of char production temperature. [16]*

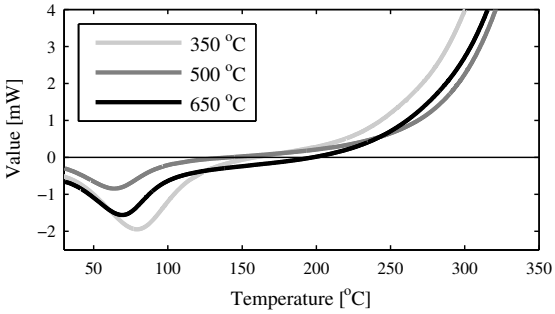

Figure 5.4: *DSC profiles of three different char samples. The vertical axis shows the measured power which is produced or absorbed by the sample.*

heat of reaction for the three types of wood charcoal in air is measured at the University of Twente using a balance from type Mettler Toledo DSC-823. The results can be seen in figure 5.4. It can be seen that the charcoal interaction with oxygen switches from endothermic to exothermic between 150^oC and 200^oC again depending on the production temperature. From this data it can be concluded that the spontaneous

ignition of charcoal can not be lower than 150^oC. This statement is supported by the results from the spontaneous ignition experiments and by the findings of Bergström, who found that the lowest spontaneous ignition temperature for charcoal is 150^oC for a production temperature of 450^oC. It seems plausible to assume that the temperature at which the reaction switches to exothermic coincides with the spontaneous ignition temperature. This assumption also clarifies why the char bed temperature is always lower than the air temperature when ignition did not take place, since the reaction is still endothermic.

Wood

Wood reacts also complex, but the kinetics of several types of wood are well documented and can be measured more easily than those of charcoal. Often, wood pyrolysis is modeled by the sum of the pyrolysis of its main components (i.e. hemicellulose, cellulose and lignin), see for example the work of Grønli et al., Yang et al., Órfão et al. and Branca et al. [40, 96, 63, 21]. Although the reported kinetics diverge to a great extent, the reported temperature ranges at which the components pyrolyze do not differ much. It appears that hemicellulose is the most reactive and decomposes between around 220^oC and 315^oC [96]. Cellulose decomposes between 315^oC and 400^oC and lignin decomposes slowly over a wide temperature range ($160^oC - 900^oC$). So for temperatures below 300^oC, wood degradation can be attributed to hemicellulose degradation to a great extent. The heat of hemicellulose pyrolysis is measured by Beall [11]. He found a value of $159.9 kJ/kg$ for softwood hemicellulose pyrolysis in nitrogen in the temperature range of $180 - 350^oC$.

The most important conclusions that can be drawn from these papers [40, 96, 63, 21, 11] are:

- the degradation of wood for temperatures up to 300^oC can be attributed to the hemicellulose degradation;
- wood pyrolysis is slightly exothermic at temperatures between 180^oC and 350^oC mainly due to the hemicellulose pyrolysis;
- the heat of reaction of hemicelluloses pyrolysis is $159.9 kJ/kg$ [11];
- between 320^oC and 380^oC the endothermic cellulose pyrolysis determines the heat of reaction.

The kinetics of hemicellulose pyrolysis temperatures below 300^oC can be expressed as follows:

$$K = \frac{d\rho_w}{dt} = \frac{d\rho_{hc}}{dt} = k_{hc} \exp\left(-\frac{E_{hc}}{RT}\right) \rho_{hc} \tag{5.2}$$

With ρ_w the density of wood, ρ_{hc} the density of the hemicellulose in the wood, k_{hc} the pre-exponential factor, E_{hc} the activation energy, R the ideal gas constant and T the temperature of the wood. Most of the kinetic data found in the literature do not focus on the low temperatures encountered in the spontaneous ignition experiments. However, Órfão et al. [63] have carried out TG analyses on wood, cellulose, hemicellulose and lignin at low temperatures. They give the kinetics for the pyrolysis of the three wood components in nitrogen but they also found that in air the pyrolysis reactions occur at lower temperatures. They do not mention the kinetic data for hemicellulose in air, but it can be found by fitting an Arrhenius equation on their TGA curve. The result is: $E_{hc} = 107 kJ/mol$ and $k_{hc} = 8.9 \cdot 10^8\ 1/s$.

5.3.2 Convective heat transfer

The convective heat transfer flux is expressed as:

$$\dot{q}''_{conv} = h(T_a - T_b) A_s d_b \tag{5.3}$$

In which h is the heat transfer coefficient and A_s is the specific surface area of the packed fuel. The heat transfer coefficient h can be found according to Bird et al. [17] as follows:

$$\begin{aligned} h &= \frac{k(1-\phi)}{d_p}\left(2.19Re^{1/3} + 0.78Re^{0.619}\right)Pr^{1/3} \\ \text{with:} \quad Re &= \frac{d_p Q}{\nu(1-\phi)} \end{aligned} \tag{5.4}$$

In this, ν is the kinematic viscosity of the air flowing through the bed, k is the thermal conductivity of the air and Q is the superficial air velocity at the local air temperature (which is the preheat temperature in this case). The term d_p is an equivalent particle diameter which is defined as:

$$d_p = \frac{6(1-\phi)}{A_s} \tag{5.5}$$

It can be shown that for cubic particles the equivalent diameter d_p equals the particle diameter for a bed porosity of 0.67. This porosity is close to the porosities of packed fuel beds found in practice. For spheres, this relation is true per definition.

Now the two needed heat fluxes are known from equations (5.1) and (5.3). The next step is to derive relations for the spontaneous ignition and the critical air temperature.

5.3.3 Finding the critical temperature

At the critical point (point 2 in figure 4.1) the heat produced by hemicellulose pyrolysis and the heat lost by convection have the same value and the same gradient. This can be expressed as (with $\Delta\dot{q}'' = \dot{q}''_{react} - \dot{q}''_{conv}$):

$$\begin{cases} \dfrac{d\Delta\dot{q}''}{dT} & = 0 \\ \\ \Delta\dot{q}'' & = 0 \end{cases} \tag{5.6}$$

From this system the spontaneous ignition temperature and the critical air temperature can be found.

When the relations (5.1-5.3) are substituted in (5.6), the system can be written as:

$$\begin{cases} hA_s = \dfrac{k_{hc}E_{hc}}{RT_{si}^2}\exp\left(-\dfrac{E_{hc}}{RT_{si}}\right)\rho_{hc}\Delta H \quad \text{(gradient)} \\ \\ hA_s(T_{si} - T_{a,c}) = k_{hc}\exp\left(-\dfrac{E_{hc}}{RT_{si}}\right)\rho_{hc}\Delta H \quad \text{(value)} \end{cases} \tag{5.7}$$

From this set, the critical air stream temperature ($T_{a,c}$) and the spontaneous ignition temperature (T_{si}) can be found.

$$\begin{aligned} T_{si}\frac{R}{E_{hc}} &= \theta_{si} = \frac{1}{2}\frac{1}{W_{-1}(-\Phi)} \\ T_{a,c}\frac{R}{E_{hc}} &= \theta_{a,c} = \frac{1}{4}\left[\frac{1+2W_{-1}(-\Phi)}{W_{-1}^2(-\Phi)}\right] \\ \text{with} \quad \Phi &= \sqrt{\frac{hA_sE_{hc}}{4k_{hc}\rho_{hc}\Delta HR}} \end{aligned} \tag{5.8}$$

The dimensionless spontaneous ignition temperature θ_{si} and the critical air temperature $\theta_{a,c}$ are made by scaling the dimensional temperatures with E_{hc}/R. . The expression $W_{-1}(-\Phi)$ is the -1-branch of the Lambert-W function. The parameter Φ can be considered the ratio of the convective cooling (hA_s) and a term defined by the heat gained by the reaction $\left(\frac{E_{hc}}{k_{hc}\rho_{hc}\Delta HR}\right)$.

The dimensionless critical temperature and spontaneous ignition temperature are plotted in figure 5.5(a) against Φ. It will be shown later that in the experiments Φ is in the order of 10^{-4}. The plot shows that for $\Phi > 0.5\cdot10^{-5}$ the temperatures only increase slightly. On the other hand, for $\Phi < 0.5\cdot10^{-5}$, the temperatures decrease

quickly with decreasing Φ. This shows the large difference in spontaneous ignition temperatures when there is no cooling (Φ = 0) or when just a little cooling is present. The spontaneous ignition temperature is predicted slightly higher than the critical air temperature. Figure 5.5(b) shows the dimensional spontaneous ignition and critical air temperatures as a function of the air velocity. Also here it can be seen that when no air flow is present, spontaneous ignition can occur at very low temperatures. However, ignition times will be very long.

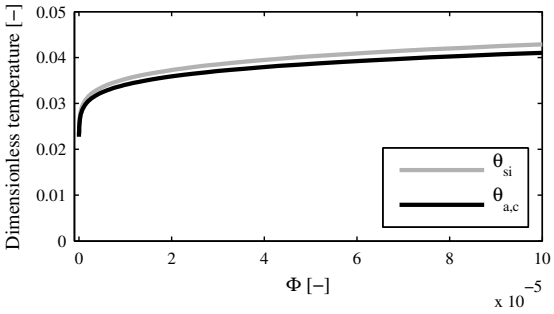

(a) The predicted dimensionless critical air temperature (black lines), and spontaneous ignition temperature (grey lines) as a function of Φ.

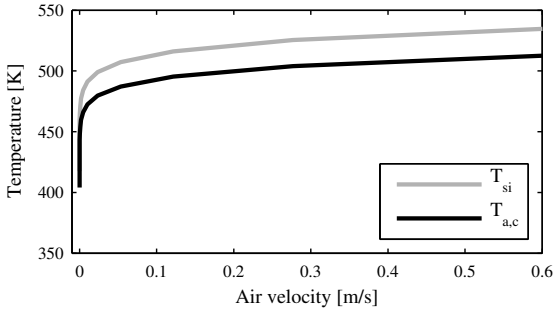

(b) The predicted dimensional critical air temperature (black lines), and spontaneous ignition temperature (grey lines) as a function of the air velocity.

Figure 5.5: *The predicted dimensionless (a) and dimensional (b) critical air temperature and spontaneous ignition temperature.*

5.4 Results and discussion

The model is used to calculate the spontaneous ignition temperature and the critical air temperature of a packed bed of wood chips. The results are compared with the experimental results presented in section 4.4.1.

The values of the model parameters are summarized in table 5.1. With this data, the spontaneous ignition temperature and the critical air temperature for wood can be calculated. The results are plotted against Φ in figures 5.6(a) and 5.6(b). In the same figure, the measured temperatures for wood are plotted as well. It is noted that these temperatures are non-dimensionalized by multiplying by R/E_{hc}. Because both the dimensionless spontaneous ignition temperature and the critical air temperature only depend on Φ, the experimental results have to be expressed by Φ as well. This makes it straightforward to also include the experimental results from the wood chips with added inert in the figures.

Table 5.1: *Parameters for wood spontaneous ignition analysis. For wood pyrolysis, the hemicellulose component is used.* [a] *The hemicellulose content in wood is around* 30%*, with a packed density of wood of* $200 kg/m^3$*, the packed density of hemicellulose is* $60 kg/m^3$*. The properties of air are at* $200^o C$*.*

variable	value	ref.
k_{hc}	$8.9 \cdot 10^8\ s^{-1}$	extracted from [63]
ρ_{hc} [a]	$60\ kg/m^3$	est.
E_{hc}	$107\ kJ/mol$	extracted from [63]
ΔH	$159.9\ kJ/kg$	[11]
A_s	$260\ m^2/m^3$	est. from geometry
d_p	$9\ mm$	calculated
Pr	0.68	[14]
ν	$34.6 \cdot 10^{-6}\ m^2/s$	[14]
k_a	$0.039\ W/mK$	[14]
ϕ	0.6	est.

The figures show a good comparison between the measured values and the model results. The figures also show that the results from the experiments with the added inert follow the trend of the other results. This shows that the parameter Φ is an appropriate parameter to describe the spontaneous ignition and critical air temperatures.

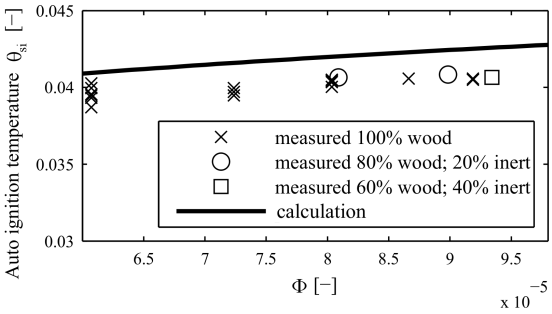

(a) The calculated dimensionless spontaneous ignition temperature (θ_{si}) for wood (line). The experimental data are shown as well [86]. The ×-symbols denote the results for pure wood and the ◯-symbols and □-symbol denote the results for wood mixed with $20wt\%$ and $40wt\%$ inert respectively.

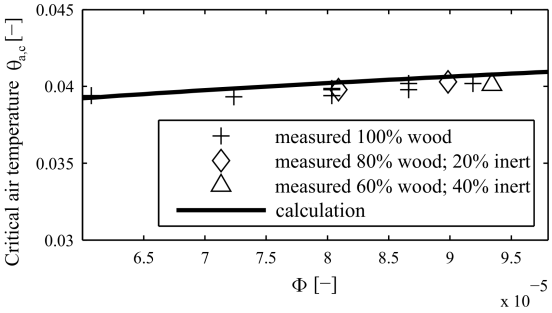

(b) The calculated dimensionless critical air temperature ($\theta_{a,c}$) for wood (line). The experimental data are shown as well [86]. The +-symbols denote the results for pure wood and the ♢-symbols and △-symbol denote the results for wood mixed with $20wt\%$ and $40wt\%$ inert respectively.

Figure 5.6: *The calculated and measured dimensionless spontaneous ignition (a) and dimensionless critical air temperature (b) for wood chips as a function of the air flow velocity.*

5.4.1 Ignition time

The time needed for the bed to ignite can not be predicted by the current model, but with an instationary energy balance the ignition times can be estimated as follows:

$$c_{p,b}\frac{d\rho_b T_b}{dt} = \Delta\dot{q}'' - \frac{d\rho_m}{dt}H_{evap} \tag{5.9}$$

With ρ_b the total (wet) density of the fuel bed, which decreases when the drying proceeds and rho_m is the moisture density in the wood, H_{evap} is the heat of evaporation of water en the subscript $_b$ denotes the bed properties. The heat flow needed for the evaporation of the moisture can be modeled with a first order Arrhenius reaction according to [22] with $k_m = 5.13 \cdot 10^{10} 1/s$, $E_{evap} = 88 kJ/mol$ and $\Delta H_m = -2.44 MJ/kg$. The moisture content is defined as follows:

$$moisture = \frac{\rho_m}{\rho_b} 100\% \tag{5.10}$$

Differential equation (5.9) has been solved numerically with the values listed in table 5.1 as input parameters. Figures 5.7 shows the results for the ignition time according to this equation for a dry fuel as a function of the air velocity for different air temperatures. Figure 5.8 shows the results for the ignition time as a function of the air velocity for different values of the moisture content.

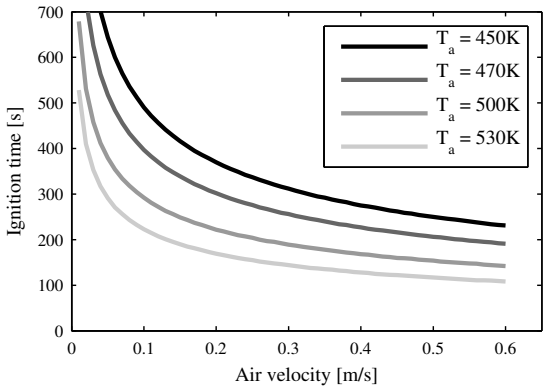

Figure 5.7: *The ignition times predicted by equation (5.9) as a function of the primary air velocity for different values of the air temperature for completely dry fuel.*

The ignition time values found in the experiments are in the order of 5-10 minutes with an air temperature of $503K$. The figure shows that this value is under-predicted for a dry fuel which is probably caused by not taking the heating of the steel reactor wall into account. It is predicted that for an increasing air velocity, the ignition time decreases. This is caused by an increased heat transfer coefficient, so the fuel heats faster. An increasing air temperature decreases the ignition time which is also due to an increased convective heat transport and a faster heating fuel. An increased moisture content significantly increases the ignition time, which is clearly caused by the time needed to dry the fuel. It is noted that the ignition temperatures are not likely to change with changing moisture content, because at the moment of ignition nearly all moisture is evaporated from the particles.

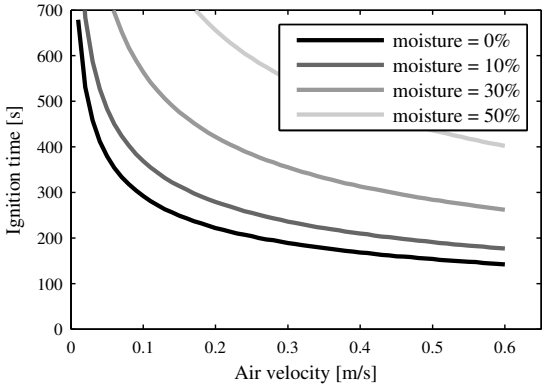

Figure 5.8: *The ignition times predicted by equation (5.9) as a function of the air velocity for several values of the moisture content. The primary air temperature is* $500K$

In Semenov's analysis a uniform temperature distribution inside the particles is assumed. The time required to heat the core of the 1cm thick particles to 225^oC with an air temperature of 230^oC is about 3 minutes while the calculated time to ignition is less than two minutes. Hence, the assumption of an uniform temperature inside the particles does not hold in this case. This will result in an under-prediction of the measured ignition times. However, due to the low heating rates used in the experiments to determine the spontaneous ignition and the critical air temperature the times to achieve ignition are an order longer, so uniform temperatures inside the particles will occur in these experiments and thus Semenov's analysis can be properly used.

5.4.2 Deep fuel bed

The model described in this chapter is a zero dimensional model. This means that there are no temperature gradients in the fuel bed. Also the experiments which are used to validate the model [86] are done with a shallow fuel layer to be able to assume a zero dimensional process. However, in the experimental work described in chapter 4 also some experiments in a deep fuel bed are described. In this case, the temperature gradients along the height of the fuel bed can not be ignored. A remarkable result from these experiments is that the fuel layer does not ignite at the grate.

For an air flow velocity of $0.2m/s$, the ignition took place at $20cm$ above the grate (see figure 4.12). With an air flow velocity of $0.3m/s$ ignition occurred $35cm$ above the grate (see figure 4.13). This behaviour is probably caused by the conduction of

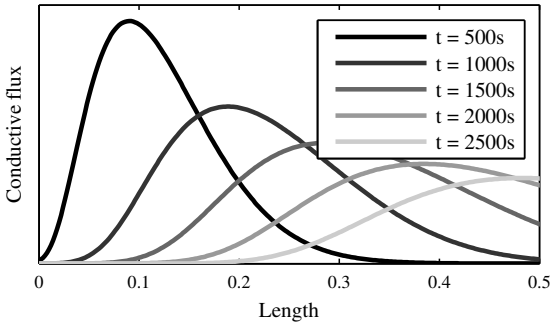

Figure 5.9: *The nett conductive flux over the length of a packed bed heated by a preheated gas stream at several times.* $Q_0 = 0.3 m/s$.

heat through the fuel bed. In this case, Semenov's analysis (see figure 4.1) should be extended with an extra heat flux, resulting from conduction. With the present (zero dimensional) model, it is not possible to predict this, because conduction needs at least one dimension. However, the conductive heat flux can be analyzed separately to explain the effects seen in the experiments.

The nett conductive flux through a small slab of the bed can be expressed as (with x increasing from the grate to the top of the fuel bed):

$$\Delta \dot{q}''_{cond} = k_b \frac{\partial^2 T_b}{\partial x^2} \Delta x = \rho_b c_{p,b} \frac{\partial T_b}{\partial t} \Delta x \tag{5.11}$$

The second equality is Fouriers law. For an inert packed bed heated by a preheated air stream, the nett conductive heat flux is shown in figure 5.9. The heat transfer coefficient from equation (5.4) is used again and the effective thermal conductivity of the wood fuel bed is $0.054 W/mK$. The figure shows that the nett conductive flux has a maximum which moves along the air stream direction. The maximum appears in the region where the fuel bed heats the fastest (this can also be seen in the right hand side of equation (5.11)). So, when the lower layers are heated up to the air stream temperature, the convective flux is zero from that moment on and the maximum travels downstream.

A similar figure can be made for several air velocities. This is seen in figure 5.10 which shows the nett conductive flux along the bed after 2000 seconds for several air velocities. The figure shows that for an increasing velocity, the maximum nett conductive flux is located higher in the bed. For an air velocity of $0.2 m/s$ the peak lies around $0.28 m$ and for an air velocity of $0.35 m/s$ the peak can be found at around $0.38 m$.

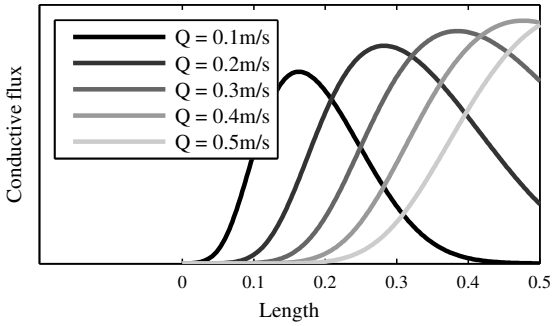

Figure 5.10: *The nett conductive flux along the bed heated by a preheated gas stream for several gas velocities after at* $t = 2000s$.

These heights are close to the heights at which ignition is observed in the experiments for these air velocities.

When the nett conductive heat flux would be included in Semenov's analysis (figure 4.1), it can be shown that the ignition does not have to take place directly above the grate. Due to the maximum conductive flux, which is higher up in the bed, the runaway reactions might start there as well. To be able to predict the time and location of ignition, it is recommended to develop a detailed transient 1D model.

5.5 Conclusions and recommendations

A theory is presented to describe spontaneous ignition seen in packed beds. An analytical model is derived from this theory to calculate the critical primary air temperatures and the spontaneous ignition temperatures for a packed bed of wood. A parameter Φ is derived which is a ratio of convective heat loss and heat gain by the reaction. The model over-predicts measured values of the ignition temperatures by $6-7\%$. Despite the over-prediction, the trends as a function of Φ are predicted well. Results from spontaneous ignition experiments for wood with added inert also follow these trends well. Although the accuracy of the value of Φ needs to be improved for the current situation, it is shown that the parameter is able (and sufficient) to describe the spontaneous ignition temperature for wood.

With the presented theory, the ignition phenomena occurring during char experiments can be explained, however, no quantitative analysis can be given. It seems plausible to assume that the temperature at which the heat of reaction of char oxida-

tion becomes exothermic coincides with the spontaneous ignition temperature. This temperature depends strongly on the char production temperature and is between 150 and 200^oC. The interaction between char and oxygen should be studied further. This will result in a more accurate description of reaction kinetics and heats and predictions can be made for spontaneous ignition of char as well.

In general, air preheating is only used in the drying zone of a municipal waste or biomass incinerator. The waste approximately needs 20 minutes to travel through this zone so when primary air temperatures higher than 230^oC are used ignition can (and will, in case of only dry wood) occur already in the first half of the drying zone. Ignition in the first zone can even happen with wood with a moisture content of 50%. It has to be kept in mind that waste has a higher moisture content than the wood used in the experiments and also the kinetics and heat of reaction will be different. However, RDF showed a lower spontaneous ignition temperature and a shorter ignition time than wood [86].

Despite the fact that at very low air velocities, the needed air temperature to ignite the wood or RDF is the lowest (see figure 5.5) the time needed for ignition is very long (see figure 5.7). An optimal combination of the air velocity and temperature should be found.

6

Piloted ignition

To gain insight in the startup of a waste incinerator, this chapter deals with piloted ignition. This type of ignition is especially relevant at startup procedures, because an external ignition source (a pilot) is present in the form of startup burners. A newly developed model is described to predict the piloted ignition times of wood, PMMA and PVC. The model is based on the lower flammability limit and the adiabatic flame temperature at this limit. The incoming radiative heat flux, sample thickness and moisture content are some of the used variables. Not only the ignition time can be found with the model, but also the mass flux and surface temperature at ignition. The predicted ignition times agree reasonably well with experiments for softwoods. For hardwoods, PMMA and PVC the predicted ignition times agree well with experimental results. Due to a significant scatter in the experimental data the mass flux and surface temperature found with the model are hard to validate. The model is applied on the startup of the combustion process in a municipal waste incineration plant. For this process a maximum primary air flow is derived. When the primary air flow is above this maximum air flow, no ignition can be obtained.

6.1 Introduction

The startup of a waste incineration plant is a time consuming process and usually oil or gas fired startup burners are used. Generally, these burners have a (combined) power of about 60% of the thermal input of the waste incineration and are located about 10 meters above the fuel bed [35]. To heat up the flue gas cleaning train to operating temperatures, the waste is not fed until the furnace temperature reaches 850^oC.

High carbon monoxide emissions may occur during startup of the waste combustion process. Carbon monoxide is mainly a product of a bad air to fuel ratio. When too less air is fed, the fuel is incompletely converted which results in carbon monoxide emissions. When too much air is provided, the fuel bed will be cooled down locally which also may result in carbon monoxide emissions. During startup it is difficult to determine how much waste is burning, so the required amount of primary and secondary air is also hard to determine.

To improve the startup of a waste incinerator, knowledge of the ignition behaviour of the waste is important. To investigate this, the piloted ignition times of several materials found in MSW is dealt with in this chapter. Firstly a literature review is presented to get an overview of the available models to determine the piloted ignition times for several materials. After this, a model is developed to calculate the ignition times for wood, PVC and PMMA as a function of external radiative heat flux, material thickness and moisture content. The model is validated with experimental data from the literature. The model also predicts the surface temperature of the sample and the mass flux of the pyrolysis gases out of the sample at ignition. These results are also compared to experimentally found values. After the validation of the model with lab scale experimental results, the model is applied on the full scale waste combustion process. A maximum primary air flow above which ignition can not occur is determined.

6.2 Literature review

A lot of research is done to find this so called time to ignition for all kinds of materials and several models are developed to predict ignition times. To model ignition it is inevitable to determine when a flame extinguishes and this is the fundamental point where most of the models differ. We can divide the models found in the literature into two groups:

- models that use (mostly) measured solid phase properties such as surface temperature or mass flux out of the solid as a criterion for extinguishing (or igni-

tion), see for example [82, 8, 12, 60]. In this case the behaviour of the ignition of the gas phase is lumped to the solid phase.

- models that use flame properties such as flame temperature and stoichiometry as a criterion for extinguishing, see for example [70, 5, 57].

The advantage of the models from the first group is that the results are more straightforward and close to engineering situations. The second group however is physically more sound. The model presented in this chapter can be placed in the second group, because it uses the adiabatic flame temperature and the lower flammability limit to determine the threshold for extinguishing. Because the here developed model shows strong resemblance with the models from Rasbash et al. [70], Atreya [5] and Lyon and Quintiere [57], their models will be reviewed.

Rasbash et al. [70] calculated a critical mass flux of volatiles out of the material needed for a flame which is in contact with a surface to sustain. They give two criteria for ignition: (1) the flame temperature should be higher than a certain critical value and (2) the heat losses from the flame may not exceed a critical value. For the critical flame temperature they use the constant flame temperature of $1600K$ for most hydrocarbons close to extinction. This criterion for extinction is well founded by experiments done by several researchers and is a "lower flammability like" criterion. For the heat losses, they pose that the maximum allowed heat lost to the surface is 0.3 times the heat gained by the combustion for common organic vapors. It has to be noted that they assume stoichiometric combustion. They calculate values for the critical mass flux for PMMA of about $2g/m^2s$. Their experiments show critical mass fluxes of $4-5.5g/m^2s$, so they under-predict the critical mass flux by a factor two. For piloted ignition it seems more appropriate to assume the gas to ignite at the lower flammability limit instead of stoichiometric conditions. The lower flammability limit assumption will result in a higher required critical mass flux, because more energy is needed to heat the excess air to the flame temperature.

The model for the critical mass flux from Atreya [5] is derived from the model from Rasbash et al. Also Atreya assumes stoichiometric combustion. However, he does not use the heat loss parameter introduced by Rasbash et al. Instead, he uses only the constant flame temperature of $1550K$ for most hydrocarbons close to extinction. Atreya calculates critical heat fluxes for wood of about $1.5g/m^2s$ which he says are somewhat lower than measured data from the literature. It is useful to note that the used temperature criterion is valid for most hydrocarbons. For the pyrolysis gas from wood, which is a mixture of CO, CO_2, H_2 and a fraction of hydrocarbons, this criterion should be reconsidered. Also for MMA, which is the product of PMMA pyrolysis, this criterion does not hold. Ishizuka and Tsuji [48] found that for hydrogen this flame temperature close to extinction is $1013K$. The flame temperature of pyrolysis gas from wood close to extinction would be lower than $1550K$, resulting in a under-prediction

of the critical mass flux. Since Atreya still under-predicts the mass flux (with his higher temperature) indicates that the stoichiometric assumption has more influence than the temperature assumption. In other words: the amount of excess air which has to be heated to the flame temperature has a stronger effect that the actual temperature to which it should be heated.

Lyon and Quintiere predict the critical mass flux by using the more or less constant critical energy density of $1.9 MJ/m^3$ for any hydrocarbon diffusion flame at the lower flammability limit. This is an experimentally determined value. They use this critical energy density to calculate the lower flammability limit. As with the constant flame temperature at the lower flammability limit, this criterion is not valid for gases other than hydrocarbons. It can be easily shown that the used relation between the energy density criterion and the lower flammability limit does not hold for for example MMA (which has a critical energy density of $0.65 MJ/m^3$), CO ($1.39 MJ/m^3$) and H_2 ($0.44 MJ/m^3$). With their analysis, Lyon and Quintiere find a critical mass flux (for transient ignition as they call it) of $1 g/m^2 s$ for a wide range of plastics (including PMMA) which is in line with the values they report from Drysdale and Thomson [30]. However, Drysdale and Thomson use a different definition for the critical mass flux and found a value of $1.80-2.04 kg/m^2 s$ (note that this corresponds with the value calculated by Rasbash et al. [70]).

The model presented in this chapter will only use properties of the gas at the lower explosive limit and the constant flame temperature approach from Atreya by including other gases than hydrocarbons.

6.3 Theory

When a material is heated in for example a cone calorimeter it will start to release mostly flammable gases. If the concentration of these flammable gases is high enough to ignite (i.e. when the gases are above the lower flammability limit), a continuous pilot such as a repeatedly fired spark will ignite the gases. From this moment, three situations are possible:

- The just created flame does not have enough energy to sustain itself. More energy will be lost to the surroundings than the flame generates and the flame will extinguish. This results in the flashes observed by Arteya [5] and Rasbash et al. [70]. This will happen in early stages of heating when the flame looses much energy to the solid surface which is still relatively cold.
- The flame does have enough energy to overcome the losses, but more gases are burnt than created. This can happen when there is accumulation of gases

around the pilot rather than a continuous stream of gases. This will also result in a flash.

- The flame creates enough energy and the mass flow of gases out of the solid is continuous and sufficient. This will result in a stable flame.

Figure 6.1 [27] is very useful to illustrate the three situations. The figure visualizes several ignition parameters of a mixture of a flammable gas and air (or oxygen). The x-axis denotes the temperature of the gas mixture and the y-axis gives the concentration of the flammable gas. In our case the interesting regions appear on the right side of the saturation curve (temperatures higher than the flash point). For concentrations below the lower flammability limit and above the upper flammability limit, the mixture is not flammable. The auto-ignition temperature and the flame temperature are drawn as a function of the concentration. At the beginning of the heating of a sample in the cone calorimeter, the gas around the pilot is at point 1 (the temperature and concentration are low). At a certain point, the concentration of the pyrolysis gases might be at point 2. The gases are now on the lower flammability limit and will be ignited by the pilot. If the heat produced by the flame is not enough (i.e if it does not reach the auto-ignition temperature, see point 3), the flame will extinguish (the gas will fall back to around point 1). If the flame temperature reaches the auto-ignition temperature (point 4), a sustained flame is obtained.

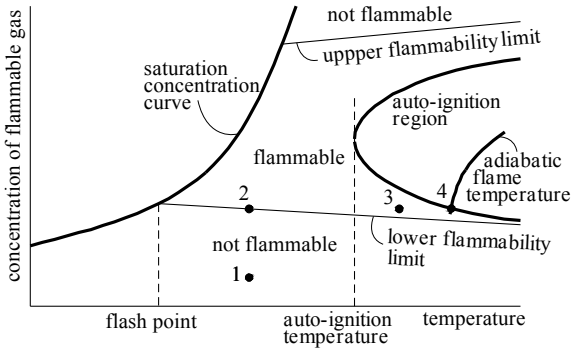

Figure 6.1: *Relationships between various flammability properties. Adopted from [27]. The flame temperature line and points 1-4 are added.*

It is difficult to find the ignition temperature for a gas at its lower flammability limit. Fortunately it can be shown that the ignition temperature is very close to the adiabatic flame temperature at the lower flammability limit. A widely accepted view is that the flammability limits are encountered when the reaction rate is less than a certain critical value [58]. Williams [95] combines this idea with a single step Arrhenius reaction to describe the combustion reaction. He derives that the term $exp(-E/RT_{ad})$ should

be above a critical value. When the activation energy E and the ideal gas constant R are assumed constant as a function of temperature, the adiabatic flame temperature should be higher than a critical value (i.e. auto-ignition temperature) and the flammability limits are found when the adiabatic flame temperature equals this auto-ignition temperature.

However, when flammability limits are measured, heat losses are always present. This means that the adiabatic flame temperature will never be reached and the measured flammability limits will be narrower than expected. Indeed, it is widely recognized that the flammability limits depend on the used apparatus [56]. Williams [95], however, posed that the amount of heat losses from a flame does not influence the limits too much. Spalding [81] analytically determines how the temperature of an hydrocarbon flame at the lower flammability limit (LFL) behaves due to heat losses. With his analysis and evaluation it can be found that:

$$T_{fl} = 0.92\,T_{ad,LFL} \tag{6.1}$$

Law and Egolfopoulos [56] approach this relation numerically and they found the following relations.

$$\begin{aligned} T_{fl} &= 0.942\,T_{ad,LFL} \quad \text{for a methane/air flame} \\ T_{fl} &= 0.962\,T_{ad,LFL} \quad \text{for a hydrogen/air flame} \end{aligned} \tag{6.2}$$

This is a very useful property in our analysis because the adiabatic flame temperature at the lower flammability limit can be determined on forehand for a gas. With an energy balance just after ignition, it can be calculated if the flame reaches the temperature needed. In this analysis, the relation found by Spalding (6.1) is used. Because, according to Williams, the heat losses have not much influence on the flammability limits, the criterion is not very strict. It will be shown later that differences in model predictions for the different criteria are small indeed.

6.4 The model

The purpose of the model is to find the ignition times for several materials as a function of incoming radiative heat flux, sample thickness and moisture content. To find the ignition time several steps are carried out:

1. determine the adiabatic flame temperature ($T_{ad,LFL}$) at the lower flammability limit of the pyrolysis gas. For this, the composition of the pyrolysis vapors has to be known.

2. calculate the temperature of the reacted gas-air mixture (T_{fl}) at the moment of the pilot. (it is assumed that the gas is at the LFL at the moment of the pilot). For this, the mass flux of pyrolysis vapors out of the sample has to be calculated.
3. if $T_{fl} > 0.92 T_{ad,LFL}$ ignition occurs and the analysis is over, if not, the heating and pyrolysis of the sample continues until $T_{fl} > 0.92 T_{ad,LFL}$;

For point 2, the energy and mass balances of the solid phase are needed to calculate the mass flux of pyrolysis vapors out of the sample. To calculate the temperature at the moment of the piloted ignition the energy balance in the gas phase is needed. The three steps are elaborated in the sections below.

6.4.1 Step 1: Adiabatic flame temperature

The adiabatic flame temperature at the lower flammability limit follows from:

$$T_{ad,LFL} = \frac{\Delta H}{c_{p,g}(\nu_{LFL} + 1)} + T_0 \tag{6.3}$$

To evaluate this temperature, the composition of the pyrolysis products should be known.

6.4.2 Step 2: Just reacted mixture temperature

The basis of the model are the energy and mass balances for the solid phase. The sample with the mass and energy fluxes is shown in figure 6.2. In order to calculate the temperature of the burning pyrolysis vapors, the mass flux out of the sample has to be known. This mass flux on his turn depends on the temperature of the sample. Firstly the energy balance of the solid phase will be derived and consequently the mass balance of the solid phase will be given.

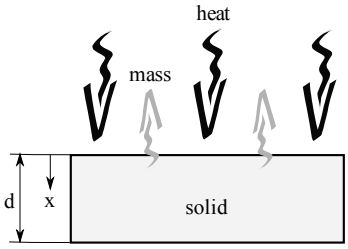

Figure 6.2: *Schematic overview of the solid phase.*

Solid phase energy balance

The energy balance is given by:

$$c_{p,s}\frac{\partial \rho_s T}{\partial t} = k\nabla^2 T - c_{p,g}\dot{m}''_{g,loc}\nabla T - \frac{\partial \rho_s}{\partial t}\Delta H \tag{6.4}$$

The local mass flux of gases through the particle at position x is denoted by $\dot{m}''_{g,loc}$. Just before ignition, the pyrolysis reaction is still slow and the terms $\dot{m}''_{g,loc}$ and $\frac{\partial \rho_S}{\partial t}$ can be neglected in the energy balance. Besides, the thermal properties of the solid are regarded constant with temperature. These simplifications result in the following energy balance for the solid phase:

$$\frac{\partial T}{\partial t} = \alpha\nabla^2 T \tag{6.5}$$

The boundary condition at one side is an adiabatic one and at the other side external radiation comes in:

$$\begin{aligned} &\frac{\partial T}{\partial x} = -\tau\frac{\dot{q}''}{k} \quad \text{at} \quad x = 0 \\ &\frac{\partial T}{\partial x} = 0 \quad \text{at} \quad x = d \\ &T = T_0 \quad \text{at} \quad t = 0 \end{aligned} \tag{6.6}$$

The energy balance consists of a standard heat equation with Neumann boundary conditions at both sides. The parameter τ is explained below.

Beaulieu and Dembsey [13] state that, unless the pyrolysis vapors, all radiation emitted by an external source reaches the particle. They embedded a Schmidt-Boelter gage in the sample surface to measure the radiative heat flux reaching the particle. Their results show that the heat flux only changes very slightly when the pyrolysis starts. However, pyrolysis gases can condensate on the cooled gage and the condensation released energy will be interpreted by the gage as radiation. This will result in an over-prediction of the actual radiative heat flux.

Kashiwagi [51] measured that a significant part of the radiation is blocked by the gas. He measured a attenuation of radiation by the pyrolysis gas as high as 80% for PMMA at high heat fluxes (up to $174 kW/m^2$). His findings are in line with the ones from Di Blasi [19]. Park and Tien [65] are able to predict the measured transmittances from Kashiwagi. The radiative flux $\dot{q}''$ has to be multiplied with the transmittance τ of the

gas. The transmittance is defined as the fraction of radiation which is transmitted through the gas. Because the value of the transmittance is not precisely known, a sensitivity analysis will be done.

Solid phase mass balance

The mass balance of the solid fuel is given by:

$$\begin{aligned} \frac{\partial \rho_s}{\partial t} &= \sum_i K_i + D\nabla^2 \rho_s \\ \text{with} \quad K_i &= -k_i \exp\left(-\frac{E_i}{RT}\right) \rho_i^{n_i} \end{aligned} \tag{6.7}$$

The initial condition is:

$$\rho_s = \rho_0 \quad \text{at} \quad t = 0 \tag{6.8}$$

In this, K_i are the reaction rates of the several pyrolysis reactions and D is the diffusion term for pyrolysis gases coming out of the sample. As has been said before, just before ignition, the reaction is still slow and the diffusion term can be assumed to be infinitely fast compared to the reaction. The mass balance is now determined by the pyrolysis reaction(s) and all gases which are formed due to this are transported out of the particle infinitely fast.

The total mass flux out of the particle (with infinitely fast diffusion) is given by:

$$\dot{m}_g'' = \int_{x=0}^{d} \frac{\partial \rho_s}{\partial t} dx \tag{6.9}$$

With some assumptions, the mass and energy balances can be solved analytically, but this will result in very complex and maybe too simplified relations. Therefore, the balances are solved numerically by finite differences.

Gas phase

The energy balance in the gas phase just after ignition is (per unit mass of gas):

$$A\dot{m}_g'' c_{p,g}(\nu_{LFL} + 1)(T_{fl} - T_0) = A\dot{m}_g'' \Delta H - hA(T_{fl} - T_s) \tag{6.10}$$

The solid surface temperature is denoted with T_s. With this equation the temperature of the gas mixture (T_{fl}) at the moment of the pilot can be determined. However,

in general the pyrolysis gas is a mixture of a wide range of components. The composition of this mixture depends, among others, on the pyrolysis temperature. The equivalence ratio at the lower flammability limit, heating value and specific heat are the average values in the mixture. In most practical cases, one component is available abundantly (e.g. MMA in PMMA pyrolysis) and the gas can be assumed to completely consist of this component. With this approximation, which has to be made for every type of solid fuel, the properties of the pyrolysis gas can be determined.

From the energy balance (6.10) it follows that the flame temperature at the moment of the pilot is:

$$T_{fl} = \frac{T_{ad,LFL} + T_s \Phi}{1 + \Phi} \qquad \text{with} \quad \Phi = \frac{h}{\dot{m}''_g c_{p,g} (\nu_{LFL} + 1)} \tag{6.11}$$

If the heat losses to the solid (h) are zero, equation (6.11) gives the adiabatic flame temperature.

6.4.3 Step 3: Ignition?

If the criterion from Spalding (equation (6.1)) is fulfilled, ignition is obtained. When the T_{fl} is substituted in that criterion, the result is:

$$\frac{T_{ad,LFL} + T_s(t_{ign})\Phi(t_{ign})}{1 + \Phi(t_{ign})} = 0.92 T_{ad,LFL} \tag{6.12}$$

The time at which this is true is defined as the ignition time t_{ign}. Equations 6.7 and 6.9 are used to calculate the mass flux and equation 6.5 is used to calculate the surface temperature. The radiative heating of the gases is neglected due to the relative small distance between the sample and the pilot. The transient system is solved by finite differences until the criterion from 6.12 is fulfilled.

6.5 Results

Beaulieu et al. [13] measured ignition times for several materials as a function of different heat fluxes. They used a modified cone calorimeter apparatus for this. From this research, the results for pine, PMMA and PVC are used to validate the model from section 6.4. Also data from Harada [41] on pine, hiba abor-vitae and oak, data From

Kashiwagi [51] on oak and PMMA and data from Rhodes and Quintiere [73] on ignition times for PMMA are used for validation. The used model parameters are listed in table 6.1.

Table 6.1: *The data used in the calculations.* [a] *Pyrogas consists of 40 vol% CO, 30 vol% CO_2, 15 vol% $\geq C_7$ and 10 vol% CH_4 [62]. Properties of this mixture is the sum of the components contribution.* [b] *The equivalence ratio at the lower flammability limit is derived from the lower flammability limit itself.* [c] *The PVC pyrolysis gases are mainly heavy hydrocarbons. Because the relevant properties of heavy hydrocarbons do not differ to much, octane is chosen as a modeling gas.*

	hardwood oak zelkova		softwood pine hiba abor-vitae		PMMA		PVC	
$\rho_s(kg/m^3)$	750	[41]	420	[14]	1190	[38]	1380	[14]
$ln(k_1/s^{-1})$	6.84	[40]	6.36	[40]	21.89	[32]	34.13	[80]
$E_1(kJ/mol)$	100	[40]	100	[40]	190	[32]	388.2	[80]
$\rho_{1,0}$	$0.28\rho_0$	[40]	$0.34\rho_0$	[40]	$0.0303\rho_0$	[32]	$0.193\rho_0$	[80]
n_1	1		1		1.9	[32]	1	[80]
$ln(k_2/s^{-1})$	17.97	[40]	17.40	[40]	27.01	[32]	7.59	[80]
$E_2(kJ/mol)$	236	[40]	236	[40]	263.7	[32]	110.4	[80]
$\rho_{2,0}$	$0.34\rho_0$	[40]	$0.35\rho_0$	[40]	$0.0187\rho_0$	[32]	$0.377\rho_0$	[80]
n_2	1		1		2.19	[32]	1	[80]
$ln(k_3/s^{-1})$	0.60	[40]	0.53	[40]	10.657	[32]	8.5	[80]
$E_3(kJ/mol)$	46	[40]	46	[40]	118.9	[32]	149.8	[80]
$\rho_{3,0}$	$0.14\rho_0$	[40]	$0.11\rho_0$	[40]	$0.337\rho_0$	[32]	$0.316\rho_0$	[80]
n_3	1		1		1.30	[32]	1	[80]
$ln(k_4/s^{-1})$	10.05	[40]	9.15	[40]	15.976	[32]		
$E_4(kJ/mol)$	127	[40]	105	[40]	199.2	[32]		
$\rho_{4,0}$	$0.03\rho_0$	[40]	$0.01\rho_0$	[40]	$0.614\rho_0$	[32]		
n_4	1		1		1.21	[32]		
$\alpha(mm^2/s)$	0.188	[82]	0.12	[14]	0.10	[38]	0.11	[14]
$k(W/mK)$	0.19	[14]	0.15	[14]	0.18	[38]	0.15	[14]
modeling gas	pyogas [a]	[62]	pyogas [a]	[62]	MMA	est.	octane [c]	est.
$\Delta H(MJ/kg)$	10.8	calc.	10.8	calc.	26.7	[93]	44.9	[47]
ν_{LFL} [b]	13.3	calc.	13.3	calc.	15	[67]	25	[47]

Figure 6.3 shows the results for the hard- and softwoods from Beaulieu et al. (pine), Harada (pine, hiba abor-vitae, red oak and zelkova) and Kashiwagi (oak). It can be seen that the experimental data for softwoods shows a rather large scatter. This can be caused by differences in the experimental method or wood type used by the two researchers. The calculated ignition times are lower than the measured values. The trend for softwood is predicted reasonably well.

For hardwood the data from the two researchers agree well with one another. It is noted that the sample thickness (10mm or 20mm) does not influence the ignition time for the heat fluxes used. The calculated ignition times from the model correspond well with the experimental results.

Figure 6.4 shows the measurement data from Beaulieu et al. (PMMA and PVC), Kashiwagi (PMMA) and Rhodes et al. (PMMA) and the calculation results from the model. The results from Kashiwagi differ a bit from the data from the other two researchers. This can be caused by the different sample thickness. However, Kashiwagi poses that for his experiments the samples can be regarded thermally thick [51]. A more likely reason for the different results from Kashiwagi can be the different experimental setup. He uses a closed chamber in which the fuel is located. This means the pyrolysis gases will accumulate above the sample, causing a lower transmittance. This will result in longer times to ignition. For PVC only one set of data is found in literature. For PMMA the model is in good agreement with the results from Beaulieu et al. and Rhodes et al. The data of Kashiwagi however is not well predicted. For PVC the model over-predicts the experimental data for low to medium heat fluxes. This over-prediction can be caused by the relatively unknown decomposition mechanisms of PVC.

Harada [41] found that the time to ignition scales linearly with k^2/α, which is $188 \cdot 10^3 W^2/m^4K^2$ for softwood and $192 \cdot 10^3 W^2/m^4K^2$ for hardwood. These two values are close together, so it is expected that the ignition times are close as well. However, both the experiments and the model show a difference which is higher than can be expected from this analysis. This indicates that not only the thermal properties, but also kinetics play a role in the ignition times.

6.6 Discussion

6.6.1 Sensitivity analyses

Two sensitivity analyses are carried out. The first one deals with the uncertainty in the transmittance, the second one deals with the variation of the ignition criterion.

In the description of the model in section 6.4, it is posed that not all radiation reaches the surface. Kashiwagi [51] has measured how much radiation is blocked by the pyrolysis gases. From his PMMA measurements it follows that only about $20\% - 50\%$ of the radiation is transmitted through the gas. Because of this uncertainty, a sensitivity analysis is carried out.

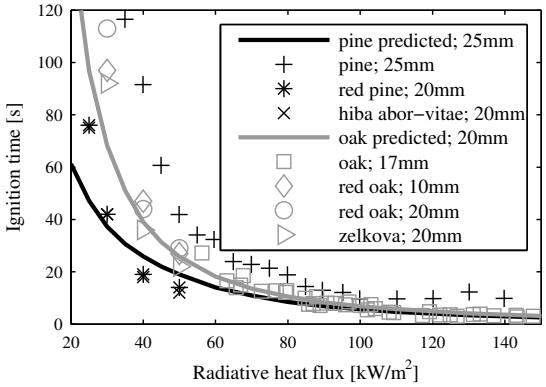

Figure 6.3: *Results for several softwoods (black line and symbols) and several hardwoods (gray line and symbols) with* $\tau = 0.5$. *The experimental data is adopted from [13, 41, 51].*

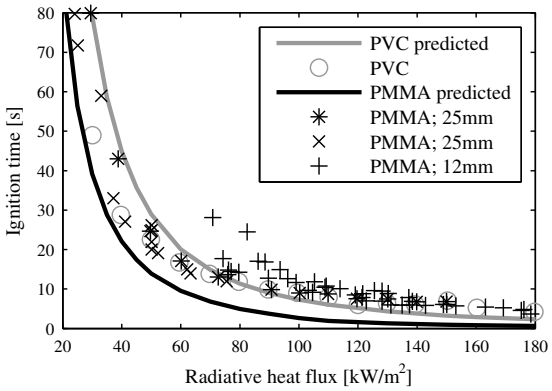

Figure 6.4: *Results for PMMA (black line and symbols) and PVC (gray line and symbols) with* $\tau = 0.5$. *The experimental data is adopted from [13, 73, 51].*

Figure 6.5 shows the results of the model for four different values of the transmittance of the gases. Also the experimental results presented in figure 6.4 are included in figure 6.5. The figure shows that for low radiative fluxes, the calculation with $\tau = 0.5$ compares best with the experimental data and for high fluxes $\tau = 0.3$ and $\tau = 0.2$ do. This result is in line with the findings of Kashiwagi that at low fluxes the transmittance is higher than for high fluxes. This can be explained by the fact that with a higher flux, more pyrolysis gas is created in a shorter time and the gas density will be higher. This

will result in a lower transmittance. For low heat fluxes, the pyrolysis gas has the time to dilute, resulting in a higher transmittance. To make the model more accurate, the transmittance τ in the model should be a function of the incoming radiative heat flux.

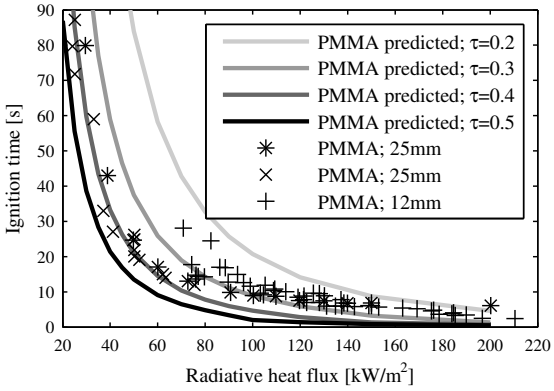

Figure 6.5: *Predicted ignition times for PMMA for several values of the transmittance of radiation of the pyrolysis gas. Experimental data is adopted from [13, 73, 51].*

Figure 6.6 shows the model results for the three criteria for the flame temperature mentioned in equations (6.1) and (6.2). The figure shows that the differences between the three criteria are very small. This shows that the ignition criterion is not very strict indeed.

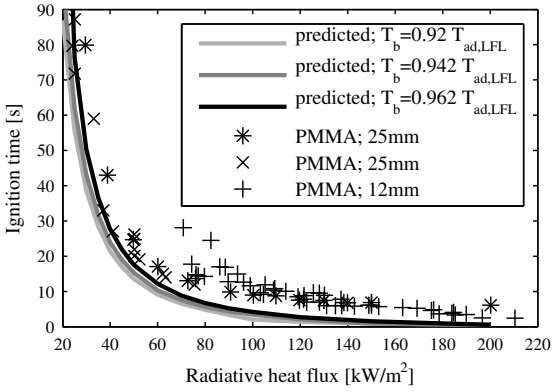

Figure 6.6: *Predicted ignition times for PMMA for the three criteria from equations (6.1) and (6.2) with* $\tau = 0.5$. *Experimental data is adopted from [13, 73, 51].*

6.6.2 Influence of sample thickness

In figures 6.7 and 6.8 the ignition time for respectively PMMA and PVC are plotted as a function of sample thickness for five values of the heat flux. The figures show that for heat fluxes higher than $120 kW/m^2$ the thickness of the sample has hardly any effect on the ignition time. On the other hand, for a heat flux of $20 kW/m^2$ the effect of sample thickness is considerable for samples thinner than $10 mm$. The figure shows that in the heat flux range considered in this work, samples thicker than $10 mm$ can be regarded thermally thick. This conclusion is in line with the statement from Kashiwagi [51] that his PMMA samples of $12 mm$ are thermally thick. The figures show that all PMMA and PVC samples used in the from literature cited experiments are thermally thick.

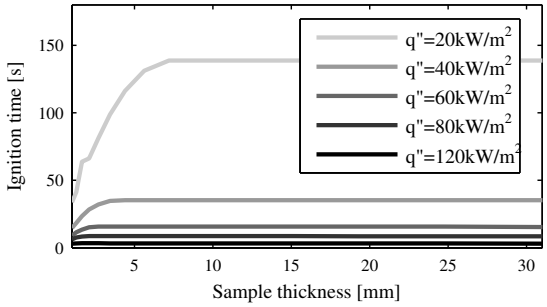

Figure 6.7: *Predicted ignition times as a function of PMMA sample thickness for five heat fluxes.* $\tau = 0.4$.

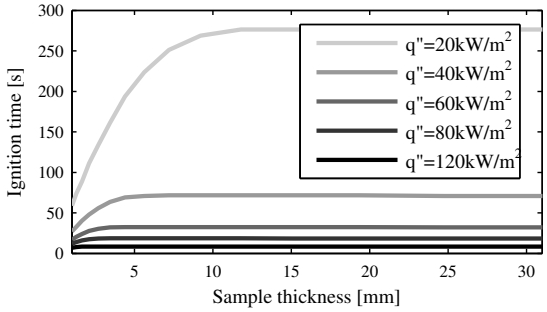

Figure 6.8: *Predicted ignition times as a function of PVC sample thickness for five heat fluxes.* $\tau = 0.4$.

6.6.3 Influence of moisture content

The influence of the moisture content on the ignition times for red oak can be seen in figure 6.9 for five heat fluxes. The moisture evaporation is modeled by a first order Arrhenius equation with $A_m = 5.13 \cdot 10^{10} s^{-1}$, $E_m = 88 kJ/mol$ and $\Delta H_m = -2.44 MJ/kg$ [22]. The diffusion of the water vapor out of the particle is assumed to be much faster than the evaporation rate due to the relatively low thickness of the heated zone. It can be seen that the ignition times significantly increase with increasing moisture content.

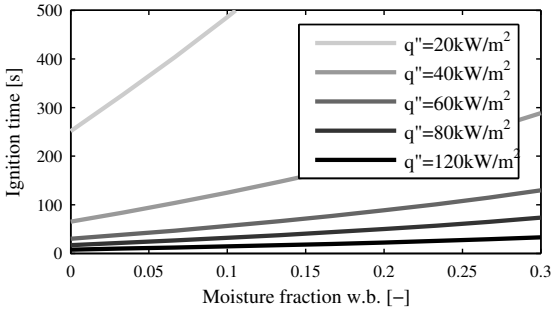

Figure 6.9: *Predicted ignition times as a function of the moisture content for red oak for five heat fluxes. The sample thickness is* $25mm$ *and* $\tau = 0.4$.

6.6.4 Surface temperature and mass flux

Figure 6.10 shows the calculated surface temperature of PMMA and red oak at the moment of ignition as a function of the incoming radiative heat flux. The slope discontinuities are caused by the iteration in the numerical solution method. It can be seen that the surface temperature at ignition of both materials is almost independent of the heat flux. Experimental data found in the literature are summarized in table 6.2. The measured surface temperature at ignition for PMMA seems to be rather reproducible. However, the current model under-predicts the measured values from the literature quite a bit. Besides, the trend is not predicted well. The measured temperatures for red oak show some more scatter, but the model predictions are within the measured data. However, again, the trend is not predicted well. This can be caused by a relatively long delay in ignition in the experiments with higher heat fluxes due to the time needed for the gas to mix with oxygens. Another reason for the discrepancy can be the few used experimental datasets from literature. It is difficult to derive a clear trend from these sets.

Figure 6.11 shows the mass flux out of the PMMA and red oak at ignition. Also the mass flux is predicted to be independent of the heat flux. Measured mass fluxes from the literature are summarized in table 6.2 as well. The model predictions compare well with the data from Rasbash et al. [70] for PMMA and Bamford et al. [9] for wood. In general it can be concluded that there is a wide scatter in the data summarized in the table. Nelson et al. [59] review some measured mass flux data. They pose that the results might be test-specific. Due to the scatter it is difficult to define either a critical surface temperature or critical mass flux for ignition.

Table 6.2: *Experimental data from the literature on surface temperature and mass flux at ignition.*

material	$T_s[K]$	$\dot{m}''_g[g/m^2 s]$	$\dot{q}''[kW/m^2]$	ref.
PMMA	650 – 700		75 – 155	[51]
PMMA	520 – 550	4 – 5.5	12 – 28	[70]
PMMA	520 – 630		15 – 75	[45]
PMMA		1.80 – 2.04	13 – 33	[30]
red oak	780 – 700		75 – 155	[51]
red oak	553 – 623		27 – 76	[44]
wood		2.5		[9]
wood		4 – 5		[70]

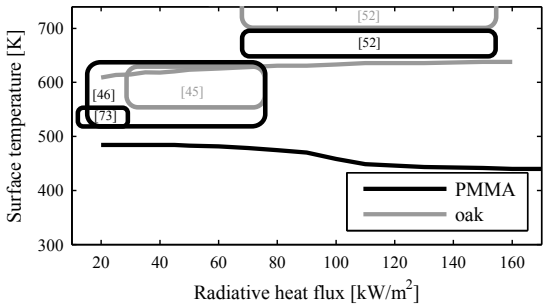

Figure 6.10: *The calculated surface temperature of PMMA and red oak at ignition as function of the incoming heat flux. Experimental data from the literature is shown as well.* $\tau = 0.5$

6.7 Application on waste combustion

The presented model assumes that there is always just enough air to create a mixture which is at its lower flammability limit. In a waste incineration plant, the amount of

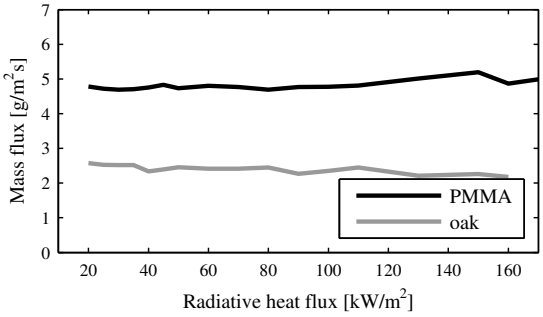

Figure 6.11: *The calculated mass flux out of PMMA and red oak at ignition as function of the incoming heat flux.* $\tau = 0.5$

available air is dictated by the primary air flow rate. In this case, it can not be assumed that the created pyrolysis gases are at their lower flammability limit and therefore, this lower flammability limit criterion is not fulfilled at any time. Besides, the criterion for the adiabatic flame temperature presented in (6.12) can not be used in the case of a waste incinerator plant because the pyrolysis gases are not always at the lower flammability limit.

The two criteria for ignition in a waste incineration plant will be (and in any other gas ignition case):

$$T_{fl} \geq T_{ign} \tag{6.13}$$

$$\dot{m}''_g \geq LFL \cdot \dot{m}''_a \tag{6.14}$$

The latter criterion can be fairly easily evaluated, because the air velocity $\dot{m}''_a$ is a known parameter and when the waste composition is known, the LFL can be approximated. The gas flux $\dot{m}''_g$ can be calculated by equation (6.9). However, the first criterion is more difficult because the ignition temperature is not known for any concentration of the pyrolysis gases (in fact, it is only known for the stoichiometric and the lower flammability limit case). If it can be shown that the first criterion is met before the second one, only the second one has to be considered. We can derive an air flow at which both the criteria are just fulfilled. This air flow gives the transition between the two criteria. The criteria are:

$$T_{fl} = 0.92\, T_{ad,LFL} \tag{6.15}$$

$$\dot{m}''_g = LFL \cdot \dot{m}''_a \tag{6.16}$$

When (6.11) is used, the transition air flow can be shown to be:

$$\dot{m}''_{a,t} = \frac{h(0.92T_{ad,LFL} - T_s)}{LFL \cdot T_{ad,LFL} c_{p,g}(1-0.92)(\nu+1)} \tag{6.17}$$

When the actual air flow is lower than this transition air flow, the gas mixture can be beyond the lower flammability limit, but it has not enough energy to reach the ignition temperature. In this situation, the second criterion (6.14) is fulfilled before the first one (6.13). So the first one should be considered. On the other hand, when the actual air flow is higher than the transition air flow, the gas mixture has enough energy to reach the ignition temperature before the mixture is at the lower flammability limit. In this case the first criterion (6.13) is met before the second one (6.14) and only the second one should be considered:

$$\begin{aligned} \dot{m}''_a < \dot{m}''_{a,t} \quad &\Rightarrow \quad \text{criterion (6.13)} \\ \dot{m}''_a > \dot{m}''_{a,t} \quad &\Rightarrow \quad \text{criterion (6.14)} \end{aligned} \tag{6.18}$$

With $T_s = 300K$ the transition air flow for wood is $0.1 kg/m^2 s$ and for PMMA it is about $0.05 kg/m^2 s$. The primary air flow rates generally encountered in waste incineration plants are in the order of $0.3 kg/m^2 s$, which is higher than the transition air flow. This means that in waste combustion only criterion (6.14) has to be considered.

For a surface temperature of $650K$ (which is about the temperature of the surface at ignition for red oak, see figure 6.10) the transition air flow for red oak is $0.017 kg/m^2 s$. Because this transition air flow is evaluated at the surface temperature at ignition, this is the transition air flow for red oak in practice.

To calculate the ignition time in this case, the convective cooling of the air flow should be included in the solid energy balance (6.4). The convective heat loss due to the primary airflow is:

$$\dot{q}''_{conv,loc} = h_a(T_s - T_a)A_s \Delta x \tag{6.19}$$

In which h_a is the heat transfer coefficient, T_a is the air temperature and A_s is the specific surface area of the fuelbed. The heat transfer coefficient h_a can be found according to Bird et al. [17] as follows:

$$\begin{aligned} h_a &= \frac{k(1-\phi)}{d_p}\left(2.19Re^{1/3} + 0.78Re^{0.619}\right) \\ \text{with:} \quad Re &= \frac{d_p Q}{\nu(1-\phi)} \end{aligned} \tag{6.20}$$

Figure 6.12 shows the calculated ignition times for red oak as a function of the air flow rate for several values of the radiative heat flux for red oak. As has been explained

before, below air flow rates of $0.017 kg/m^2 s$, the model is not valid due to another ignition criterion, so no data is given there. At $0.017 kg/m^2 s$ the results for the ignition time are the same as presented in figure 6.3. For air flows higher than the maximum air flow no ignition can be obtained. This is due to a limited gas mass flux out of the solid fuel as can be seen in figure 6.13. This figure shows the mass flux out of a red oak sample for several heat fluxes until the surface temperature reaches $1000K$. The profiles show a maximum depending on the radiative heat flux. If the air flow is too high (higher than the maximum gas flux divided by the lower flammability limit), the gas mixture will not be able to reach the lower flammability limit at any time. On the other hand, when the air flow is too low, the upper flammability limit (UFL) might be reached and no ignition can take place. In this case, criterion (6.14) is replaced by: $\dot{m}''_g \leq UFL \cdot \dot{m}''_a$. For pyrogas, $UFL \approx 6LFL$ and when it is assumed that also at the upper flammability limit $T_{ign} = 0.92 T_{ad,UFL}$ is valid, it can be estimated that the minimal air flow is $m_{a,t} \frac{LFL}{UFL} = 0.0028 kg/m^2 s$ for 20% moist red oak.

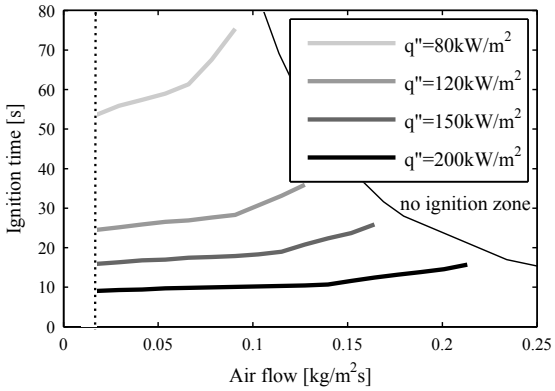

Figure 6.12: *Predicted ignition times as a function of the air flow for red oak. Below* $0.017 kg/m^2 s$ *the model is not valid, so no data is given there. The right top zone is the zone where no ignition can take place. The sample thickness is* $25mm$ *and* $\tau = 0.4$. *The moisture content is 20% w.b.*

With the air flow rates considered here, the heat lost to the air by convective cooling is in the order of a few kW/m^2. This heat loss is small compared to the radiative heat flux. Hence, the problems with ignition are not caused by convective cooling, but by the dilution of the gas mixture to values below the lower flammability limit.

This is useful information for the startup of a waste incineration plant. The air flow should be kept between a maximal and a minimal value. To avoid a long heating time and emissions, an high heat flux should be applied. Based on the calculations for 20% moist red oak, it can be advised to keep the air flow at least above $0.0028 kg/m^2 s$ and

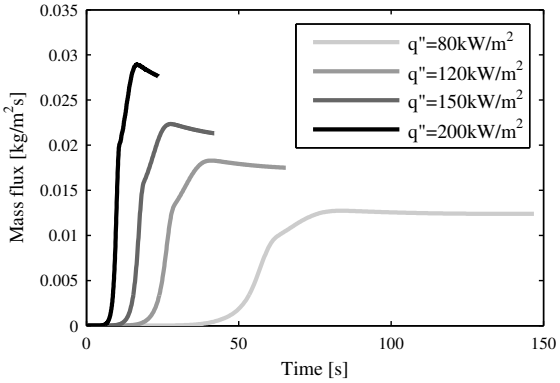

Figure 6.13: *The calculated volatile mass flux evolution for red oak for several radiative heat fluxes. The sample thickness is* $25mm$ *and* $\tau = 0.4$. *The moisture content is 20% w.b.*

below about $0.05 kg/m^2 s$ (see figure 6.12). Even for relative high heat fluxes, the air flow should be kept low during startup to not exceed the maximum air flow.

6.8 Conclusions

In this chapter, a model is presented to predict the ignition times for hardwood, softwood, PMMA and PVC as a function of an incoming radiative heat flux. The criterion for ignition is that the flame temperature of the just reacted volatiles is 0.92 times the adiabatic flame temperature at the lower flammability limit. Conclusions which can be drawn from the model are:

- A model is developed to calculate the ignition times, surface temperatures at ignition and mass fluxes at ignition for several materials as a function of moisture content, primary air flow and incoming radiative heat flux.
- Comparison with experiments from literature showed that the model predicts the ignition times reasonably well. The model prediction for soft wood seems on the low side. For hard wood the predictions agree with the experimental results. Ignition times for PMMA are well predicted. The ignition times for PVC, however, are slightly over-predicted.
- The model results show that the ignition time decreases with lower moisture content and higher incoming heat flux. The sample thickness only has significant influence for low heat fluxes and sample thicknesses below $7mm$

- The model predicts that the surface temperature and the mass flux at ignition are both independent of the incoming radiative heat flux. However, comparison with literature data is difficult due to a significant scatter in this data.
- The model is applied on the ignition of municipal waste on a grate and a minimum and maximum primary air flow is derived. When the primary air flow is not between these two limits, no ignition can take place. The maximum air flow decreases with increasing incoming radiative heat flux.
- It is unlikely that the cooling effect of primary air flow results in a difficult ignition. This can rather be attributed to the dilution of the pyrolysis gases by the primary air flow.

7

Application on waste combustion

Some mechanisms during ignition of solid fuels and packed beds are discussed in the previous chapters. In this chapter this knowledge is translated back to waste incineration.

7.1 Introduction

The objective of this work is to gain insight in the ignition process of municipal solid waste. Based on the knowledge gained from the previous chapters from this thesis, important material properties which determine the ignition phenomena are derived. As described in the first chapter of this thesis, MSW is an inhomogeneous fuel, while most models are based on a homogeneous fuel bed. The effect of the inhomogeneity of a fuel bed on the ignition phenomena is described in this last chapter.

In the first part of this chapter attention is paid to the shape of the ignition front. The influence of mixtures of different materials is investigated. In the second part an expression for the location where the front hits the grate is derived. It is shown that the currently developed two dimensional model for the front movement predicts it to hit the grate sooner than the generally applied one dimensional model. In the last section of this chapter some guidelines for the initial startup are derived.

The combustion and ignition of waste on grate can be described by several characteristic lengths. Figure 7.1 shows these characteristic lengths: L_{fl} is the distance from the entrance of the furnace to the flame and L_f is the distance from the entrance of the furnace to the ignition front. Because this distance is not the same over the bed height is is expressed as a function of this bed height h. The flame at the surface of the fuel bed at L_{fl} is caused by piloted ignition under a radiative heat flux. Chapter 6 deals with piloted ignition and can be used to estimate L_{fl}. In chapter 3 a model is developed to calculate the velocity of the ignition front inside the fuel bed and this chapter can be used to estimate $L_f(h)$. The location where the front hits the grate is $L_f(H_b)$.

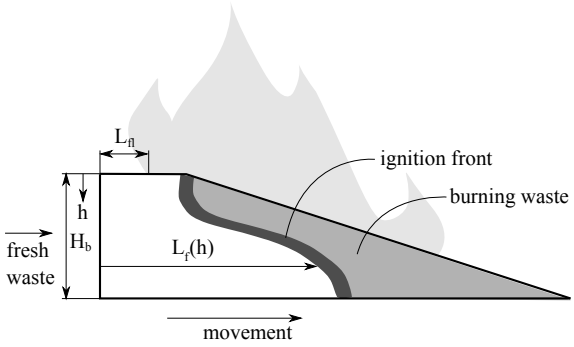

Figure 7.1: *Several characteristic lengths describing the waste combustion process. L_{fl} is the distance from the entrance of the furnace to the flame and $L_f(x)$ is the distance from the entrance of the furnace to the ignition front as a function of the bed height h.*

7.2 Ignition of flames

To predict L_{fl} the horizontal velocity of the fuel bed should be multiplied by the time to (flaming) ignition. Section 6.4 describes a model to predict the time to ignition for a certain material as a function of the incoming radiative heat flux. When this heat flux and the horizontal velocity of the waste are known, the location of the flames can be estimated. When the radiation of the flame is taken into account, the location of the flame can be estimated at any time with this method.

CFD calculations carried out by van den Broek [87] show that in the first zone the radiation on the fuel bed is between 150 and $200 kW/m^2$. If we now use the model described in chapter 6 a time to ignition can be calculated. However, figure 6.12 shows that for 20% moist red oak particles the primary air flow should not exceed $0.23 kg/m^2 s$ ($0.19 m/s$) to obtain ignition. As has been explained in chapter 6, beyond this velocity no ignition can take place at radiative heat fluxes below $200 kW/m^2$ because the concentration of the flammable vapors is too low compared to their lower flammability limit. This maximum air flow of $0.23 kg/m^2 s$ is in the order of the one generally applied in the first zone of waste incinerators. Note that waste also contains inert components. This will result in less flammable gases and thus even less primary air is needed to dilute the gases below their flammability limit. From this it follows that the maximum primary air flow will be even lower in the case of a higher inert fraction. Very close to the flame, the radiative heat flux will be higher than $200 kW/m^2$ and figure 6.12 shows that in this region, the maximum primary air flow increases rapidly with increasing heat flux and a flammable mixture can be reached at higher primary air flows. This means that in practice, the location of the flames (L_{fl} in figure 7.1) is likely to be determined by the point where the maximum air flow is larger than the primary air flow. It can be expected that this will be close to the flame.

7.3 Ignition front movement

For the stability of the process it is useful to be able to predict (and influence) the location of the ignition front. For example: if the flames are too close to the entrance of the furnace, the risk of chute fire exists. But not only the location of the flames is of interest, also the location of the front deeper inside the layer is important to ensure proper burnout.

The movement of the front can be split up in a horizontal and a vertical component (the movement in the third direction is left out this analysis) as has been shown in chapter 3.2. The following can be derived for the location of the front $L_f(x)$ (see also

figure 7.2):

$$\frac{dL_f}{dh} = \frac{v_{b,h}(h) - v_h(h, L_f(h))}{v_{b,v}(h) - v_v(h, L_f(h))} \tag{7.1}$$

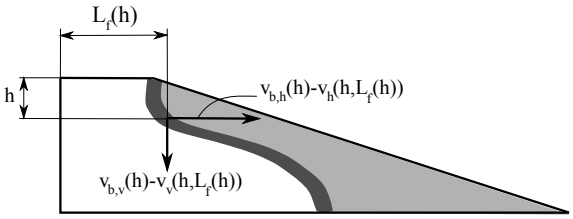

Figure 7.2: *The two components of the ignition front movement at position* $(h, L_f(h))$

In practice the velocity of the bed ($v_{b,h}$ and $v_{b,v}$) are functions of the bed height. However, the average superficial bed velocity is considered here. This means that $v_{b,v} = 0$ and $v_{b,h}(h) = v_b$, with this assumption, local mixing is eliminated. Note that the values for v_h and v_v should be considered at the ignition front at position h: $(h, L_f(h))$. This makes it difficult to integrate the expression.

Because equation (7.1) does not give the location of the front explicitly, one point of the front should be known to predict the ignition front contour. A straightforward choice for this point is $L_f(0)$. This point is a function of thermal and chemical properties of the fuel bed, furnace radiation and bed velocity. Details on this can be found in section 3.5.4.

To find the movement of the front, next to the value of $L_f(0)$, also the front velocities at all location along the ignition front should be known. As an alternative to this, average front velocities can be used. Both options will be discussed in the next sections.

7.3.1 Local front velocities

In chapter 3 it is derived that the ignition front velocity is determined by two processes:

- the time needed to achieve glowing combustion;
- the heat transfer inside the fuel bed.

Several researchers [101, 85] determined that, especially for small particles, glowing is likely to start when most of the particle is pyrolized. When the pyrolysis reactions are faster than the heating of the fuel, the time needed to achieve glowing combustion (which can also be called the time to glowing ignition) is determined by the thermal

mass of the fuel bed ($\rho_b c_{p,b}$). This is true for high heating rates or thermally thick particles. The analysis in chapter 6 showed that for the heat fluxes generally encountered in waste combustion, particles thicker than $10mm$ can be regarded thermally thick. So generally it can be assumed that in waste combustion the time to glowing ignition is determined by the thermal mass $\rho_b c_{p,b}$

For some fuel beds the heat transfer inside the fuel bed is determined by the actual thermal conductivity of the fuel bed (for example dense beds). For other fuel beds the radiation inside the fuel bed determines the heat transfer inside the bed. In both cases the heat transfer inside the bed can be expressed as k_{eff}/d_f. For a more detailed analysis, the reader is referred to section 3.2. The ignition front velocity for a homogeneous fuel bed can be approximated by the ratio of the effective thermal conductivity (which is either radiation or conduction) and the time to glowing ignition (which is determined by the thermal mass of the fuel bed for particles larger than $10mm$, as described before):

$$v_f \approx \frac{k_{eff}}{d_f \rho_b c_{p,b}} = \frac{\alpha_{eff}}{d_f} \tag{7.2}$$

For a more precise prediction, equation (3.17) can be used.

In figure 7.3 the two processes listed above are estimated for several bed materials. In the lower (grey) part of the figure materials are located through which no ignition front can travel. These materials are either inert, or they have a too low char content such as most plastics. The higher the thermal mass, the lower these materials are in the figure. The upper (white) part of the figure lists the materials through which an ignition front is able to propagate. As can be seen with the help of equation (7.2), ignition fronts in materials which are more to the upper-right part of the figure have a higher velocity than ignition fronts in materials close to the origin of the graph.

Inert materials

Also inert materials have a value for k_{eff} and ρc_p but obviously, no ignition front can travel through these materials. When an inert material is added to a charring material it depends on the properties of the inert material whether it will speed up or slow down the ignition front. The properties of the mixture can be estimated by averaging the properties of an inert particle with the properties of the neighboring fuels over a thickness of the combustion front. It can be derived that if too much inert is present it is impossible for an ignition front to propagate. Figure 7.3 shows that this is the case when the properties of this average material are in the grey zone. This will be the case if the heat gained by the char oxidation is smaller than the heat lost by the relatively

cold primary air flow. With the help of equation 3.17 from chapter 3 the front velocity through this average material can be determined.

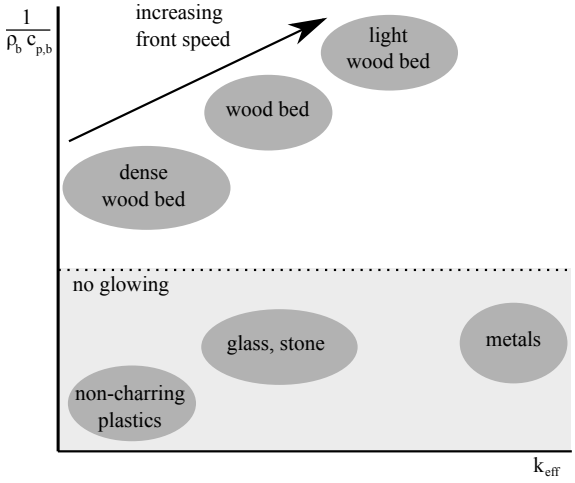

Figure 7.3: *Schematic view of the time to achieve glowing ($\rho_b c_{p,b}$) and effective heat transfer (k_{eff}) for several bed materials.*

Inhomogeneous fuel bed

For an inhomogeneous fuel bed no clear single ignition front can be observed. This is caused by the mixture of fuels with a different α_{eff} (if we assume d_f to be constant) resulting in different ignition front velocities through these materials.

When the ignition front velocities in both directions are known in all locations of the bed and $L_f(0)$ is known, the front shape can be determined with equation (7.1).

7.3.2 Average front velocities

For an inhomogeneous fuel bed which composition is continuously changing the exact location of the ignition front at any time is not that important. More important is where the ignition front hits the grate. When an isotropic waste layer is assumed (which is reasonably for large volumes), an average front velocity $\boldsymbol{v_f}$ can be used to predict the average location where the ignition front hits the grate so the grate can be prepared for high temperatures. Because the average $\boldsymbol{v_f}$ is no function of x anymore,

equation (7.1) can be integrated when $\boldsymbol{v_f}$ is substituted:

$$\begin{aligned} &\int_{\boldsymbol{L_f}(0)}^{\boldsymbol{L_f}(h)} d\boldsymbol{L_f} = \int_0^h \left(\frac{v_b(h)}{\boldsymbol{v_f}} - 1 \right) dh \\ &\text{with:} \quad \boldsymbol{v_f} = \sum_i v_{f,i} \sqrt[3]{\chi_i} \end{aligned} \tag{7.3}$$

As has been explained before, the bed velocity is regarded uniform, so $v_b(h) = v_b$. In this equation $\boldsymbol{L_f}$ is the average front location and χ_i is the volume fraction of component i. Note that the velocity is averaged over a length and not over a volume. Hence the velocity is proportional with the cube root of χ_i. Solving equation (7.3) results in:

$$\boldsymbol{L_f}(h) = h \left(\frac{v_b}{\boldsymbol{v_f}} - 1 \right) + \boldsymbol{L_f}(0) \tag{7.4}$$

Comparison with the 1D situation

When a one dimensional approach is followed (no horizontal front movement: $v_h(h, L_f(h)) = 0$ in equation (7.1)), the location of the front can be expressed as:

$$\boldsymbol{L_f}(h) = h v_b / \boldsymbol{v_f} + \boldsymbol{L_f}(0) \tag{7.5}$$

So when $v_b / \boldsymbol{v_f} >> 1$ in equation (7.4) the influence of the horizontal propagating front can be ignored and equation (7.4) reduces to the 1D situation (7.5).

As has been derived earlier, a first order approximation for the local front velocity is $v_i \approx \alpha_{eff,i} / d_f$. Analogous to this, the average front velocity can be defined as:

$$\begin{aligned} &\boldsymbol{v_f} \approx \frac{\boldsymbol{\alpha_{eff}}}{d_f} \\ &\text{with:} \quad \boldsymbol{\alpha_{eff}} = \sum_i \alpha_{eff,i} \sqrt[3]{\chi_i} \end{aligned} \tag{7.6}$$

The relation for the average front velocity (7.6) can be substituted in equation (7.4) for the 2D situation:

$$\boldsymbol{L_f}(h) = h \left(\frac{v_b d_f}{\boldsymbol{\alpha_{eff}}} - 1 \right) + \boldsymbol{L_f}(0) \tag{7.7}$$

and equation (7.5) for the 1D situation:

$$\boldsymbol{L_f}(h) = h \frac{v_b d_f}{\boldsymbol{\alpha_{eff}}} + \boldsymbol{L_f}(0) \tag{7.8}$$

Now, the horizontal propagating front can be ignored if $v_b d_f / \boldsymbol{\alpha_{eff}} >> 1$. Note that $v_b d_f / \boldsymbol{\alpha_{eff}} = Pe$ as has been used in section 3.2. In that chapter it is derived that $Pe \approx 2$ and two dimensional effects can not be ignored. Equations (7.7) and (7.8) show that for $Pe = 2$, the front in the 2D situation is twice as steep as in the 1D situation. This means that in the 2D situation the front is predicted to hit the grate earlier than predicted by a 1D approach. A schematic view of the difference of the two predictions is shown in figure 7.4.

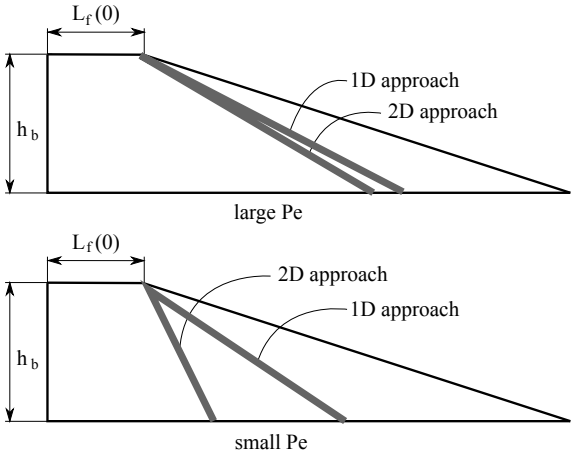

Figure 7.4: *Qualitative view of the difference of the two predictions for different Péclet numbers*

In this figure it is assumed that $L_f(0) = 2$ meters, $Pe = 2$ and $h_b = 1$ meter. In the 1D approach it is calculated that the front reaches the grate at 4 meters from the fuel inlet, while in the 2D approach this occurs at 3 meters from the fuel inlet.

The location of the ignition front can be influenced by either the bed velocity or the bed properties (d_f and α_{eff}) which have all three a linear influence on the location where the front hits the grate. The flame on top of the fuel bed can be moved by varying the primary air velocity at the first zone. If it is made sure that the air velocity in the first zone is high enough to not obtain ignition, the risk of a chute fire can be reduced.

7.4 Startup

Up till now this chapter only deals with the continuous waste combustion process. However, the initial startup of a waste incineration plant is important as well and

should be as clean and short as possible. During this startup an auxiliary oil or gas burner is used to heat up the furnace and to ignite the fuel bed. With the help of the insight gained in previous chapters, something can be said about the ease of the startup for several bed materials. It will be shown that despite some materials ignite very easily, no sustainable ignition front can be achieved.

Figure 7.5 shows the piloted ignition time (vertical axis) and the ignition front velocity (horizontal axis) for several bed materials. According to Harada [41], the ignition time is linearly dependent on k^2/α, so this is used in the figure. Note that these are not effective or bed parameters, but parameters for the solid material.

The figure shows that several materials do not allow an ignition front to propagate, even when these materials are easily ignited. This happens mostly for materials with a very high volatile to char ratio such as plastics. Also some materials do not ignite in the gas phase (flaming), but an ignition front can travel through it very fast. This is the case for materials with an very low volatile to char ratio.

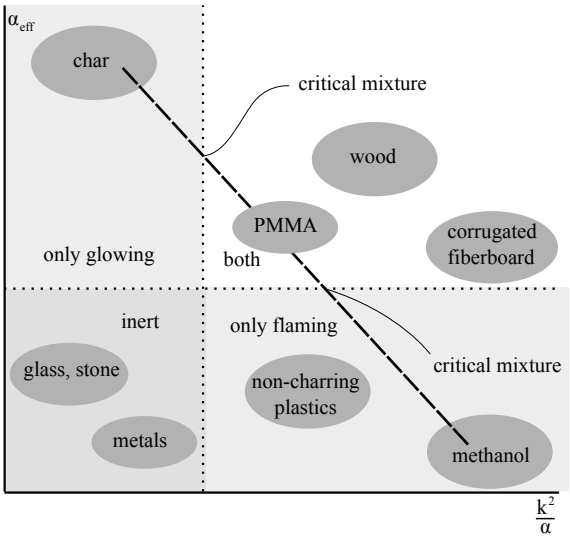

Figure 7.5: *Schematic view of the ignition front velocity and piloted ignition times for several materials and mixtures.*

During the 1D experiments in the glass tube described in chapter 3 it appeared difficult to ignite the wood bed by putting non-charring firebrands on top of the bed. However, char soaked in methanol appeared to be a very effective way of igniting the wood bed. This can be explained with the help of figure 7.5. The non-charring firebrands only ignite flaming but create no ignition front. On the other hand, char can

create a ignition front, but this is difficult to ignite. When the amount of methanol in the char is between certain limits, the mixture is easy to ignite and is able to create an ignition front.

This can be applied on the startup of a waste incinerator. To ensure a easily ignitable fuel bed and the development of a stable ignition front, the initial mixture should be in the upper-right quadrant.

7.5 Conclusions

The theories and models developed in this thesis are developed for model fuels and uniform process conditions. However, the models can be applied on practical situations as occurring in municipal solid waste incinerators. The models and theories show that in a full scale waste incinerator:

- the ignition front velocity is proportional to the thermal diffusivity of the fuel bed;
- for small Péclet numbers, the ignition front is up to twice as steep as is predicted by 1D models;
- the ignition of the waste layer at its surface is determined by the primary air velocity at this zone;
- easy flammable materials do not ensure easy startup;

7.6 Recommendations for further research

Further research can be based on this work in two ways: (1) to validate the translations done in the current work to full scale waste and biomass combustion and (2) to apply the results to a full scale combustion process.

To validate the translations to full size waste and biomass combustion done in the current work, measurements are needed in full size plants. Measurements of the gas composition at several location in a full size burning fuelbed can reveal if flashback in waste combustion does not occur in practice as is derived from models in chapter 2 Measurements of the influence of the furnace radiation on the ignition front velocity in an actual plant would give interesting data to complement the work done in chapter 3.

This work explores some possible ignition mechanisms in solid fuel combustion on a grate in a rather fundamental way. Although translations to full scale waste combustion are made in some chapters, the application of the results from this work on full scale waste and biomass combustion requires more research. A possible topic could be to find optimal process settings and fuel to reduce the emissions from the startup of a furnace. Another topic could be to investigate the influence of ignition of the waste by preheated primary air. This project has started in 2009 at the University of Twente. Finally, the influence of local fuelbed properties on the ignition front velocity requires further research to produce more detailed information on this relation.

Nomenclature

A	stoichiometric switch (0 or 1)
A	surface area $[m^2]$
A_s	specific surface area $[m^2/m^3]$
C	radiation constant $[-]$
c_p	specific heat $[J/kgK]$
D	diffusivity $[m^2/s]$
d	length $[m]$
d_p	(effective) particle diameter $[m]$
E	activation energy $[J/mol]$
Ex	excess energy parameter $[-]$
e	emissivity $[-]$
F	radiation exchange factor $[-]$
H_{evap}	latent heat of evaporation $[J/kg]$
h	heat transfer coefficient $[W/m^2K]$
	height $[m]$
K	reaction rate $[kg/m^3s]$
k	thermal conductivity $[W/mK]$;
k	pre-exponential factor $[1/s]$
k_t	total effective solid thermal conductivity $[W/mK]$
L	characteristic length $[m]$
LFL	lower flammability limit $[m^3/m^3]$
Lo	loss parameter $[-]$
M	molar mass $[kg/mol]$
$\dot{m}''$	surface mass flux $[kg/m^2s]$
$\dot{m}'''$	volumetric mass flux $[kg/m^3s]$
Nu	Nusselt number $[-]$
n	order of reaction
p	pressure $[Pa]$
Pe	Péclet number $[-]$
Pr	Prandtl number $[-]$
Q	primary air velocity $[m/s]$
$\dot{q}''$	heat flux $[W/m^2]$
R	ideal gas contant, $(8.314 J/molK)$
Re	Reynolds number $[-]$
T	temperature $[K]$
t	time $[s]$
v	velocity $[m/s]$
x	Cartesian coordinate $[m]$
Y	mass fraction $[-]$

Greek symbols

α	thermal diffusivity $[m^2/s]$
ΔH	heat of reaction $[J/kg]$
ε	porosity $[-]$
η	stoichiometric mass number $[kg/kg]$
θ	dimensionless temperature $[-]$
κ	radiation approximation term $[W/m^2K^2]$
ν	kinematic viscosity $[m^2/s]$
ν	stoichiometric number $[-]$
ρ	density $[kg/m^3]$
σ	Stefan-Boltzmann constant, $(5.67 \cdot 10^{-8} W/m^2K^4)$
τ	transmittance $[-]$
ϕ	equivalence ratio $[-]$
Φ	ignition parameter $[-]$
χ	volume fraction $[-]$
ψ	dimensionless velocity $[-]$

Subscripts

0	initial, surrounding
a	air
ad	adiabatic
al	alumina

avg	average
b	bed
c	char, critical
$cond$	conduction
dry	dry
eff	effective
$evap$	evaporation
f	front
fl	flame
$furn$	furnace
g	gas
h	horizontal
hc	hemicellulose
i	component i
i	inner
ign	ignition
LFL	at lower flammability limit
loc	local
m	moist
o	outer
p	particle
r	reactor
rad	radiation
s	solid
s	surface
s	specific
sat	saturation
si	spontaneous ignition
t	transition
$tube$	tube
v	vertical
w	wood
$wall$	wall

Bibliography

[1] Emissieregistratie (Pollutant Release & Transfer Register).

[2] Afsteken vuurwerk (in Dutch). Technical report, Rijkswaterstaat - Waterdienst, 2008.

[3] *Afval Energie Bedrijf - maximaal rendement uit afval, brochure*. Gemeente Amsterdam Afval Energie Bedrijf, 2008.

[4] E. Achenbach. Heat and flow characteristics of packed beds. *Experimental Thermal and Fluid Science*, 10:17–27, 1995.

[5] A. Atreya. Ignition of fires. *Philosophical Transactions of the Royal Society A: Mathematical, Physical and Engineering Sciences*, 356(1748):2787–2813, 1998.

[6] V.S. Babkin, A.A. Korzhavin, and V.A. Bunev. Propagation of premixed gaseous explosion flames in porous media. *Combustion and Flame*, 87:182–190, 1991.

[7] V.S. Babkin and Y.M. Laevskii. Seepage gas combustion. *Combustion, Explosion and Shock Waves*, 23(5):531–547, 1987.

[8] V. Babrauskas. Ignition of wood a review of the state of art. *Interflam*, Proc. 9th Intl. Conf.:71–88, 2001.

[9] C.H. Bamford, J. Crank, and J. Malan. On the combustion of wood. part I. *Proceedings of the Cambridge Phil. Soc.*, 42:166–182, 1946.

[10] Kenneth Barbalace. The history of waste. environmentalchemistry.com, Aug 2003.

[11] F.C. Beall. Differential calorimetric analysis of wood and wood components. *Wood Science and Technology*, 5:159–175, 1971.

[12] Patricia A. Beaulieu. *Flammability characteristics at heat flux levels up to* $200 kW/m^2$ *and the effect of oxygen on flame heat flux*. PhD thesis, Worcester Polytechnic Institute, October 2005.

[13] Patricia A. Beaulieu and Nicholas A. Dembsey. Flammability characteristics at applied heat flux levels up to $200 kW/m^2$. *Fire and Materials*, 32:61–86, 2008.

[14] A. Bejan. *Heat Transfer*. Number 0-471-50290-1. John Wiley & Sons, Inc., 1993.

[15] A. Bejan and A.D. Kraus. *Heat Transfer Handbook*. John Wiley & Sons, 2003.

[16] H. Bergström. *Handbok för kolare (in Swedish)*. Jernkontoret, Uppsala, Sweden, fourth edition, 1947.

[17] R.B. Bird, W.E. Stewart, and E.N. Lightfoot. *Transport phenomena*. Number 0-471-41077-2. John Wiley & Sons, Inc., 2 edition, 2002.

[18] C.J.M. Blankert. TGA-MS experiments on different biomass fuels. Technical report, University of Twente, 2008.

[19] C. Di Blasi. Modeling and simulation of combustion processes of charring and non-charring solid fuels. *Prog. Energy Combust. Sci*, 19:71–104, 1993.

[20] P. Bovy. The effect of preheated primary air on the grate of a furnace. Master's thesis, Eindhoven University, 2007.

[21] C. Branca, A. Albano, and C. Di Blasi. Critical evaluation of global mechanisms of wood devolatilization. *Thermochimica Acta*, 429:133–141, 2005.

[22] Kenneth M. Bryden, Kenneth W. Ragland, and Christopher J. Rutland. Modeling thermally thick pyrolysis of wood. *Biomass and Bioenergy*, 22:41–53, 2002.

[23] Valeri Bubnovich and Mario Toledo. Analytical modelling of filtration combustion in inert porous media. *Applied Thermal Engineering*, 27(7):1144 – 1149, 2007.

[24] V.I. Bubnovich, S.A. Zhdanok, and K.V. Dobrego. Analytical study of the combustion waves propagation under filtration of methane-air mixture in a packed bed. *International Journal of Heat and Mass Transfer*, 49(15-16):2578 – 2586, 2006.

[25] G.J. Cheng, A.B. Yu, P. Zulli, and D.L. Xu. Radiation heat transfer in random packing of mono-sized spheres. *Proceedings of the 4th World Congress on Particle Technology, Paper*, 313, 2002.

[26] J. Cooper and W.L.H. Hallett. A numerical model for packed-bed combustion of char particles. *Chemical Engineering Science*, 55:4451–4460, 2000.

[27] D.A. Crowl and J.F. Louvar. *Chemical Process Safety*, chapter 6, Fire and Explosions, pages 225–289. Prentice Hall, Inc., 2nd edition, 2002.

[28] J.H. Damink. Combustion of premixed gas in an inert packed bed. Master's thesis, University of Twente, 2007.

[29] Kirill V. Dobrego, Serguey A. Zhdanok, and Eduard I. Khanevich. Analytical and experimental investigation of the transition from low-velocity to high-velocity regime of filtration combustion. *Experimental Thermal and Fluid Science*, 21(1-3):9 – 16, 2000.

[30] D.D. Drysdale and H.E. Thomson. Flammability of plastics II: Critical mass flux at the firepoint. *Fire Safety Journal*, 14:179–188, 1989.

[31] M. Fatehi and M. Kaviany. Adiabatic reverse combustion in a packed bed. *Combustion and Flame*, 99(1):1–17, 1994.

[32] M. Ferriol, A. Gentilhomme, M. Cochez, N. Oget, and J.L. Mieloszynski. Thermal degradation of poly (methyl methacrylate)(PMMA): modelling of DTG and TG curves. *Polymer Degradation and Stability*, 79(2):271–281, 2003.

[33] D.A. Frank-Kamenetskii. *Diffusion and heat exchange in chemical kinetics*. Princeton University Press, 1955.

[34] H.H. Frey, B. Peters, H. Hunsinger, and J. Vehlow. Characterization of municipal solid waste combustion in a grate furnace. *Waste Management*, 23(8):689–701, 2003.

[35] Martin GmbH für Umwelt-und Energietechnik. private communications. 2009.

[36] S.I. Futko. Mechanism of upper temperature limits in a wave of filtration combustion of gases. *Combustion, Explosion, and Shock Waves*, 39(2):130–139, 2003.

[37] S. Gaur and T.B. Reed. An atlas of thermal data for biomass and other fuels. Technical report, NREL/TP–433-7965, National Renewable Energy Lab., Golden, CO (United States), 1995.

[38] Goodfellow. Polymethylmethacrylate (PMMA, Acrylic) - Material Information. (Last visit: June 2008).

[39] R. Gort. *On the propagation of a reaction front in a packed bed.* PhD thesis, University of Twente, 1995.

[40] M.G. Grønli, G. Vàrhegyi, and C. Di Blasi. Thermogravimetric analysis and devolatilization kinetics of wood. *Ind. Eng. Chem. Res.*, 41:4201–4208, 2002.

[41] T. Harada. Time to ignition, heat release rate and fire endurance time of wood in cone calorimeter test. *Fire and Materials*, 25(4):161–167, 2001.

[42] Hans-Ulrich Hartenstein and Marc Horvay. Overview of municipal waste incineration industry in west Europe (based on the German experience). *Journal of Hazarous Materials*, 47:19–30, 1996.

[43] M.R. Henneke and J.L. Ellzey. Modeling of filtration combustion in a packed bed. *Combustion and Flame*, 117:832–840, 1999.

[44] D. Hopkins, Building, Fire Research Laboratory (US, Dept. of Fire Protection Engineering, and College Park University of Maryland. *Predicting the Ignition Time and Burning Rate of Thermoplastics in the Cone Calorimeter*. National Institute of Standards and Technology, Building and Fire Research Laboratory, 1995.

[45] D. Hopkins Jr and J.G. Quintiere. Material fire properties and predictions for thermoplastics. *Fire Safety Journal*, 26(3):241–268, 1996.

[46] H. Horttanainen, J. Saastamoinen, and P. Sarkomaa. Operational limits of ignition front propagation agianst airflow in packed beds of different wood fuels. *Energy & Fuels*, 16:676–686, 2002.

[47] F.Y. Hshieh. Predicting heats of combustion and lower flammability limits of organosilicon compounds. *Fire and Materials*, 23(2):79–89, 1999.

[48] S. Ishizuka and H. Tsuji. Experimental study of effect of inert gases on extinction of laminar diffusion flames. *Symposium (International) on Combustion*, 18(1):695–703, 1981.

[49] I.M. Ismail and P.L. Walker. Detection of low temperature carbon gasification using DSC and TGA. *Carbon*, 27(4):549–559, 1989.

[50] J+G Feuerfestbau. *Feuerfestabkleidungen in Müllheitzkraftwerken und Biomasseverbrennungsanlagen mit Rohrwandschutz-System JuSyS©Air (in German)*, 2006.

[51] T. Kashiwagi. Experimental observation of radiative ignition mechanisms. *Combustion and Flame*, 34:231–244, 1979.

[52] H. Katalambula, J. Hayashi, and T. Chiba. Dependence of single coal particle ignition mechanism on the surrounding volatile matter cloud. *Energy and Fuels*, 11:1033–1039, 1997.

[53] Wim Kloek and Karin Jordan, editors. *Waste generated and treated in Europe.* European Communities, 2005.

[54] J. T. Kuo and Chin-Lun Hsi. Pyrolysis and ignition of single wooden spheres heated in high-temperature streams of air. *Combustion and Flame*, 142:401–412, 2005.

[55] F.A. Lammers. *Ceramic-foam surface burners in high-temperature environments.* PhD thesis, Technische Universiteit Eindhoven, 2001.

[56] C.K. Law and F.N. Egolfopoulos. Unified chain-thermal theory of fundamental flammability limits. *Symposium (International) on Combustion*, 24(1):137–144, 1992.

[57] R.E. Lyon and J.G. Quintiere. Criteria for piloted ignition of combustible solids. *Combustion and Flame*, 151:551–559, 2007.

[58] A. Maček. Flammability limits: A re-examination. *Combustion Science and Technology*, 21(1):43–52, 1979.

[59] M.I. Nelson, J. Brindley, and A. McIntosh. The dependence of critical heat flux on fuel and additive properties: a critical mass flux model. *Fire safety journal*, 24(2):107–130, 1995.

[60] M.I. Nelson, J. Brindley, and A. McIntosh. Polymer ignition. *Mathl. Comput. Modelling*, 24(8):39–46, 1996.

[61] P. Nordon, B.C Young, and N. W. Bainbridge. The rate of oxidation of char and coal in relation to their tendency to self-heat. *Fuel*, 58:443–449, 1979.

[62] S. Ogawa, H. Mizukami, Y. Bando, and M. Nakamura. The pyrolysis characteristics of each component in municipal solid waste and thermal degragation of its gases. *Journal of Chemical Engineering of Japan*, 38(5):373–384, 2005.

[63] J.J.M. Órfão, F.J.A. Antunes, and J.L. Figueiredo. Pyrolysis kinetics of lignocellulosic materials - three independent reactions model. *Fuel*, 78(3):349–358, 1999.

[64] V.C. Ortmanns and G. Brem. Experimenteel onderzoek naar de emissies en uitbrand bij de verbranding van huishoudelijk afval Fase I.1 van het Parapluplan Procesoptimalisatie AVI's (in Dutch). Technical Report TNO-MEP-R 96/066, TNO, 1996.

[65] S.H. Park and C.L. Tien. Radiation induced ignition of solid fuels. *Int. J. Heat Mass Transfer*, 33(7):1511–1520, 1990.

[66] C.J. Peek. Emissies van prioritaire stoffen naar lucht in nederland 1990-2005 (in Dutch). Technical report, Milieu- en Natuurplanbureau, 2007.

[67] Pharmco-AAPER. Material safety data sheets - METHYL METHACRYLATE. MSDS 135, Rev. 2.1, 12/05, DH, August 1999 (Last visit: June 2008).

[68] K. W. Ragland, D. J. Aerts, and A.J. Baker. Properties of wood for combustion analysis. *Bioresource Technology*, 37:161–168, 1991.

[69] E. Ramström and J. Larfeldt. Indikation av förbränningssituation i nedre del av eldstad genom temperaturmätning på rostens första del (in Swedish). Technical Report 826, Värmeforsk, August 2003.

[70] D.J. Rasbash, D.D. Drysdale, and D. Deepak. Critical heat and mass transfer at pilot ignition and extinction of a material. *Fire Safety Journal*, 10(1):1–10, 1986.

[71] J. Rath, M.G. Wolfinger, G. Steiner G., Krammer, F. Barontini, and V. Cozzani. Heat of wood pyrolysis. *Fuel*, 82(1):81–91, 2003.

[72] D.O. Reimann and H. Hmerli. *Verbrennungstechnik fr Abflle in Theorie und Praxis*. Schriftenreihe Umweltschutz, Bamberg, 1995.

[73] Brian T. Rhodes and James G. Quintiere. Bruning rate and flame heat flux for pmma in a cone calorimeter. *Fire Safety Journal*, 26:221–240, 1996.

[74] J. E. L. Rogers. *Solid fuel combustion and its application to the incineration of solid refuse*. PhD thesis, Massachusetts Institute of Technology, Cambridge, Massachusetts, 1973.

[75] C. Ryu, Y.B. Yang, A. Khor, N.E. Yates, V.N. Sharifi, and J. Swithenbank. Effect of fuel properties on biomass combustion: Part I. Experiments-fuel type, equivalence ratio and particle size. *Fuel*, 85:1039–1046, 2006.

[76] J.J. Saastamoinen, R. Taipale, M. Horttanainen, and P. Sarkomaa. Propagation of the ignition front in beds of wood particles. *Combustion and Flame*, 123:213–226, 2000.

[77] N.N. Semenov. *Some problems in chemical kinetics and reactivity, volume 2*. Princeton University Press, 1959.

[78] D. Shin and S. Choi. The combustion of simulated waste particles in a fixed bed. *Combustion and Flame*, 131:167–180, 2000.

[79] B.P. Singh and M. Kaviany. Effect of solid conductivity on radiative heat transfer in packed beds. *Int. J. Mass Transfer*, 37(16):2579–2583, 1994.

[80] L. Sørum, M.G. Grønli, and J.E. Hustad. Pyrolysis characteristics and kinetics of municipal solid wastes. *Fuel*, 80:1217–1227, 2001.

[81] D.B. Spalding. A theory of inflammability limits and flame-quenching. *Proceedings of the Royal Society of London. Series A, Mathematical and Physical Sciences*, 240(1220):83–100, 1957.

[82] M.J. Spearpoint and J.G. Quintiere. Predicting the piloted ignition of wood in the cone calorimeter using an integral model - effect of species, grain orientation and heat flux. *Fire Safety Journal*, 36:391–412, 2001.

[83] P.H. Thomas and P.C. Bowes. Some aspects of the self-heating and ignition of solid cellulosic materials. *British Journal of Applied Physics*, 12(5):222–229, 1961.

[84] H. Thunman and B. Leckner. Ignition and propagation of a reaction front in cross-current bed combustion of wet biofuels. *Fuel*, 80:473–481, 2001.

[85] H. Thunman, B. Leckner, F. Niklassona, and F. Johnssona. Combustion of wood particles - a particle model for eulerian calculations. *Combustion and Flame*, 129(1-2):30–46, 2002.

[86] M. van Blijderveen, E.M. Gucho, E.A. Bramer, and G. Brem. Spontaneous ignition of wood, char and RDF in a lab scale packed bed. *Fuel*, 89(9):2393–2404, 2010.

[87] J.J. van den Broek. Modeling of a waste incinerator. Master's thesis, University of Twente, Enschede, 2005.

[88] R.P. van der Lans, L.T. Pedersen, A. Jensen, P. Glarborg, and K. Dam-Johansen. Modelling and experiments of straw combustion in a grate furnace. *Biomass and Bioenergy*, 19(3):199–208, 2000.

[89] L. B. M. van Kessel, A. R. J. Arendsen, P. D. M. de Boer-Meulman, and G. Brem. The effect of air preheating on the combustion of solid fuels on a grate. *Fuel*, 83(9):1123–1131, 2004.

[90] L.B.M. van Kessel. *Stochastic disturbances and dynamics of thermal processes*. PhD thesis, University of Eindhoven, 2003.

[91] H.A.J.A. van Kuijk. *Grate furnace combustion: a model for the solid fuel layer*. PhD thesis, Eindhoven University of Technology, 2008.

[92] N. Wakao, S. Kaguei, and T. Funzakri. Effect of fluid dispersion coefficients on particle-to-fluid heat transfer coefficients in packed beds. correlation of nusselt numbers. *Chemical Engineering Science*, 34:325–336, 1979.

[93] R.N. Walters, S.M. Hackett, and R.E. Lyon. Heats of combustion of high temperature polymers. *Fire and Materials*, 24(5):245–252, 2000.

[94] R. Warnecke. private communications. 2009.

[95] Forman A. Williams. *Combustion Theory*. Perseus Books Publishing, L.L.C., 2nd edition, 1985.

[96] H. Yang, R. Yan, H. Chen, D.H. Lee, and C. Zheng. Characteristics of hemicellulose, cellulose and lignin pyrolysis. *Fuel*, 86:1781–1788, 2007.

[97] Y.B. Yang, Y.R. Goh, N. Nasserzadeh, and J. Swithenbank. Mathematical modeling of solid combustion on a traveling bed and the effect of channelling. In *3rd symp. On Incineration and Flue gas treatment technology, Brussel*, July 1-4 2001.

[98] Y.B. Yang, Y.R. Goh, R. Zakaria, N. Nasserzadeh, and J. Swithenbank. Mathematical modeling of MSW incineration on a traveling bed. *Waste management*, 22:369–380, 2002.

[99] Y.B. Yang, V. Nasserzadeh, J. Goodfellow, and J. Swithenbank. Simulation of channel growth in a burning bed of solids. *Inst. Of Chem. Eng.*, 81(A):221–232, 2003.

[100] Y.B. Yang, C. Ryu, A. Khor, V.N. Sharifi, and J. Swithenbank. Fuel size effect on pinewood combustion in a packed bed. *Fuel*, 84:2026–2038, 2005.

[101] Y.B. Yang, H. Yamauchi, N. Nasserzadeh, and J. Swithenbank. Effects of fuel devolatilization on the combustion of wood chips and incineration of simulated municipal solid wastes in a packed bed. *Fuel*, 82:2205–2221, 2003.

[102] G. Zhang, X. Cai, M. Liu, B. Lin, Y. Chen, and L. Wang. Characteristic analysis of low-velocity gas filtration combustion in an inert packed bed. *Combustion Theory and Modelling*, 10(4):683–700, 2006.

[103] S. Zhdanok, L.A Kennedy, and G. Koester. Superadiabatic combustion of methane air mixtures under filtration in a packed bed. *Combustion and Flame*, 100:221–231, 1995.

Acknowledgments

Most people deserve more honor than mentioning their names at one of the last pages of a scientific book about burning trash. I would like to thank some of these people.

First of all I would like to thank Miranda for being Miranda. Thank you for being a better wife than I could wish for. Thank you for your support, your patience, your non-technical view on this work and life in general.

Secondly, I would like to thank Tim and Emma. The last thing you did is helping me to write this thesis. Despite this (or: As a result), you are absolutely a joy to have as kids. You teach me the important things in life: playing, asking why, having faith, not worrying, enjoying small things.

My family deserve to be mentioned for their unconditional support.

Gerrit, Eddy and Theo, thank you for giving me the possibility to do this PhD study. Eddy, thank you for our discussions about the experiments and for reading the piles of paper I have produced. But most of all I would like to thank you for your way of dealing with your recovery. I am glad you are alive and kicking! Gerrit, thanks for your great way of guiding my through this PhD study. I really appreciate the freedom you gave me in this work. Your creativity and your thoroughness are inspiring. The team is complete with Theo, thank you for your impressive capability to scan a page full of equations and knowing what's going on, all in two seconds. Off course, this work would not have been carried out in the first place without the funding of TNO. I am happy you gave me the possibility to be part of the NextGenBioWaste project.

I would also like to thank all students who carried out parts of this research (in no particular order): Hans, Eyerusalem, Pascal, Ilori, Desalign and Karina. The people at TNO also deserve a word of thank for our discussions and their cooperation.

My time at the university would not have been the same without the people of the ThW group. You guys (and occasionally a girl) definitely made my stay at the university much better with jokes, coffee breaks, hijacked email accounts and lots of more stuff I will be smiling about the rest of my life. I would like thank Ashiq and Miladin to share the office with me during the major part of my stay. Thank you for our discussions about food, food, relations, family, food, music, politics, food, religion and food. Jan and Artur, thanks for being my paranymphs and the promise not to attack the committee members.

I will definitely cherish the past few years of my life. Thank you!